# Clean Vehicles Consortium Project Fact Sheets

DECEMBER 2015

## U.S.-China Clean Energy Research Center

### CVC Projects


*Project 1.1.1: Characterization of Degradation Mechanisms in Li-Ion Batteries ..... 1*

*Project 1.1.2: In-Situ Neutron Depth Profiling of Lithium Ion Battery Materials for Improved Electrochemical Performance and Aging Models ..... 6*

*Project 1.1.3: Li-ion Battery Aging and Internal Degradation Mechanisms ..... 11*

*Project 1.1.4: Manufacturing of Pouch Cells for Battery Degradation Studies ..... 15*

*Project 1.2.1: Advanced Battery Chemistries ..... 19*

*Project 1.2.2: Fundamental Understanding of Li-Air Reaction Mechanisms ..... 22*

*Project 2.1: Fundamental Autoignition Chemistry of Advanced Biofuels ..... 26*

*Project 2.2: Chemical and Physical Models for Novel Fuels ..... 29*

*Project 2.4: Integrated Powertrain and Aftertreatment System Control for Clean Vehicles ..... 32*

*Project 2.8: Energy Conversion ..... 36*

*Project 3.1: Electrical Variable Traction-Transmission (EVTT) System Based on DMP Machine ..... 39*

*Project 3.2: Efficient and High Power Density Electric Powertrain ..... 42*

*Project 3.3.1: Rapid System Integration through Modular Configuration ..... 45*

*Project 3.3.2: Intelligent Fault Diagnosis and Prognosis ..... 49*

*Project 3.4.1: Adaptive Battery Management System On and Off the Grid ..... 56*

*Project 3.4.2: Data-Based Techniques for Battery-Health Prediction ..... 61*

*Project 4.2: Cost-Effective Lightweight Materials ..... 65*

*Project 4.3.2: Joining Multi-Material Structures – ..... 68*

*Project 4.3.3: Electrically Assisted Friction Stir Welding for Joining Dissimilar Materials ..... 71*

*Project 4.4: Hybrid Materials Interface Increased Strength Method and Modeling ..... 77*

*Project 4.5: Multi-Material Lightweight Body Subsystem and Vehicle Optimization ..... 81*

*Project 5.2: Vehicle–Grid System Modeling for Technology Deployment ..... 83*

*Project 5.3: Control Strategies for Vehicle-Grid Integration ..... 86*

*Project 5.4: A Wireless Magnetic-Resonance Power Transmission System for EV Charging ..... 88*

*Project 6.1: Life Cycle Assessment of Wireless Charging of Electric Vehicles ..... 94*

*Project 6.2: Fuel Mix Strategies and Constraints*.....98
*Project 6.4.1: Fleet Modeling on China's Electric Vehicle Development* .....101
*Project 6.5.1: Evaluating the Significance of Allocation Methods on Interpretation of Lightweighting Results*.....104
*Project 6.5.2: Improving Precision of Electricity Grid Modeling for Electrified Vehicle Sustainability Assessments* .....107

# Characterization of Degradation Mechanisms in Li-Ion Batteries

***Joint Project***


## U.S. Research Team Lead

- D.W. McComb, The Ohio State University
- Bharat Bhushan, The Ohio State University
- Marcello Canova, The Ohio State University
- Raymond Cao, The Ohio State University
- Terry Conlisk, The Ohio State University

## U.S. Partners

- The Ohio State University
- Argonne National Laboratory
- University of Michigan
- Sandia National Laboratories
- Oak Ridge National Laboratory

## China Research Team Lead

- Feiyu Kang, Tsinghua University
- Xiangming He, Tsinghua University
- Borong Wu, Beijing Institute of Technology
- Daobin Mu, Beijing Institute of Technology

## China Partners

- Tsinghua University
- Beijing Institute of Technology


## Research Objectives

The project team aims to improve the robustness of current-generation lithium-ion batteries via detailed characterization of degradation and aging mechanisms. In addition, the project is formulating design principles based on the knowledge of degradation and aging mechanisms to improve battery cycle life.

## Technical Approach

- Generate aged cells by accelerated electro-thermal protocols that are representative of actual driving conditions for electric vehicles (EVs), hybrid EVs (HEVs), and plug-in HEVs
- Conduct multi-scale ex situ analysis of the anodes and cathodes harvested from unaged and aged cells for changes in physical and morphological structures, surface deposits, micro structures, phase fraction, active lithium concentration, etc.
- Perform electrical and electrochemical characterization at nanoscale using an atomic force microscope (AFM)
- Apply the aging mechanism data to calibrate and evaluate the microscale models for battery performance

## Significant Results

Previously acquired commercial cells from A123 (LiFePO4, 20Ah, prismatic) have been successfully aged in battery cyclers. A refined EELS (electron energy loss spectroscopy) methodology for identifying light elements (lithium in this case) that involves special sample preparation techniques as well as minimization of beam induced damage in the transmission electron microscope during analysis has been developed.

Two sample preparation techniques have been used. In the first type, cathode material (powder) is extracted using a razor blade and subsequently ground in a pestle and mortar to obtain a fine powder with electron transparent regions. This powder is sprinkled on a lacey film support transmission electron microscopy grid for EELS analysis. This is a fast method for determination of phases forming in the cathode but lacks information on spatial correlation between nanoparticles in the cathode. Figure 1 shows a scanning transmission electron microscopy – high angle annular dark field detector (STEM-HAADF) image of the cathode nanoparticles sprinkled on a grid as an inset to several low loss EELS spectra acquired from within a nanoparticle over several exposures lasting for five seconds each. The lithium–K edge is clearly visible (marked) after four exposures demonstrating a lack of beam damage either during specimen preparation or EELS analysis.

In the second technique, electron transparent thin foils are created in a focused ion beam instrument using a procedure with modified parameters of ion beam voltage, ion beam current and ion beam milling angle on specimen surface [1]. The parameters are designed to minimize knock-on damage to the lithium during ion beam milling. This technique retains spatial correlation between various nanoparticles in the original cathode. Figure 2 shows EELS spectra taken from several areas of the FIB foil extracted from a cathode (blue box region). The spectra shows variation in the shape of the Li-K edge across the sample. At this point, variations in the edge structure are purely qualitative and attempts to quantify them are being pursued. Such spectra can be acquired from regions as small as 20nm, allowing phase determination at the nanoparticle level.

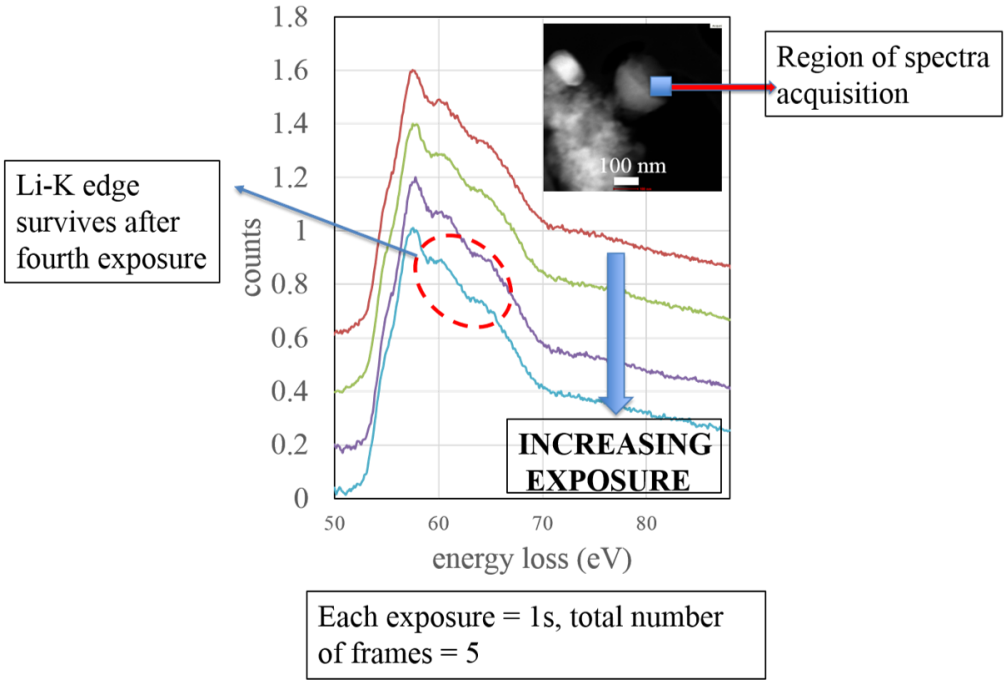


**Figure 1: EELS spectra obtained from a region within a LiFePO4 nanoparticle powder (STEM-HAADF image in inset) obtained from a battery cathode, sprinkled on a lacey support film TEM grid. The lack of beam damage over several exposures is demonstrated.**

Scanning Transmission Electron Microscopy- Electron Energy Loss Spectroscopy (STEM-EELS) was used to simultaneously obtain images of the cathode microstructure and also acquire energy loss spectra in the low loss regime (-10 → 90eV). Multiple Linear Least Squares (MLLS) fitting was used to prove that the phase composition of aged cathodes did not correspond to a linear combination by weight of FePO4 and LiFePO4 phases which prompted further probng of the local electronic structure. Lorentz oscillator modelling was used to interpret the electronic structure using the obtained low loss EELS data. We developed a tool to track that can track these changes to a very high spatial resolution (nm) irrespective of the complex phase composition. We also used the data to study electronic structure evolution in these cathodes with aging and its implications to local chemical bonding environments in the cathode. The data suggests that the electronic structure of the cathode is homogenized as the battery is aged. These results have been discussed in more detail in the quarterly reports presented in 2015 and are summarized in Figure 5 below. A hypothesis of Li-Fe antisite defects was proposed to explain the trends in electronic structure and used to explain the observed system level trends of capacity loss in the battery with aging. Future work must focus on capturing these phenomena in a real time environment (in-situ), perhaps using some of the recently developed liquid cell TEM technology.

The team has developed and utilized in-situ AFM technique for studying aging mechanism in LiFePO4 cathode [2]. Project team has developed an in-situ AFM cell that is easy to assemble in a glove box. In the in-situ AFM cell design, special attention was paid to limit the electrolyte evaporation during in-situ experiments. In-situ AFM cell performed on par with a commercial Li-ion battery at C rates below C/10. Diffusion limitations (i.e., distance between working and counter electrodes is around 2.5 mm) and non-ideal counter electrode (CE) to working electrode (WE) surface area ratio (i.e., CE is ring shaped to accommodate AFM probe) dictates in-situ experiments to be performed at C/10 rate or below. In-situ AFM experiments conducted on LiFePO4 cathode revealed that particle size changes during discharge showed a wide distribution indicating the inhomogeneous nature of the cathode surface, Figures 3 and 4.

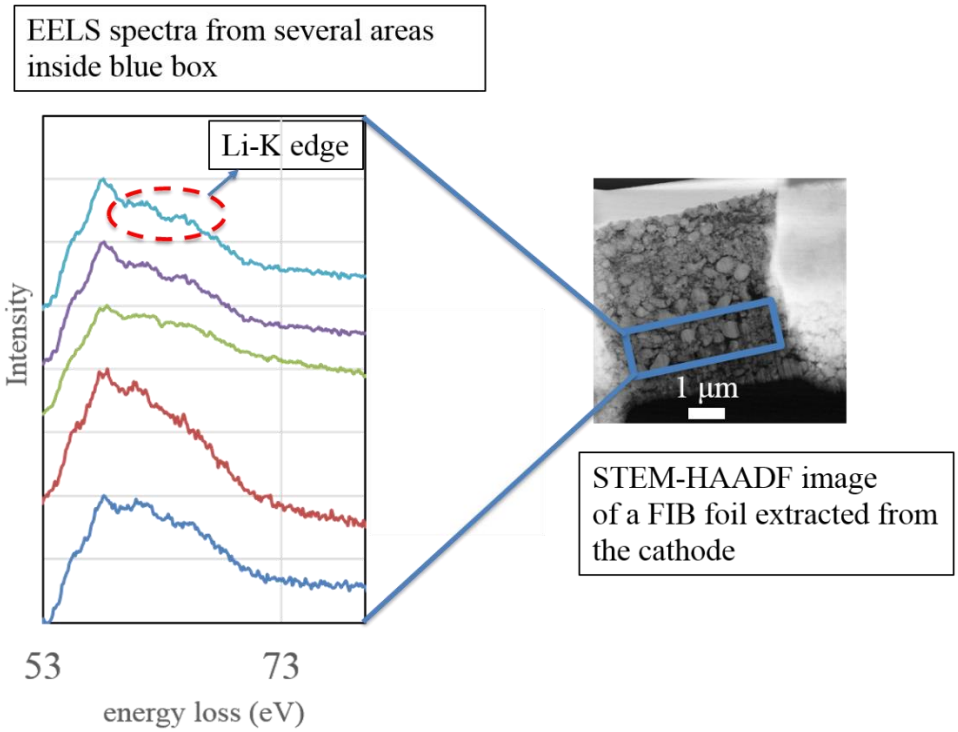


**Figure 2: EELS spectra obtained from several regions within the blue box marked in the STEM-HAADF image on the right**

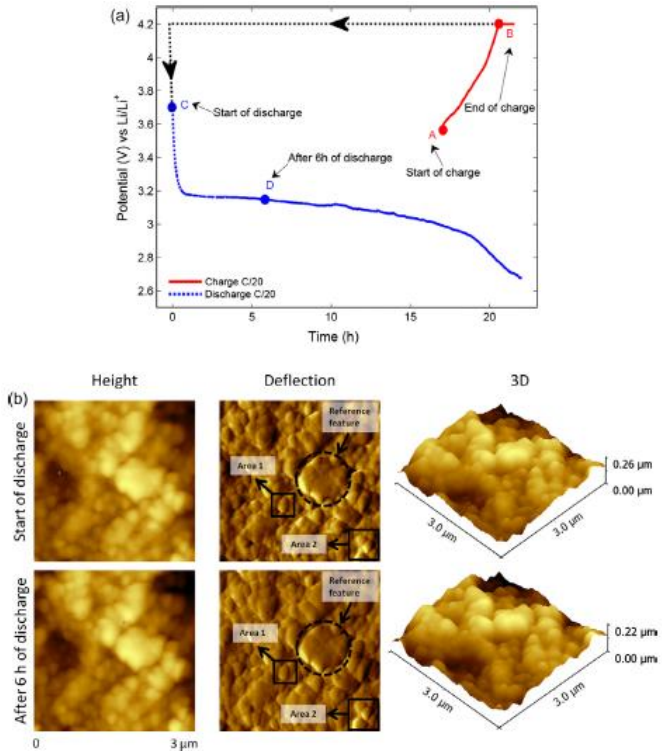


**Figure 3: (a) In-situ LiFePO4 cycling data. (b) AFM images at the start and after 6 h of discharge.**

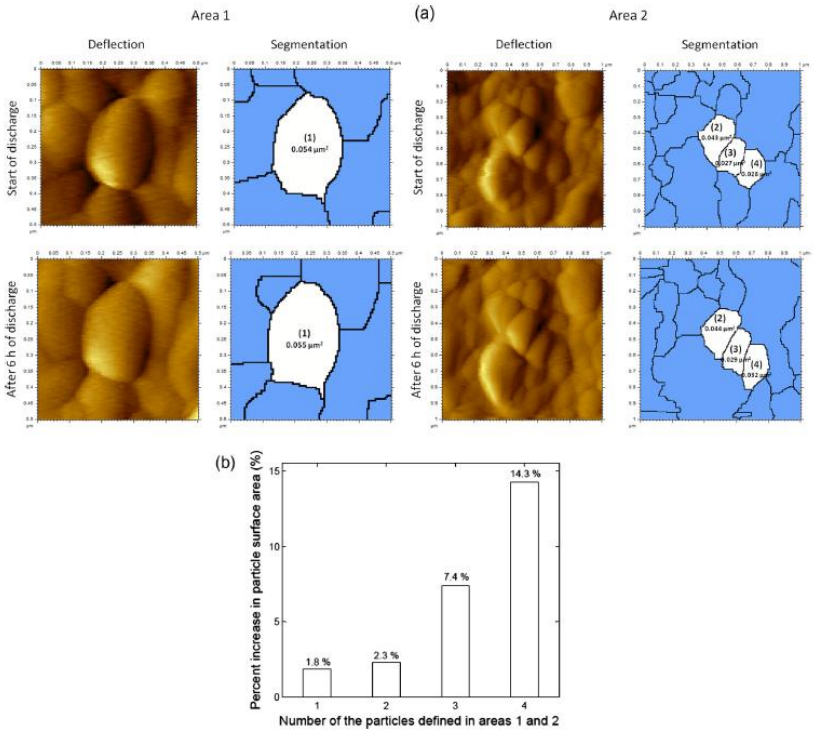


**Figure 4: (a) Deflection and segmented images of areas 1 and 2 given in Figure 4(b). Four LiFePO4 particles were analyzed for surface area change, (b) percent increase in particle surface area after 6 h of discharge at C/20 rate.**

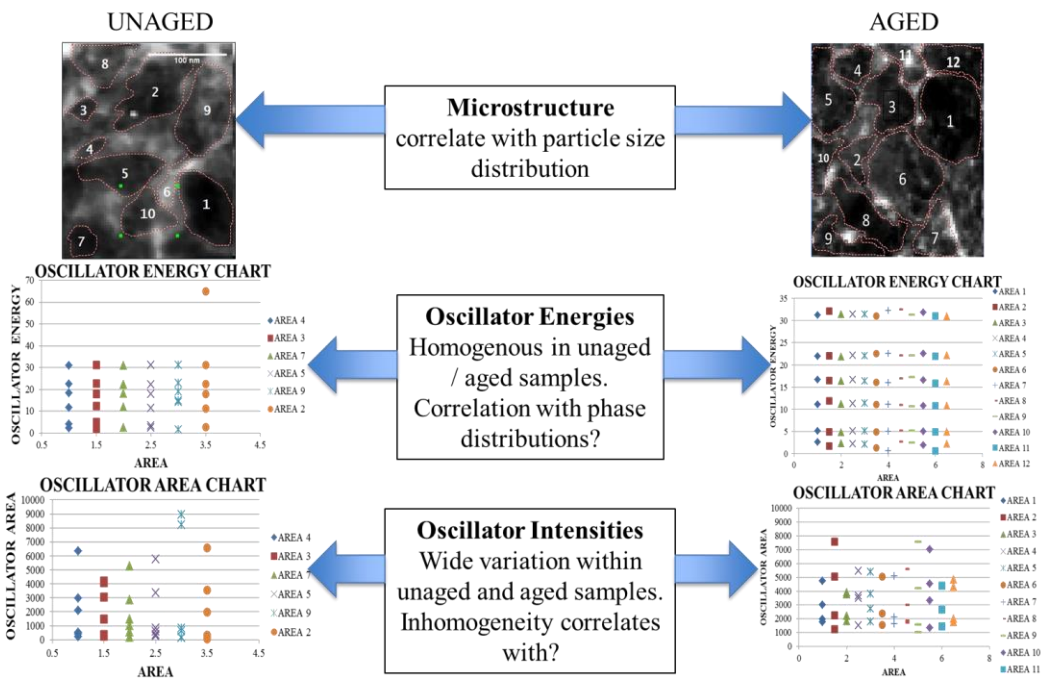


**Figure 5: STEM microstructure images of unaged and aged samples with specific nanoparticles marked from which electronic structure data was obtained (plots below). Various colors in the plot represent various nanoparticles marked in the microstructure.**

## Future Plans

Future work needs to focus on performing experiments to probe structure and chemistry of the cathode with nanometer spatial resolution in a real time environment (in-situ). These experiments will provide deeper insight into the role of defect structures and metastable phases in the aging mechanism of LiFePO4 battery cathodes. The team will also continue utilizing in-situ AFM technique to understand aging phenomenon in LiFePO4 cathode. The team started studying aging mechanism in thin film samples, which are especially useful for fundamental understanding of the aging mechanism since

they only include active material (i.e., LiFePO4) as compared to composite cathodes (i.e., LiFePO4 active material, carbon coating and binder); therefore, thin film samples allow studying the aging mechanism of LiFePO4 active material in isolation.

## Expected Outcomes

- A refined EELS methodology for light element analysis in battery materials
- In situ AFM capabilities for direct analysis of morphological changes and electrochemical performance of LiFePO4
- A robust understanding of aging mechanisms in batteries as a function of aging protocols and cell design and shape
- Parameters to quantify and relate evolution of microstructure in the cathode with the system-level aging metrics

## References/Publications


1. Gilchrist, J. B., Basey-Fisher, Toby. H., Chang, S. C'E., Scheltens, F., McComb, D. W. and Heutz, S. (2014), Uncovering Buried Structure and Interfaces in Molecular Photovoltaics. Adv. Funct. Mater., doi: 10.1002/adfm.201400345
2. Demirocak, D. E. and Bhushan, B. (2014), In situ atomic force microscopy analysis of morphology and particle size changes in Lithium Iron Phosphate cathode during discharge. J Colloid and Interface Sci., vol. 423, pp. 151-157.

# In-Situ Neutron Depth Profiling of Lithium Ion Battery Materials for Improved Electrochemical Performance and Aging Models

***Cooperative Project (U.S.)***


## U.S. Research Team Lead

- **Marcello Canova, The Ohio State University**
- **Raymond Cao, The Ohio State University**

## U.S. Partners

- **The Ohio State University**


## Research Objective

- To establish a direct method to measure the lithium intercalation in the anode and cathode of commercial lithium-ion batteries
- To establish a technique to conduct in situ measurement of the lithium concentration distribution in the anode and cathode of lithium-ion cells during cell utilization (discharging – charging)
- To identify the effect of aging and shape factors on the lithium intercalation in anode and cathode through direct in situ measurements
- To improve the accuracy of performance and aging models through better understanding of the relation between degree of lithiation and state of charge, diffusion kinetics and concentration in liquid and solid phase in the cell

## Technical Approach

- Improve capabilities of ex situ and develop in situ methodology for the analysis of lithium-ion electrode materials at The Ohio State University's (OSU's) Research Reactor
- Develop a lithium-ion coin cell design, enabling for in situ NDP measurements
- Conduct in situ and ex situ NDP to quantify the lithium concentration in the surface region of electrodes and relate the findings to cell-level testing results (electrochemical impedance spectroscopy, cycling data, calorimetry)
- Achieve a systematic design of an experiment to evaluate the lithium concentration profile in electrode samples harvested from new and aged cells, and relate the experimental results to cell usage data
- Analyze experimental results from in situ and ex situ NDP of lithium-ion cell electrodes through electrochemical modeling that is inclusive of aging (e.g., SEI growth models)

## Recent Progress

**Q1 2015**

In this quarter we fabricated a sealed electrochemical cell and investigated the charging/discharging of a series of materials including a high voltage Li1.21Ni0.15Mn0.54Co0.10O0.79 (NMC) electrode, high power density lithium titanate (Li4Ti5O12, LTO), and high energy LixSny electrode, and conducted neutron depth profiling experiments. The purpose is to validate that in-situ neutron depth profiling can be used for a wide range of battery materials.

The structure of the assembled cell can be found in the previous quarter report. The NMC samples were supplied by Argonne National Lab, while the LTO samples were from Idaho National Lab (INL). The thickness of the NMC were about 60 µm and approximately only the charged particles generated from 5 µm deep into the surface can contribute to the signal. The electrolyte sandwich between the NMC and the Li metal is composed of a 25 µm Celgard (80% porosity) immersed in a conventional carbonate electrolyte (1.0 M LiPF6 in 1:1 w/w EC: DMC), which is the channel to transport

Li+ ions between the NMC electrode and the Li foil. The 300 µm Li foil serves as both the counter and reference electrode. A 7.5 µm Kapton® film covers the top surface of the NMC electrode sealing the cell from leaking electrochemical substances to vacuum, and also stops the alpha particles avoiding signal interference of the measured triton signal. We also investigated a 2.5 µm thick Mylar window that will substantially reduce the stopping power therefore improving the effective penetration depth for study. The in-situ NDP experiment was conducted at the National Institute of Standards and Technology's (NIST) Center for Neutron Research (NCNR), while all experimental design optimization was conducted at OSU's facility. The setup can be found in the previous report. The battery sample receives a cold neutron beam with a flux of 1.0 x 109 /cm2-s during a controlled charging/discharging rate of C/10. NDP spectra collected during charge/discharge cycles were recorded every 15 min. The resolution is low thus the curves are smoothed by using 100 data average. However, the resolution can be improved by integrating the signal from multiple 15 min period NDP spectra or channels. From these results we conclude that during the charging process, 1) changes in the Li+ ion concentration was observed in the bulk of the NMC sample 2) the Li+ concentration increases uniformly and steadily within the observed region. A 48% decrease in the Li concentration was observed by integrating the Li concentration under the NDP spectra, this change amounts to a 1.47 mAh charge passed during 50.4% of delithiation. The Li concentration from NDP correlates very well with the charged passed during electrochemical delithiation. This research helped the understanding of Li transportation in NMC battery and validated in-situ NDP can be used for a wide range of materials including a high energy density LiSn, fast charging/discharging LTO and high voltage NMC electrodes.

**Q4 2014**

The activities of Q4 2014 focused on continuing the verification of the in-situ NDP characterization process, specifically by applying this measurement technique to diagnose the lithiation and delithiation in different electrode materials provided by national laboratory partners and from self-synthesized.

To this extent, several experiments were conducted at NIST in December 2014. Several half-cell samples were built using three different materials:

1. LTO, with samples provided by Idaho National Laboratory;
2. NMC, with samples provided by Argonne National Laboratory;
3. LiSn, from samples synthesized at OSU by Dr. Co's team.

## Significant Results

In the second year, we have fabricated a sealed electrochemical cell at OSU and successfully demonstrated in situ study of lithium transportation in a living cell using the NDP facility, as shown in Figure 1 (A) and (B). At the National Institute of Standards and Technology (NIST), the snapshots of lithiation/delithiation of a thin Sn foil (ca. 12.5 µm) were studied and are shown in Figure 1 (C).

NDP spectra collected during charge/discharge cycles were recorded every 5 min during a potentiostatic hold at +0.4 V vs. Li/Li+ (lithiation) over a period of 12 hrs, amounting to ca. 200 mAhr/g.

The real-time evolution of the Li distribution at 60 min intervals is shown in Figure 2. Prior to lithiation (Figure 2 black dashed line), the Li signal in the electrolyte region (-5 to 0 µm) of 6.2 × 1020 atom/cm$^3$ corresponds to the concentration of Li in 1M $LiBF_4$. Upon lithiation, it is evident that an enrichment of Li at the near surface region (up to 2 µm) of Sn is prevalent (0 to 260 min), followed by the diffusion of Li into the bulk. The surface concentration of Li reaches a steady state at 1.9 × 1022 atoms/cm$^3$ by 680 min (equivalent to ca. 200 mAhr/g).

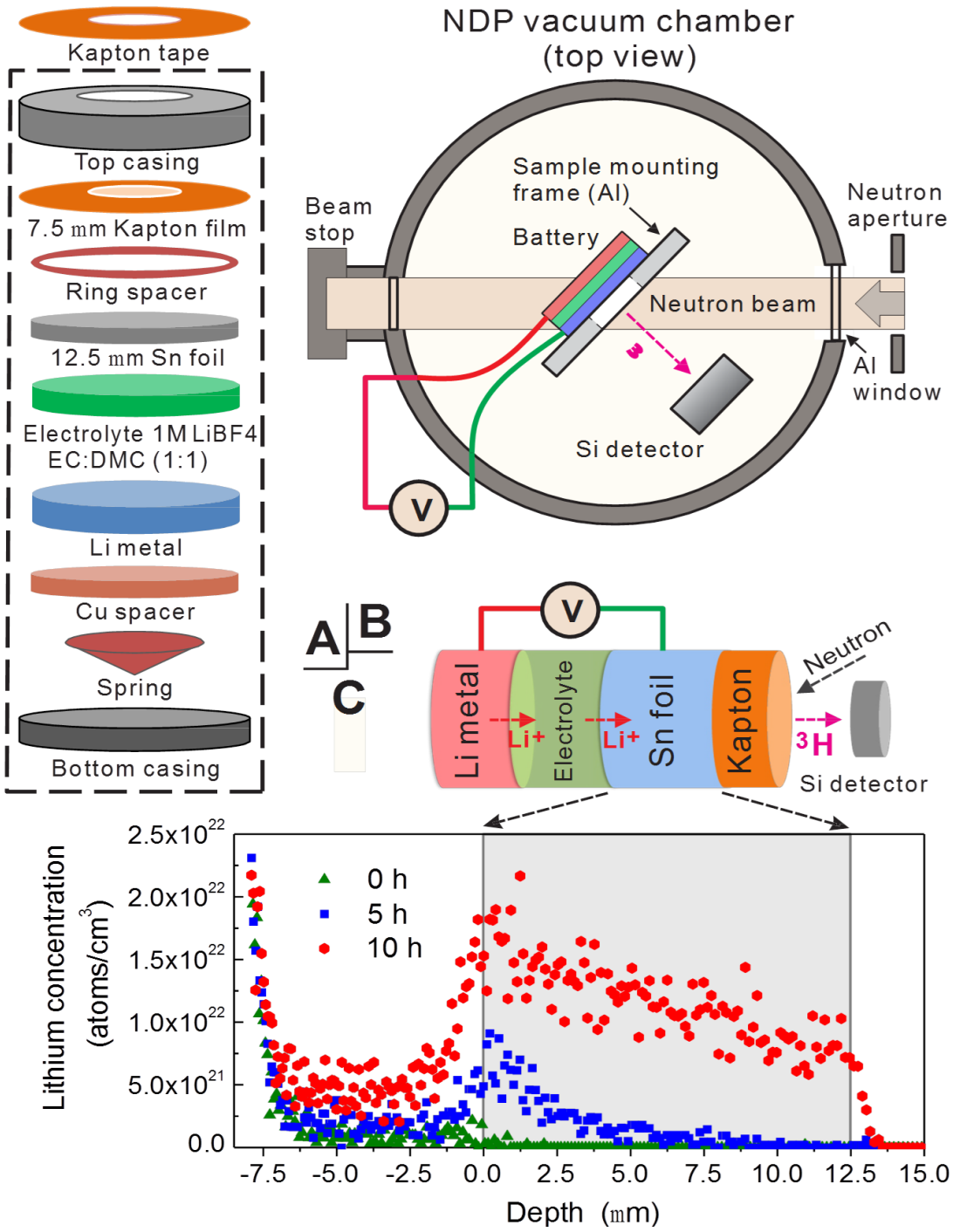


**Figure 1. (A) A schematic representation of the battery components; (B) illustration of the NDP setup; and (C) a snapshot of the in situ NDP spectra showing Li transport during charging/discharging a battery.**

The experiment conducted also elucidated an interesting phenomenon occurring in the electrolyte region. Figure 2 shows an increase in the concentration of the electrolyte upon charge at relatively uniform increments with time. This increase can be attributed to increased concentration of Li salt due to solvent consumption during the formation of the SEI or due to a decrease in volume from the expansion of the electrodes. Another possible explanation is the preferential migration of 6Li towards the Sn during lithiation induced enrichment of 6Li. We exhibited the kinetics of Li reactions, intercalation, and transport by in situ NDP, providing information that is indispensable in the advancement of materials for energy storage.

This work is published at Angewandte Chemie (IF: 13) and was picked by the editors as a very important publication.

## Future Plans

With the successful completion of the goal set in year 1 -2, our future plan is to apply the developed technology to battery characterization of higher-rate and more commercialized products. To achieve this goal, we will continue to apply in situ NDP technology to lithium-ion battery studies to improve the understanding of lithium transport within electrodes and interface processes that occur during cycling behavior of new and aged batteries.

This diagnostic tool complements the multi-scale characterization studies that are being conducted at OSU to investigate the degradation mechanisms in lithium-ion battery materials due to cycle aging.

The unique ability of NDP to provide non-destructive and quantitative measures of lithium concentration in the surface region of electrodes will provide essential data for improved electrochemical performance and aging models. The aging models can then predict the life of the battery with a higher confidence level and can prove vital in diagnostic and prognostic applications for full-scale, production-level batteries.

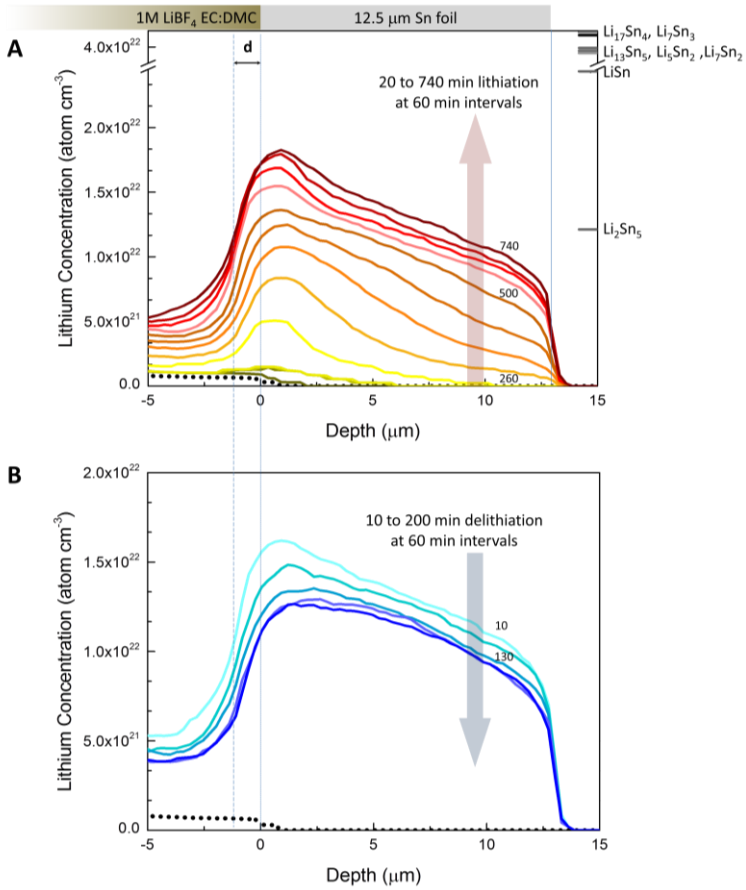


Figure 2. Lithium concentration profiles within a 12.5 μm Sn foil as a function of time (dashed) before electrochemical lithiation, (A) Lithiation spectra plotted every 60 min interval from 20 min to 740 min at 0.4 V vs. $Li/Li^+$(reaching approx. 200 mAhr/g); (B) Delithiation spectra plotted every 60 min interval from 10 min to 200 min delithiation at 1.0 V vs. $Li/Li^+$.

## Expected Outcomes

- Demonstration of the in situ NDP capability for battery diagnostics
- Definition of methods to combine the ex situ and in situ NDP experimental results with the design and calibration of system-level electrochemical models for lithium-ion battery performance prediction
- Investigation of the growth of the SEI layer in lithium-ion cell anodes with NDP-based methods to provide dynamic information for modeling and simulation
- Collaborations created with Chinese and industrial partners to develop applications of NDP-based measurement techniques

## Recent Publications


- Danny X. Liu, Jinghui Wang, Pan Ke, Jie Qiu, Marcello Canova, Lei. R. Cao and Anne C. Co, "In Situ Quantification and Visualization of Lithium Transport with Neutrons," Angewandte Chemie International Edition 53.36 (2014): 9498-9502.
- Jinghui Wang, Danny Liu, Anne Co, Marcello Canova, R. Gregory Downing, Lei R. Cao, "Profiling lithium distributions in Sn anode of Lithium-Ion Batteries with neutrons". Journal of Radioanalytical and Nuclear Chemistry. Vol. 301, no. 1: 277 - 284. 2014.
- Shrikant C. Nagpurea, Padhraic Mulligan, Marcello Canova,Lei R. Cao, "Neutron depth profiling of Li-ion cell electrodes with a gas-controlled environment". Journal of Power Sources. Vol. 248, 489-497. 2014.
- Chuting Tan, Kwan Yee Leung, Danny X. Liu, Marcello Canova, R. Gregory Downing, Anne C. Co, Lei R. Cao, "Gamma radiation effects on Li-ion battery electrolyte in neutron depth profiling for lithium quantification", Journal of Radioanalytical and Nuclear Chemistry. 2015.

## Presentations

- A. Co, "In Situ Characterization of Li Transport in LiSn Anodes with Neutrons." Presented at 2014 ECS and SMEQ Joint International Meeting. Cancun, Mexico (2014)
- (INVITED) A. Co, Seminar Presenter. "Sn as an Alternative Anode Material in Li-Ion Batteries." Presented at 248th ACS National Meeting. San Francisco, California, United States (2014)
- (INVITED) A. Co, "Electroactive Thin Films for Chemical Conversion and Energy Storage." Presented at Gordon Research Conference in Electrochemistry. Ventura, California, United States (2014)
- (INVITED) A. Co, "Electrochemical Characterization of Sn as an Alternative Anode Material in Li-Ion Batteries." Presented at Pittcon 2013 Society for Electroanalytical Chemistry (SEAC) - Highlighting Young Investigators (2013)
- D. Liu, A. Casaday, A. Co, "Electrochemical and Spectroscopic Characterization of Sn as an Alternative Anode in Lithium-Ion Batteries." Presented at Pittcon 2014 Conference and Expo. Chicago, IL, United States (2014)
- (INVITED) L. Cao, "Imaging and Quantifying Lithium in a “living” Li-ion Battery with Neutrons." Argonne National Lab Chemical Sciences and Engineering (CSE) Division Colloquium, Argonne, Illinois, United States (Dec 2014)

## News and Media Items

“First-Ever Look Inside a Working Lithium-Ion Battery”, by Pam Frost Gorder
(http://news.osu.edu/news/2014/09/08/first-ever-look-inside-a-working-lithium-ion-battery/)

# Li-ion Battery Aging and Internal Degradation Mechanisms

***Joint Project***


## U.S. Research Team Lead

- Kevin Leung, Sandia National Laboratories
- Don Siegel, University of Michigan
- S. S. Babu, The Ohio State University
- Marcello Canova, The Ohio State University
- Raymond Cao, The Ohio State University
- S. Nagpure, The Ohio State University

## U.S. Partners

- Sandia National Laboratories
- The Ohio State University
- University of Michigan
- Argonne National Laboratory
- Oak Ridge National Laboratory

## China Research Team Lead

- Xiangming He, Tsinghua University
- Xinping Qiu, Tsinghua University
- Borong Wu, Beijing Institute of Technology

## China Partners

- Tsinghua University
- Beijing Institute of Technology


## Research Objectives

The objective of this project is to predict atomic-length-scale electrolyte and cathode degradation mechanisms (e.g., Mn[II] dissolution) from spinel $LiMn_2O_4$ oxides, a promising prototype material for cathodes in lithium-ion batteries. In addition, the project is investigating electrolyte decomposition on the oxide surface, possibly synergistic with $LiMn_2O_4$ degradation. A second objective is to apply similar methods to study the stability of electrolytes on lithium-air cathode surfaces.

## Technical Approach

- Use electronic structure density functional theory (DFT), including DFT with Hubbard augmentation of d-electrons ("DFT+U") and hybrid DFT functionals
- Use both geometry optimization and finite-temperature molecular dynamics calculations

## Significant Results

The project team has recently published[1] their work on modelling initial electrolyte decomposition reaction of ethylene carbonate (EC) on the dominant[2] (111) surface of $LiMn_2O_4$ (LMO) cathode. The methodology suggested by Karim et al.[3] was used to obtain the most stable $LiMn_2O_4$ bulk crystal and (111) surface structures. It was found that EC undergoes a two-step degradation reaction.

The first step (Figure 1(a)) is the rate determining proton abstraction from EC to the LMO (111) surface. A small second barrier after the transition state is primarily due to the rotation of the surface hydroxyl. The second step (Figure 1(b)) involves ring opening of the proton abstracted EC which turns out to have a smaller barrier. In both of these reactions, at least one electron is transferred from the EC molecule to the surface.

[1] N. Kumar; K. Leung; D. J. Siegel, "Crystal Surface and State of Charge Dependencies of Electrolyte Decomposition on LiMn2O4 Cathode." *J. Electrochem. Soc.* **2014**, *161*, E3059–E3065.

[2] M.R. Huang, C. W. Lin, H. Y. Lu, "Chrystallographic faceting in solid-state reacted $LiMn_2O_4$ spinel powder," *Appl. Surf. Sci.* 177, 103 (2001).

[3] A. Karim, S. Fosse, and K. Persson, "Surface structure and equilibrium particle shape of the $LiMn_2O_4$ spinel from first-principles calculations," *Phys. Rev. B* 87, 075322 (2013).

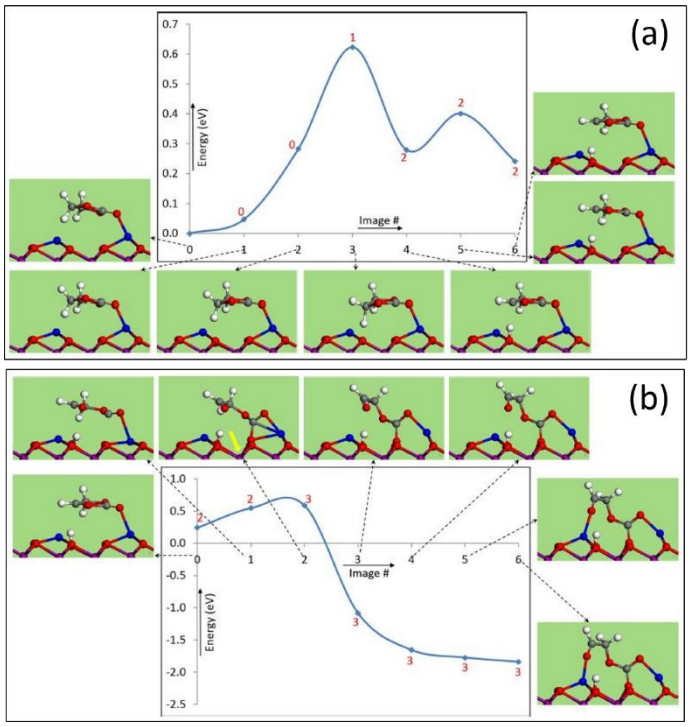


Figure 1: The two step EC decomposition reaction pathway on LMO (111) surface.

The project team also found that both of these reactions are strongly sensitive to the Li content, i.e. state of charge, of the electrode.

It is seen (Table 1) that the H-abstraction barrier decreases from +1.18 eV to +0.62 eV which translates to a 109 fold increase in the reaction rate, ignoring entropic effects and assuming Arrhenius behavior of the reactions with typical molecular vibrational prefactor of 1012 /sec at room temperature. Interestingly, this reaction is well within the typical charging/discharging rate of 1 C, i.e. about an hour. A similar Li-content dependence on the energy barrier is seen for the ring opening reaction. The fully discharge cathode has a barrierless ring opening of the H-abstracted EC. This barrier increases by a small amount to +0.35 eV when the cell reaches a higher charged state. Overall this is a much faster reaction than the H-abstraction with 106 reactions/sec. This shows that the H-abstraction barrier decreases whereas the EC's ring opening barrier increases with decreasing Li content as the battery charges from fully discharged state.

Table 1: H-abstraction and the ring opening energy barriers for varying Li content, i.e. state of charge of the LMO (111) electrode. An estimate of the reaction rate and the number of e- transferred from EC to LMO (111) slab is also reported.

| System ↓ | H-Abstraction | | |
|---|---|---|---|
| | $\Delta E_{barrier}$ (eV) | Reaction Rate at T = 300K ($sec^{-1}$) | # $e^-$ |
| $Li_{1.0}Mn_2O_4$ | +1.18 | ~$10^{-8}$ | 1 |
| $Li_{0.83}Mn_2O_4$ | +0.91 | ~$10^{-4}$ | 1 |
| $Li_{0.67}Mn_2O_4$ | +0.62 | ~$10^{1}$ | 2 |
| **System ↓** | **Ring opening** | | |
| | $\Delta E_{barrier}$ (eV) | Reaction Rate at T = 300K ($sec^{-1}$) | # $e^-$ |
| $Li_{1.0}Mn_2O_4$ | +0.00 | ~$10^{12}$ | 1 |
| $Li_{0.83}Mn_2O_4$ | +0.12 | ~$10^{9}$ | 1 |
| $Li_{0.67}Mn_2O_4$ | +0.35 | ~$10^{6}$ | 1 |

The products obtained after EC decomposition on LMO (111) surface are similar to that observed in an earlier work[4] on LMO (100) surface. On both surfaces, EC loses a proton followed by ring opening of the H-abstracted EC. However, the order of the reaction sequence is reversed on these two surfaces. As shown above, the (111) surface has a rate determining H-abstraction followed by EC ring opening. On the (100) surface, the first step of the reaction is the ring opening followed by an H-abstraction. The initial ring opening event is found to have a low (+0.48 eV) barrier on the (100) surface. However, the barriers for H-abstraction on both surfaces are similar (~+0.6 eV).

A second phase of this research has focused on electrolyte decomposition in metal-air batteries. For example, a viable Li/O2 battery will require the development of stable electrolytes that do not continuously decompose during cell operation. Recent experiments suggest that reactions occurring at the interface between the liquid electrolyte and the

[4] K. Leung, "First-Principals modeling of the Initial Stages of Organic Solvent Decomposition on $Li_xMn_2O_4$(100) Surfaces," *J. Phys. Chem. C* 116, 9852 (2012).

solid lithium peroxide (Li2O2) discharge phase are a major contributor to these instabilities. To clarify the mechanisms associated with these reactions, a variety of atomistic simulation techniques, classical Monte Carlo, van der Waals-augmented density functional theory, ab initio molecular dynamics, and various solvation models, were used to study the initial decomposition of the common electrolyte solvent, dimethoxyethane (DME), on surfaces of Li2O2. Comparisons were made between the two predominant Li2O2 surface charge states by calculating decomposition pathways on peroxide-terminated (O22−) and superoxide- terminated (O21−) facets, Figure 2.

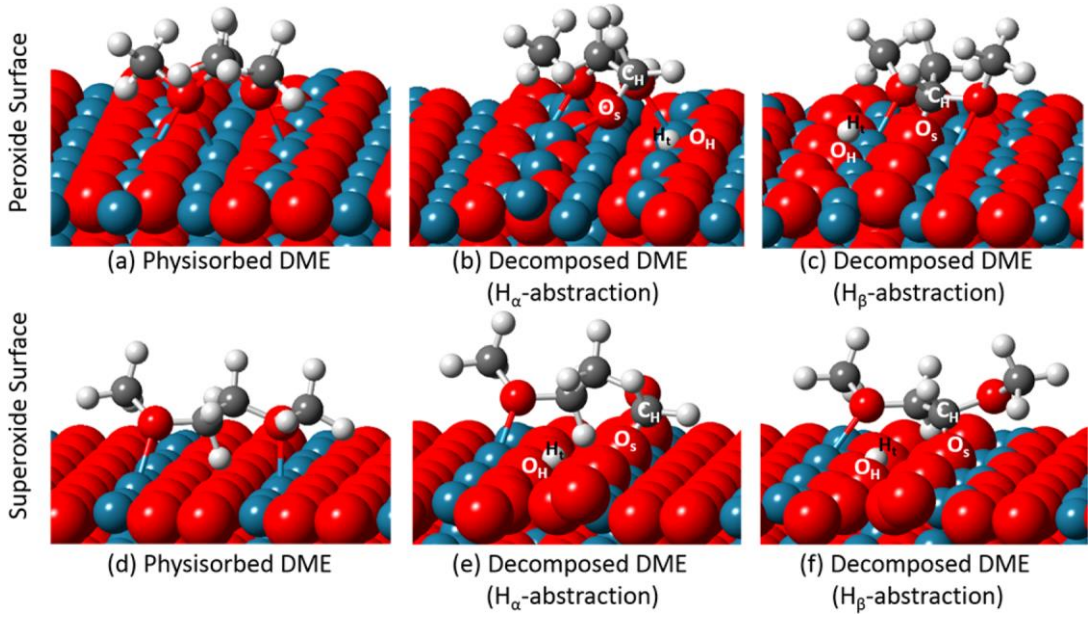


**Figure 2: Side view of the low-energy configuration for adsorbed DME on peroxide (a) and superoxide surfaces (d). H-abstracted DME adsorbed atop peroxide (b, c) and superoxide surfaces (e, f). Abstracted H can detach from either −CH3 (a, c) or −CH2− (b, d) positions within the adsorbed DME molecule. In all cases, H-abstraction results in splitting of an O2 dimer on the Li2O2 surface, generating an −OH and a surface O that nucleophilicly attacks the C from which H was abstracted. Ht: The H that is transferred from DME to the surface O2. CH: The C of DME from which Ht is abstracted. OH: One of the surface O of O2 dimer that bonds with Ht. Os: The other surface O of O2 dimer that nucleophilically attacks the CH.**

For both terminations, it was determined (Figure 3) that DME decomposition proceeds exothermically via a two-step process comprised of hydrogen abstraction (H-abstraction) followed by nucleophilic attack. In the first step, abstracted H dissociates a surface O2 dimer, and combines with a dissociated oxygen to form a hydroxide ion (OH−). The remaining surface oxygen then attacks the DME, resulting in a DME fragment that is strongly bound to the Li2O2 surface. DME decomposition is predicted to be more exothermic on the peroxide facet; nevertheless, the rate of DME decomposition is faster on the superoxide termination.

The impact of solvation (explicit vs implicit) and an applied electric field on the reaction energetics were also investigated. Our calculations suggest that surface-mediated electrolyte decomposition should out-pace liquid-phase processes such as solvent auto-oxidation by dissolved O2. This work was published in the Journal of Physical Chemistry C [1].

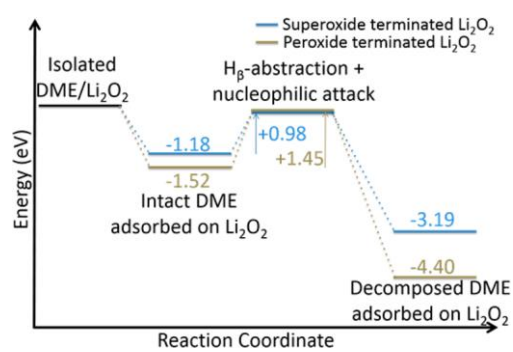


**Figure 3: Energy landscape for Hβ-abstraction from DME on peroxide and superoxide terminated Li2O2 surfaces. "Isolated DME/Li2O2" refers to a configuration where DME and the Li2O2 surface are separated. The activation barrier for H-abstraction is with respect to the "DME adsorbed on Li2O2" configuration, while the other energies are relative to the "Isolated DME/Li2O2" configuration.**

## Future Plans

The future plan is to model the LMO (111) surface covered with a layer of broken EC fragments and multilayer electrolyte similar to the experimental situation. This will allow us to model Mn dissolution. In outlying years, the effect of defects and nickel substitution on spinel oxide surfaces will be examined.

## Expected Outcomes

- Understanding of the detailed, atomistic mechanisms of manganese dissolution from spinel LiMn2O4 surfaces and electrolyte decomposition is expected to yield *insight that can better passivate such cathode oxide surfaces and prevent manganese dissolution, which is known to be a major reason for capacity fade in spinel oxide-based batteries
- Ability to inform rational design of electrolyte additives or inorganic coatings that can prevent such degradation
- Related insights that are particularly pertinent for nickel-doped high-voltage cathode materials that can more readily oxidize the electrolyte and cause further capacity fade in batteries

## References/Publications


1. Nitin Kumar, Maxwell D. Radin, Brandon C. Wood, Tadashi Ogitsu, and Donald J. Siegel, Surface-Mediated Solvent Decomposition in Li-air Batteries: Impact of Peroxide and Superoxide Surface Terminations, Journal of Physical Chemistry C, 119, 9050 (2015).

# Manufacturing of Pouch Cells for Battery Degradation Studies

***Joint Project***


## U.S. Research Team Lead

- Jianlin Li, Oak Ridge National Laboratory
- Claus Daniel, Oak Ridge National Laboratory
- David Wood III, Oak Ridge National Laboratory

## U.S. Partners

- Sandia National Laboratories
- The Ohio State University
- University of Michigan
- Argonne National Laboratory
- Oak Ridge National Laboratory

## China Research Team Lead

- Xinping Qiu, Tsinghua University
- Chuan Wu, Beijing Institute of Technology

## China Partners

- Tsinghua University
- Beijing Institute of Technology


## Research Objectives

A better understanding of the degradation mechanisms and the basic science required for the formulation of modeling tools to predict battery performance and cycle life is still largely insufficient. Establishing the relationship between system level performance parameters and material degradation (micro to nano scale) is key to improve the Li-ion battery technology. Traditionally coin cells are used to study the degradation mechanisms which may not represent the actual behavior of large format batteries in building packs and modules for EV's, and thus, insufficient to diagnose degradation mechanisms.

The objective of this project is to demonstrate manufacturing of large format pouch cells (66x99x12 mm, 100 mAh-7 Ah) and deliver those cells to other partners for battery degradation study. Battery Manufacturing Facility (BMF) will manufacture and distribute large size pouch cells to various CERC partners conducting degradation studies. BMF will also manufacture special cells with customized designs that can assist in characterization studies. The specific goal for FY15 is to investigate the stress and volume evolution in pouch cells during cycling, which provides feedbacks to battery pack design.

## Technical Approach

BMF is a largest open access battery assembly and R&D facility in US. It has a 1400 ft2 dry room with humidity < 0.1% (~-56°C d.p.) that hosts state-of-the-art equipment for every step in cell assembly.

Followings are parameters of the lithium-ion batteries processed and assembled at BMF:

- Standard Electrode Dimensions:
  - Cathode: 8.44 cm×5.60 cm
  - Anode: 8.64 cm×5.80 cm
  - 50-80 mAh per electrode with single side coating
- Current collector:
  - Cathode: Aluminum (15 µm)
  - Anode: Copper (9 µm)
- Capacity Range: 50 mAh to 7 Ah (typical 1.0 Ah)
- Solid loading:
  - Cathode (NMC532): 7.0-16.0 mg/cm2 (typical 12.0 mg/cm2)
  - Anode: 4.0-9.4 mg/cm2 (typical 7.0 mg/cm2)
  - Electrode Balance: N/P=1.0-1.2

- Uncalendered Electrode:
  - Cathode (NMC532 Thickness): 40-100µm
  - Anode Thickness: 40-90 µm
  - Uncalendered Porosity: ~50%

Cells with following specifications have been manufactured.

- Anode: A12 Graphite (Conoco Philips)/Super P Li/9300 PVDF (in NMP) binder = 92/2/6 weight. Solid loading in dispersion: 40 weight%
- Cathode: NMC532 (Toda America)/Denka carbon black/5130 PVDF (in NMP) binder = 90/5/5 weight%. Solid loading in dispersion: 45 weight%
- Electrolyte: 1.2 M LiPF6 in 3:7 EC:DMC (by weight)
- Capacity: ~1 Ah

## Significant Results

Three 1.6 Ah pouch cells were successfully assembled with NMC532 and A12 as the cathode and anode, respectively (A demo is shown in Figure 1). The electrolyte was 1.2 LiPF6 in EC:DMC (3/7 by weight). These cells demonstrated excellent and consistent performance when tested at 0.2C as shown in Figure 2. The capacity retention from all three cells is above 96% after 200 cycles.

Figure 1: A demonstration of pouch cell assembled at the Battery Manufacturing Facility at Oak Ridge National Laboratory

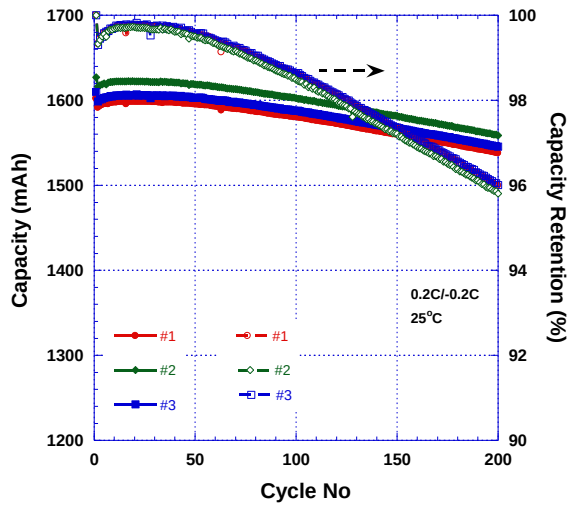


Figure 2: Cyclability and capacity retention of three 1.6-Ah pouch cells.

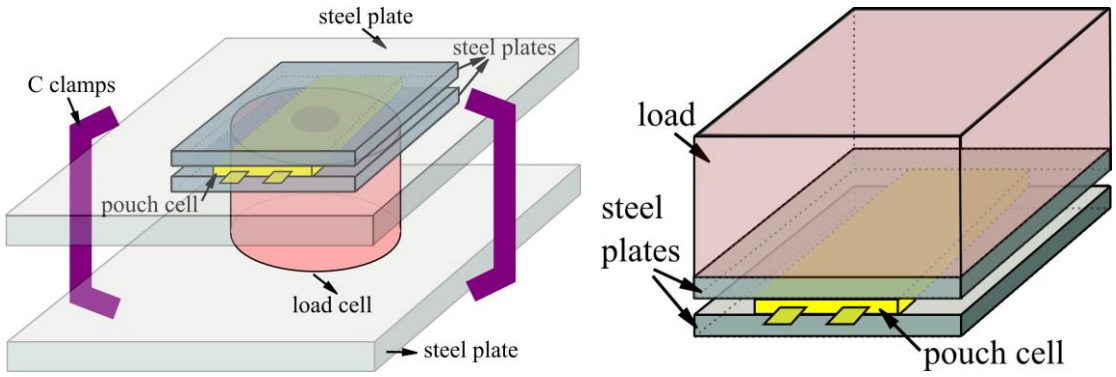


Figure 3: Experimental setup for stress and volume expansion measurement.

Stress evolution determined in one 1.6-Ah pouch cells as shown in Figure 4. Figure 4(a) shows the voltage profile of the cell after formation cycle. The stress profile follows the shape of voltage profile especially at low current (Figure 4(b)). Stress increases during charging and decreases during discharging. There also seems a plateau in stress profile during voltage plateau region. When increasing current, the plateau in stress shrinks and even disappears in the discharge process

(Figure 4 (c) and (d)). The stress also increases with increasing current and upper cutoff voltage as evidence in Figure 4 (c) and (d).

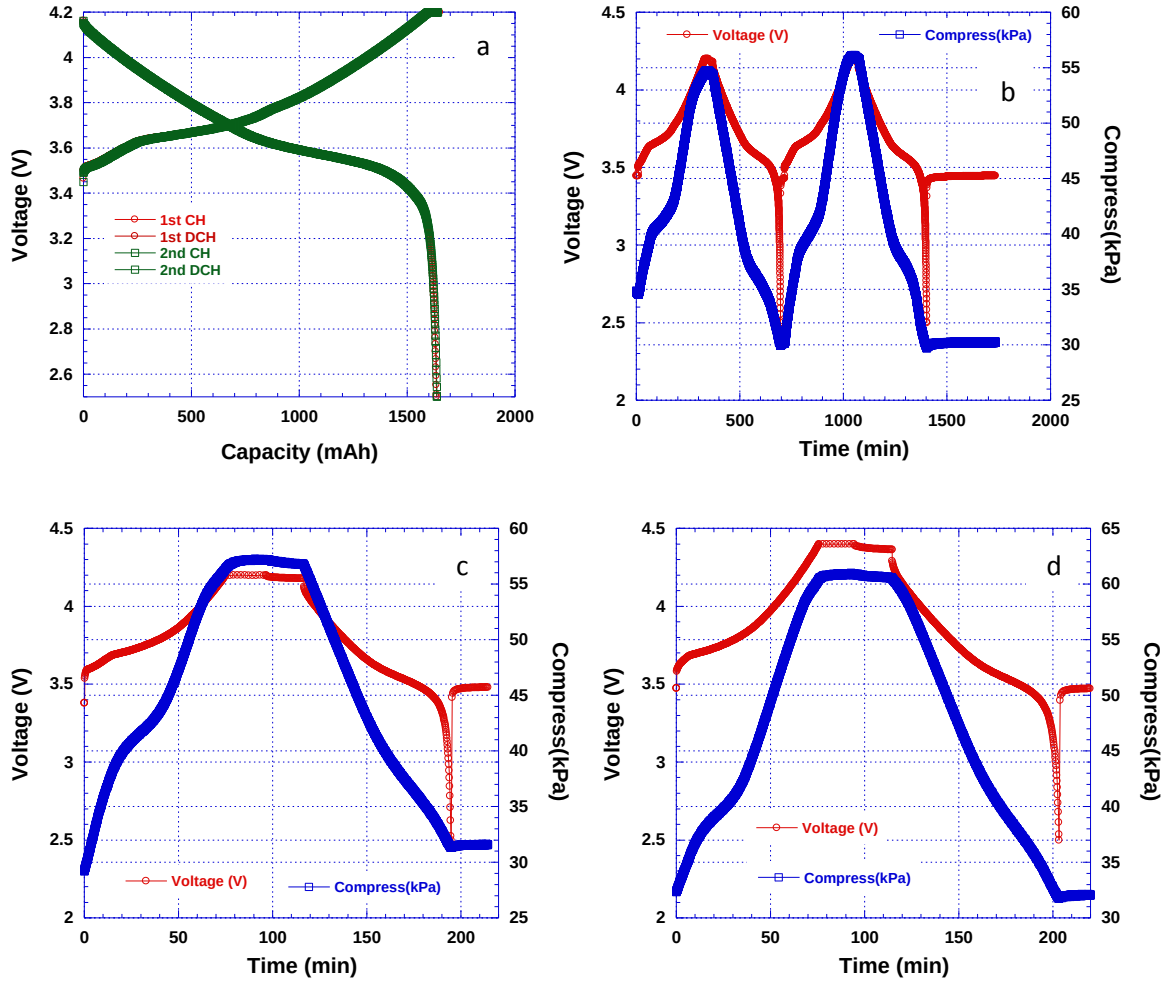


**Figure 4: Voltage profile and stress evolution of 1.6-Ah pouch cells a) voltage profile at 300mA/-300mA; b) voltage and stress profile at 300 mA/-300 mA and 2.5-4.2 V; c) voltage and stress profile at 1200 mA/- 1200 mA and 2.5-4.2 V; and d) voltage and stress profile at 1200 mA/-1200 mA and 2.5-4.4 V.**

Volume expansion measured in the same pouch cell as shown in Figure 5. As shown in Figure 5 (a), the overall volume expands during charging and contracts during discharging. It was around 1.5% at 4.2 V when charged at 300 mA. It significantly increases to above 2.0% when extending the upper cutoff voltage (UCV) to 4.3 V. The volume expansion is less significant when further extending the UCV to 4.4 V. There is also significant volume expansion when increasing charging current from 300 mA to 1200 mA at UCV of 4.2 V. The volume expansion is less significant with higher UCV or higher current (Figure 5 (b)).

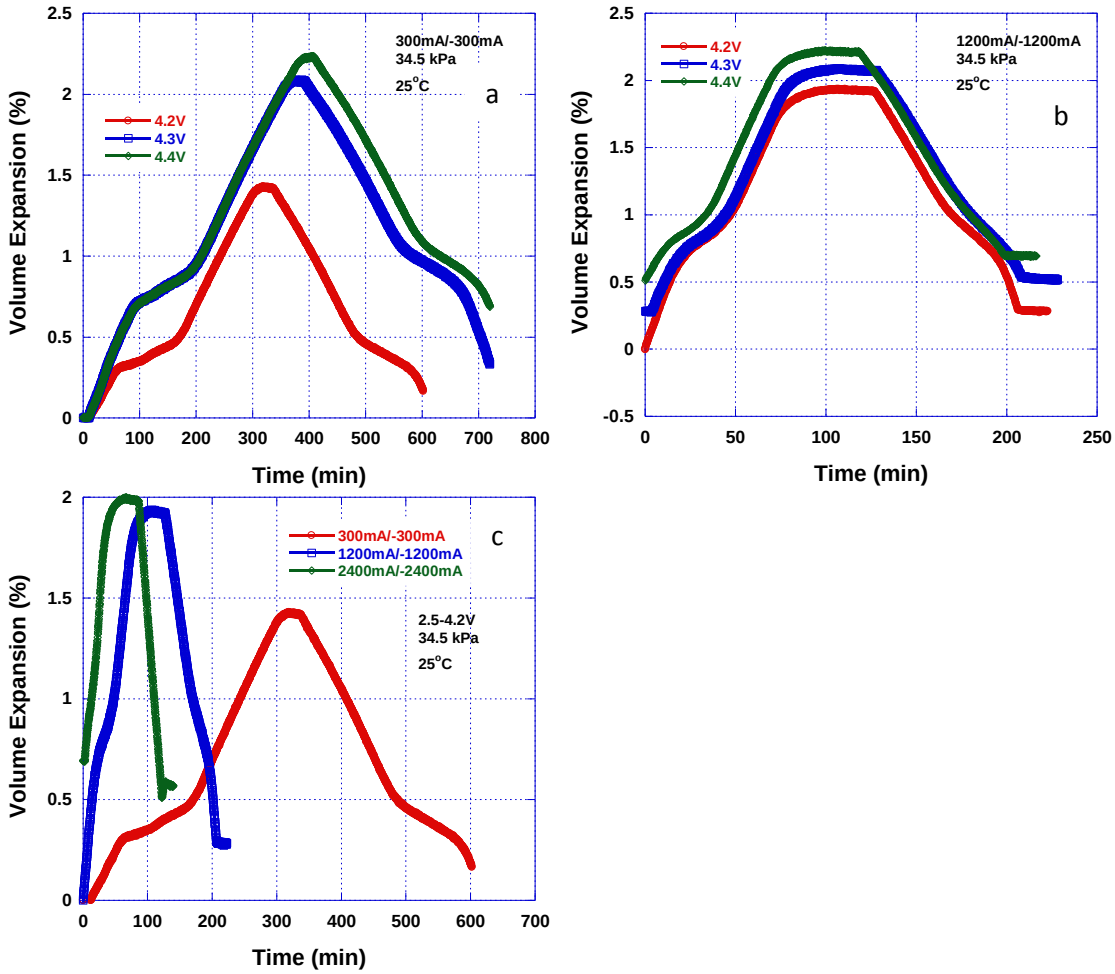


Figure 5: Volume expansion in NMC532/graphite pouch cells (a) at 300 mA/-300 mA and various upper cutoff voltages; (b) at 1200 mA/-1200 mA and various upper cutoff voltages and (c) at various currents and 4.2V upper cutoff voltage.

## Future Plans

- Characterize pouch cells with inhomogeneities and material degradation to understand the evolution of electrode structure during cycling using in-situ neutron diffraction setup.
- Continue in-depth study the volume expansion in the full pouch cells.
- Characterize volume and stress evolution in pouch cells with silicon anodes.

## Expected Outcomes

- Considerably improve our understanding of degradation mechanisms in electrodes aged in large format cells under realistic conditions
- Knowledge of stress and volume expansion information on cell level providing feedbacks to battery pack design
- Insights on stress and volume expansion on silicon electrodes providing initial information on implementing silicon anodes

# Advanced Battery Chemistries

***Joint Project***


## U.S. Research Team Lead

- Don Siegel, University of Michigan
- Yang Shao-Horn and Gerd Ceder, Massachusetts Institute of Technology
- Khalil Amine, Argonne National Laboratory

## U.S. Partners

- Argonne National Laboratory
- University of Michigan
- Massachusetts Institute of Technology

## China Research Team Lead

- Feiyu Kang, Tsinghua University
- Xiangming He, Tsinghua University
- Borong Wu, Beijing Institute of Technology
- Feng Wu, Beijing Institute of Technology

## China Partners

- Tsinghua University
- Beijing Institute of Technology


## Research Objectives

This project aims to identify the primary mechanisms that limit the performance of rechargeable metal-air batteries, including high charging potentials, poor reversibility, and limited capacity/capacity fade. Revealing these mechanisms will enable the development of rational strategies for improving performance, with the ultimate goal of translating these batteries from the laboratory bench to commercial application in electric vehicles.

## Technical Approach

- Perform a combination of first-principles computational modeling of lithium-air and sodium-air battery materials in conjunction with parallel materials characterization experiments (at partner institutions)
- Elucidate key morphological features of discharge phases in metal-air batteries
- Calculate rates of charge and mass transport in metal-air discharge phases, and explore mechanisms for enhancing transport
- More generally, uncover phenomena resulting in high charging potentials, poor reversibility, and limited capacity/capacity fade in lithium-air batteries

## Significant Results

Thanks to their high theoretical specific energy density, rechargeable non-aqueous metal-air batteries are attracting increasing attention as a potentially transformative energy storage technology. In the absence of undesirable side reactions (e.g., degradation of the solvent or carbon support), a metal-air cell can be described by the reversible reaction $xM + y/2\ O2 \leftrightarrow M_XO_Y$. This chemistry is unlike conventional lithium-ion intercalation electrodes because the solid-phase discharge product, typically a metal-peroxide or superoxide (eg., $Li_2O_2$ or $NaO_2$), nucleates and grows on the cathode during discharge, and it subsequently decomposes during recharge.

In order to achieve a high energy density, the cathode of a metal-air cell should be substantially filled with discharge phase at the end of discharge. However, our prior studies [1-4] on $LI/O_2$ systems have suggested that charge transport limitations through an ostensibly insulating discharge phase may constrain the capacity and rate capability of these cells. Therefore, a question of both practical and fundamental importance to the metal-air system is the mechanism and efficiency of charge transport through the discharge product. Unfortunately, a general mechanism for charge transport in these cathodes has yet to emerge.

Our recent efforts have focused on understanding transport in the Na-air battery system. The primary discharge product in Na-air batteries has been reported in some experiments to be sodium peroxide, $Na_2O_2$, while in others the formation of sodium superoxide, $NaO_2$, is observed. Importantly, cells that discharge to $NaO_2$ exhibit much lower charging overpotentials than those that discharge to $Na_2O_2$, suggesting a connection between round-trip efficiency and the

composition of the discharge product. These differences could arise from a higher intrinsic conductivity of the superoxide phase; however, such an explanation remains speculative given that the charge transport properties of superoxides are relatively unexplored.

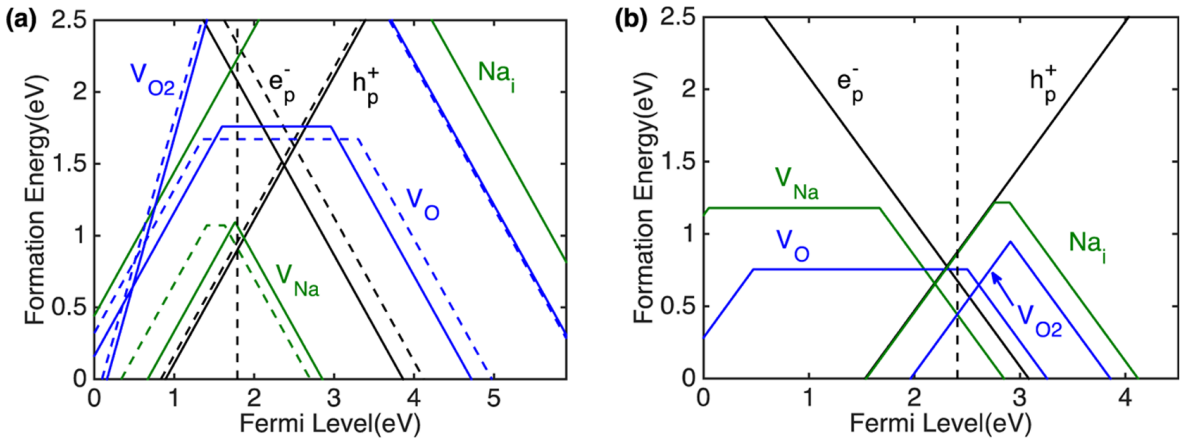


**Figure 1: Defect formation energy of the O vacancy (red lines), Na vacancy (green lines), and electron polarons and hole polarons (black lines) obtained using the HSEα (α = 0.48) hybrid functional in Na2O2 (a) and NaO2 (b). In Na2O2 (a), there are two symmetry inequivalent oxygen and sodium sites. The solid line represents the oxygen or sodium defects in the oxygen-rich layer, while the dashed line represents the oxygen or sodium defects in the oxygen-poor layer.**

In the present study [5], density functional and quasi-particle GW methods were used to comparatively assess the conductivities of $Na–O_2$ discharge phases by calculating the concentrations and mobilities of intrinsic charge carriers in $Na_2O_2$ and $NaO_2$. Both compounds are predicted to be electrical insulators, with bandgaps in excess of 5 eV. In the case of sodium peroxide, the transport properties are similar to those reported previously for lithium peroxide [4], suggesting low bulk conductivity. Transport in the superoxide has some features in common with the peroxide but also differs in important ways. Similar to $Na_2O_2$, $NaO_2$ is predicted to be a poor electrical conductor, wherein transport is limited by sluggish charge hopping between $O_2$ dimers. Different from $Na_2O_2$, in $NaO_2$ this transport is mediated by a combination of electron and hole polarons. An additional distinguishing feature of the superoxide is its ionic conductivity, which is 10 orders of magnitude larger than the electronic component. The ionic component is comprised primarily of p-type contributions from (surprisingly mobile) oxygen dimer vacancies, and from n- type contributions from negative sodium vacancies. In the context of sodium–air batteries, the low electronic conductivity afforded by $NaO_2$ suggests that enhanced bulk transport within this phase is unlikely to account for the low overpotentials associated with its decomposition. Rather, the enhanced efficiency of $NaO_2$-based cells should be attributed to other factors, such as a reduced tendency for electrolyte decomposition.

## Future Plans

- Examine stability of common electrolytes on NaO2 discharge phases
- Characterize ion cross-over properties and stability of solid state electrolytes

## Expected Outcomes

- Identification of mechanisms that most strongly impact the performance (rate capability, capacity, efficiency) of metal-air batteries
- Prediction of transport rates for cations and electrons/holes in metal-air discharge phase
- Prediction of optimal promoters to improve conductivity of discharge phases

## References/Publications


1. M. D. Radin, J. F. Rodriguez, F. Tian, and D. J. Siegel, Lithium Peroxide Surfaces are Metallic, Lithium Oxide Surfaces are Not. Journal of the American Chemical Society, 134, 1093-1103 (2012).
2. (Invited Article in Special Issue: First Principles Computations) M. D. Radin, F. Tian, and D. J. Siegel, Electronic Structure of Li2O2 (0001) Surfaces. Journal of Materials Science 47, 7564 (2012). DOI: 10.1007/s10853-012-6552-6

3. T. J. Wallington, J. E. Anderson, D. J. Siegel, M. A. Tamor, S. A. Mueller. S. L. Winkler, and O.J. Nielsen, Sustainable Mobility, Future Fuels, and the Periodic Table, Journal of Chemical Education 90, 440 (2013). DOI: 10.1021/ed3004269
4. M. D. Radin and D. J. Siegel, Charge Transport in Lithium Peroxide: Relevance for Rechargeable Metal-Air Batteries, Energy & Environmental Science 6, 2370 (2013). DOI: 10.1039/C3EE41632A. Part of Themed Issue: "Post Li-ion Batteries"
5. S. Yang and D. J. Siegel, Intrinsic Conductivity in Sodium-air Battery Discharge Phases: Sodium Superoxide vs. Sodium Peroxide, Chemistry of Materials, 27, 3852 (2015). DOI:10.1021/acs.chemmater.5b00285

# Fundamental Understanding of Li-Air Reaction Mechanisms

***Joint Project***


## U.S. Research Team Lead

- Yang Shao-Horn, Massachusetts Institute of Technology
- Gerbrand Ceder, Massachusetts Institute of Technology

## U.S. Partners

- Massachusetts Institute of Technology


## Research Objectives

The objective of this project is to fundamentally understand reaction mechanisms in metal-oxygen batteries. This year, researchers focused on understanding reaction mechanisms in Li–$O_2$ and Na-$O_2$ cells, and possible effects on parasitic reactions that can be detrimental to battery performance. Using the first-principles computation, we gained new insights into the thermodynamics and kinetics of the formation of Na-$O_2$ discharge products, which critically influence on the battery performance metrics, such as theoretical energy densities, overpotentials, as well as rate capability. We also investigated species responsible for decomposition of discharge products in Li-$O_2$ batteries with dimethylsulfoxide (DMSO)-based electrolytes and experimentally characterized decomposition products.

## Technical Approach

- Develop a computational method to correct the DFT errors in prediction of oxygen oxidation states by fitting calculated formation energies of various metal-oxides, -peroxides, and -superoxides to their experimental values.
- By applying the correction energies, predict the relative stability of sodium-oxygen compounds including $Na_2O$, $Na_2O_2$, and $NaO_2$, which are potential discharge products in sodium-oxygen batteries, as a function of temperature and oxygen partial pressure
- In addition, compute the free energies of most probable surfaces and combine with the bulk energies to obtain the particle-size dependent phase diagram
- Use x-ray diffraction (XRD), Raman and Fourier-transform infrared (FTIR) spectroscopies to understand effect of electrochemistry on discharge product chemistry and stability.

## Significant Results

Thermodynamic stability of sodium-oxygen compounds as a function of temperature, oxygen partial pressure, and particle size: The team used the first-principles computation to compute the formation free energies of sodium-oxygen compounds as a function of temperature, oxygen partial pressure, and particle size in order to investigate the formation conditions of each discharge product, i.e. $Na_2O_2$ and $NaO_2$, in sodium-oxygen batteries. The results were published in the Nano Letters.

This work has resulted in three major findings:

- In bulk, within the range of temperature and oxygen partial pressure for the operation of sodium-oxygen batteries, $Na_2O_2$ is a thermodynamically stable phase so that $Na_2O_2$ is the only possible discharge product in sodium-oxygen batteries.
- However, when it comes to the nano-regime, where the nucleation takes place, the low surface energies of NaO2 lead $NaO_2$ nanoparticles more stabilized than $Na_2O_2$.

- The critical parameter to control the formation of desired discharge product that impacts on the battery performance, in turn: When the oxygen partial pressure is high, $NaO_2$ is not only thermodynamically stabilized, but also kinetically favored to nucleate. Therefore, it is critical to ensure high enough oxygen supply to promote the nucleation and growth of $NaO_2$ as a discharge product.

The formation free energies of bulk sodium-oxygen compounds were computed by combining the DFT ground state energies, phonon vibrational energies for temperature-dependent energies of solids, and experimental temperature-dependent energies of oxygen gas. The bulk phase diagram was constructed using the calculated formation free energies (Figure 1). At 300 K and 1 atm, the standard state, $Na_2O_2$ is stable and $NaO_2$ cannot be formed under the operating conditions of sodium-oxygen batteries, e.g. T = 300 K and PO2 ⩽ 1 atm.

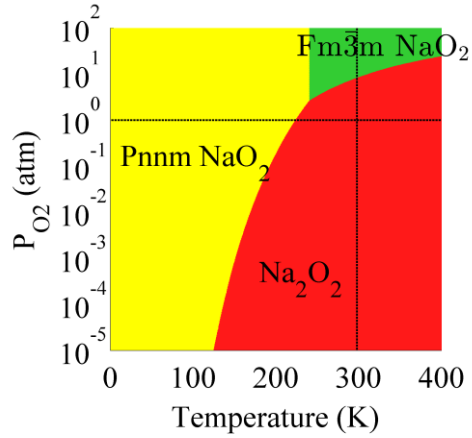


Figure 1: The predicted phase diagram of bulk sodium-oxygen compounds as a function of temperature and oxygen partial pressure.

Researchers proceeded to calculate the surface energies of $Na_2O_2$ and $NaO_2$ as a function of oxygen chemical potential, indicating that the temperature, oxygen particle pressure-dependent environmental factors were taken into account. (Figure 2) While the lowest surface energies of $Na_2O_2$ are in range of 30–45 meV/Å2, the lowest surface energy of $NaO_2$ is as low as 12 meV/Å2 within the stability window, respectively.

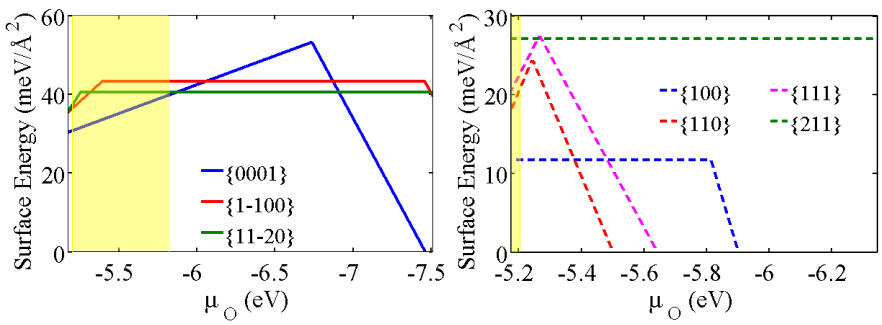


Figure 2: Calculated surface energies of (left) Na2O2 and (right) NaO2 as a function of oxygen chemical potential. The stability window for Na2O2 and NaO2 is marked by yellow boxes in (left) and (right), respectively

The calculated bulk formation energies and surface energies of sodium oxides were combined to construct a phase diagram as a function of particle size in Figure 3. Due to the lower surface energies of $NaO_2$, $NaO_2$ nanoparticles become more stable than $Na_2O_2$ at small particle size, for example, up to 6 nm at PO2 = 1 atm. Given that the structures of $NaO_2$ and $Na_2O_2$ are distinct and the energy difference between $NaO_2$ and $Na_2O_2$ is as small as 30 meV/Na at the bulk limit, the nucleated $NaO_2$ nanoparticles may grow further to micron-size.

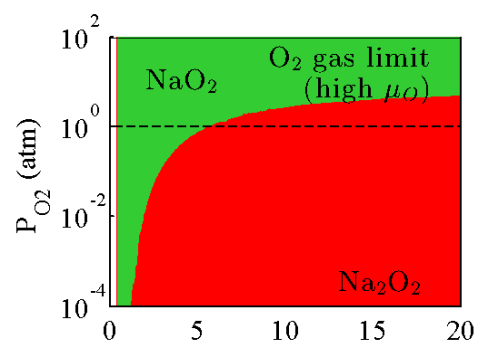


Figure 3: The predicted phase diagram of sodium-oxygen nanoparticles as a function of oxygen partial pressure and particle size.

Chemical stability of Li-$O_2$ discharge products as a function of time: We examined the chemical stability of DMSO as an electrolyte solvent for Li-$O_2$ batteries in the presence of the $Li_2O_2$ discharge product. The time-dependent stability of chemical mixtures of commercially available $Li_2O_2$ in DMSO was also examined using a variety of spectroscopic and structural techniques. The results were published in the Journal of Physical Chemistry Letters.

This work has resulted in two major findings:

- We found that the expected $Li_2O_2$ discharge product is present immediately after discharge in a DMSO-based electrolyte, but decomposes upon prolonged contact with the electrolyte into LiOH (Figure 4), and that this process is accompanied by DMSO decomposition.
- Using XRD, mass spectrometry and Raman and FTIR spectroscopies, the chemical reactivity of commercial $KO_2$ and $Li_2O_2$ powders with DMSO was investigated, and showed that the instability of $Li_2O_2$ in contact with DMSO is

greatly enhanced by the presence of superoxide anions in $KO_2$, highlighting the unique role of superoxide species in acceleration parasitic reactions in Li-$O_2$ cells.

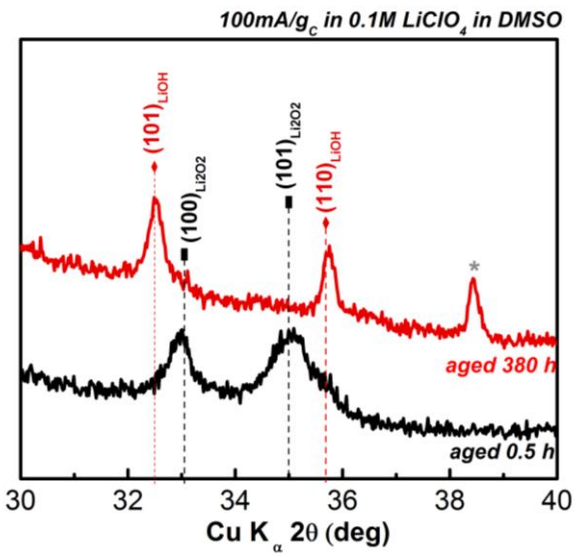


Figure 4: XRD patterns showing evolution of LiOH (red dashed lines) from $Li_2O_2$ in a carbon nanotube (CNT) electrode discharged in 0.1 M LiClO4 in DMSO after 0.5 and 380 h of aging in electrolyte following the completion of discharge. The gray asterisk denotes a peak from the Al substrate.

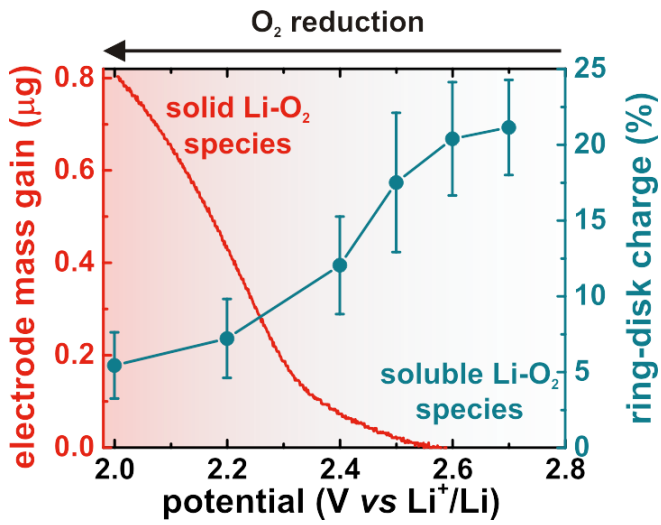


Figure 5: RRDE and EQCM measurements of the potential dependence of formation of solid and soluble reaction products and intermediates during oxygen reduction. They show a high fraction of soluble species at low overpotentials, indicative of large amounts of soluble Li+-$O_2$- while at high overpotentials, lower amounts of soluble intermediates and large mass gains are consistent with surface mediated 2e- transfer to $O_2$, as the dominant reaction mechanism for $Li_2O_2$ formation.

**Solvation effects on Li-$O_2$ reaction intermediates**

We investigated the influence of solvent on $O_2$/$O_2$- and $O_2$/Li+-$O_2$- redox potentials using the rotating and rotating ring disk electrode (RDE and RRDE) methods, respectively. Experimental results were verified with first principles computations of redox potentials based on mixed cluster-continuum solvation of $O_2$-, Li+ and Li+-$O_2$- solvation. The results were published in Angewandte Chemie. The main findings were:

- Redox potentials of $O_2$/$O_2$- vs Li+/Li are strongly influenced by $O_2$- and Li+ ion solvation – higher combined solvation energies result in higher overall $O_2$/$O_2$- vs Li+/Li potentials.
- Higher combined solvation energies result in low Li+-$O_2$- coupling and high solubility.

**Potential-dependent reaction mechanisms in Li-O2 batteries.**

We probed the origin of potential-dependent $Li_2O_2$ morphologies by examining reaction mechanisms operative at different overpotentials using RRDE and Electrochemical Quartz Crystal Microbalance (EQCM) methods (Figure 5). The results were published in the Journal of Physical Chemistry Letters. They showed that as the overpotential for oxygen reduction increased, surface-mediated 2e- $O_2$ reduction was favored over solution-mediated Li+-$O_2$- disproportionation. The latter was shown to be the dominant reaction mechanism at low overpotentials from high amounts of soluble species, and low mass-to-charge values from EQCM. The existence of toroidal and thin, particulate morphologies of $Li_2O_2$ thus corresponds to different reaction mechanisms for $Li_2O_2$ at different overpotentials.

## Future Plans

- *In situ* Raman and electrochemical quartz crystal microbalance (EQCM) experiments to directly investigate electrolyte solvent effects on $Li_2O_2$ growth mechanisms.
- X-ray absorption and emission measurements on $Li_2O_2$ in carbon-based and carbon-free lithium-oxygen battery cathodes.
- Electrolyte doping with transition metals (TMs) to examine effect of ppm-level incorporation of TMs in $Li_2O_2$ on battery rechargability (collaboration with Don Siegel at University of Michigan).

## Expected Outcomes

- Determination of factors affecting the contribution of $LiO_2$ to the microstructure of electrochemically grown $Li_2O_2$.
- Optimized cathode materials for lithium-oxygen batteries with high activity toward oxygen reduction and evolution but minimal side reactivity with electrode/electrolyte components.
- Design principles for the development of nanostructured lithium-oxygen battery cathodes with high geometric power capabilities as well as high gravimetric and volumetric energy densities.

# Fundamental Autoignition Chemistry of Advanced Biofuels

***Cooperative Project (U.S.)***


## U.S. Research Team Lead

- Craig A. Taatjes, Sandia National Laboratories
- Blake A. Simmons, Joint BioEnergy Institute, Sandia National Laboratories
- Angela Violi, University of Michigan
- Brandon Rotavera, Sandia National Laboratories
- Mohamad Akbar Ali, University of Michigan

## U.S. Partners

- Sandia National Laboratories
- Joint BioEnergy Institute
- University of Michigan


## Research Objective

Broad and detailed characterization of the chemistry and physics related to autoignition is of particular importance to national goals of renewable fuel use, such as those described in the Renewable Fuel Standard. The *Fundamental Autoignition Chemistry of Advanced Biofuels* focus area of the U.S.–China Clean Energy Research Center (CERC) effort considers a component-centered approach toward elucidating combustion fundamentals vital to the understanding of autoignition for application to fuel-flexible engines. Fuel ignition at lower temperatures is governed strongly by a sequence of reactions initiated by fuel radicals (R) reacting with molecular oxygen: $R + O_2 \rightleftharpoons RO_2$. The alkylperoxy radical $RO_2$ adduct can undergo isomerization to a hydroperoxyalkyl radical, QOOH, the class of molecules responsible for ignition-controlling chain branching at low temperatures (<~900 Kelvin [K]). Understanding the molecular structure dependence of $R + O_2$ chemistry is key for predicting performance of novel fuels and is a central focus of this part of the CERC effort.

In the past year, research has concentrated on a terpenoid fuel, limonene, that can be efficiently produced by engineered microbial fermentation of sugars liberated from lignocellulosic biomass. Hydrogenation of limonene to the more stable and energy-dense limon*a*ne (4-*iso*-propyl-1-methylcyclohexane) also forms o-cymene, an ortho-substituted aromatic whose low-temperature autoignition chemistry exhibits an "ortho-effect," a relatively increased propensity for low-temperature chain-branching in ortho-substituted aromatics. Due to significant interest in aromatic fuels, and the interest in characterizing the temperature dependence of the ortho-effect, the research team focused on o-cymene for fundamental oxidation studies, as a potentially important biofuel and as a means to study the fundamental chemistry of the ortho-effect (Figure 1).

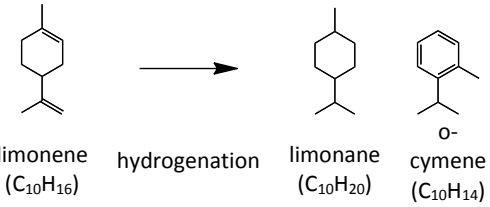


**Figure 1. Oxidation chemistry of o-cymene, studied both experimentally and computationally simultaneously leads to important fundamental characterization of a next-generation biofuel and the ortho- effect.**

## Technical Approach

- Use combined experimental and theoretical methods to determine fundamental reaction mechanisms for biofuel oxidation, especially autoignition processes that are critical for fuel-flexible, next-generation engines
  - Experimental:
    - ***Part I*** – Analyze high-resolution speciation of products from the first steps of laser-initiated oxidation of o-cymene; examine approximately 25 reaction classes for these two prototype molecules to constrain the definition of reaction mechanisms of the observed products
    - ***Part II*** – Measure of time-dependent OH and $HO_2$ radical concentrations from pulsed laser-initiated oxidation, providing critical modeling targets for combustion mechanisms
  - Theoretical: Conduct stationary point energy calculations to identify low-lying reaction pathways on R + $O_2$ potential energy surfaces

## Recent Progress

- Measurements of HO2 time histories for oxygenated cyclic biofuel (tetrahydropyran) were completed at 20 Torr and from 500 – 750 K. Complementary experiments were completed on cyclohexane, the non-oxygenated hydrocarbon analog to tetrahydropyran, in order to assess the influence of oxygenation in the initial fuel on HO2 formation.
- Photoionization mass spectrometry measurements of both tetrahydropyran and cyclohexane were completed at 10 Torr and 2 atm for three temperatures (500, 600, 700 K) to quantify the formation of HO2 co-products. In addition, the experiments revealed useful insight into the formation mechanisms of ketohydroperoxide species that are central to chain-branching and autoignition.
- Measurements of OH and HO2 for all five (5) isomers of hexene were completed at 20 Torr and from 500 – 750 K.
- Photoionization mass spectrometry measurements of all five (5) isomers of hexene were completed at 8 Torr and 550 K.

## Significant Results

The two important classes of bimolecular product channels following $O_2$-addition to alkyl radicals (R) are OH- and $HO_2$-elimination. As the $HO_2$ radical is relatively unreactive, its formation is associated with chain termination, but the OH radical is a highly effective chain carrier and is a marker for the QOOH radical chemistry that drives low-temperature chain branching and autoignition. To probe these channels for the test fuels, the project team conducted a multiplexed mass spectrometry experiment utilizing photoionization of molecular beams. These experiments can quantify the isomeric coproducts of $HO_2$ and OH in the R + $O_2$ system and hence give detailed constraints on modeling of these reactions.

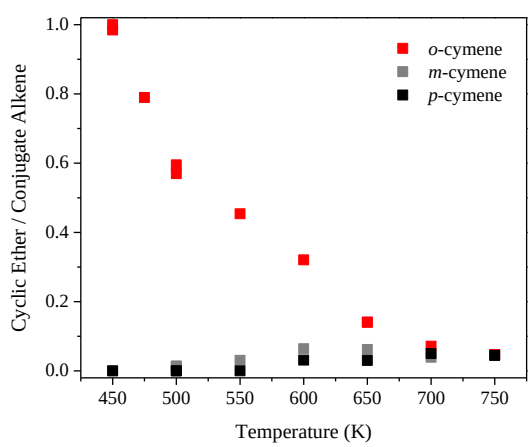


**Figure 2. Temperature-dependence of cyclic ether: conjugate alkene ratios, which reflect OH:$HO_2$ ratios, in cymene oxidation. Only o-cymene shows significant cyclic ether formation below 650 K.**

The oxidation of o-cymene was studied from 450 K to 750 K. Photolytically produced chlorine atoms abstract a hydrogen atom from the fuel molecule to form the initial radical R, which then reacts with $O_2$. Of particular interest was the influence of the ortho- configuration on the chain-propagation trend with temperature, compared to trends in m- and p-cymene. The results in Figure 2 indicate a higher yield of cyclic ether below 650 K in the oxidation of o-cymene due to facile QOOH formation and the presence of resonance-stabilized H-abstraction pathways.

Photoionization spectra (Figure 3), measured simultaneously, reflect a transition of the cyclic ether pathways initially stemming from reaction of both resonance-stabilized and non-resonance-stabilized o-cymenyl radicals at lower temperatures, to only non-resonance-stabilized radicals at higher temperatures.

## Future Plans

Ongoing analysis of experimental results and theoretical calculations are focused on the following specific areas:

- Short-term: OH/$HO_2$ concentration time histories for o-cymene
- Long-term: temperature-dependent *ab initio* rate coefficient calculations to support experimental observations of the transition from resonance- and non-resonance-stabilized ortho- radicals at lower temperatures, to only non-resonance-stabilized ortho-radicals at higher temperatures

## Expected Outcomes

- Identification of the feasibility of constraining reaction pathways
- Rate coefficient calculations
- Connection of fundamental results to CERC focus areas involving engine tests

## Seminars and Presentations

**Invited Seminar**

- "Fundamental Implications of Biofuel Structure on Low-Temperature Autoignition Chemistry in Engines", RWTH Aachen University, June 2015

**Conference Paper**

- "Analysis of OH and HO2 Time Histories Measured in Low-Temperature Oxidation of Hexene Isomers" B. Rotavera, H. Huang, I. O. Antonov, L. Sheps, J. Zádor, and C. A. Taatjes, 9th U. S. National Combustion Meeting. Organized by the Central States Section of the Combustion Institute, May 17-20, 2015, Cincinnati, Ohio

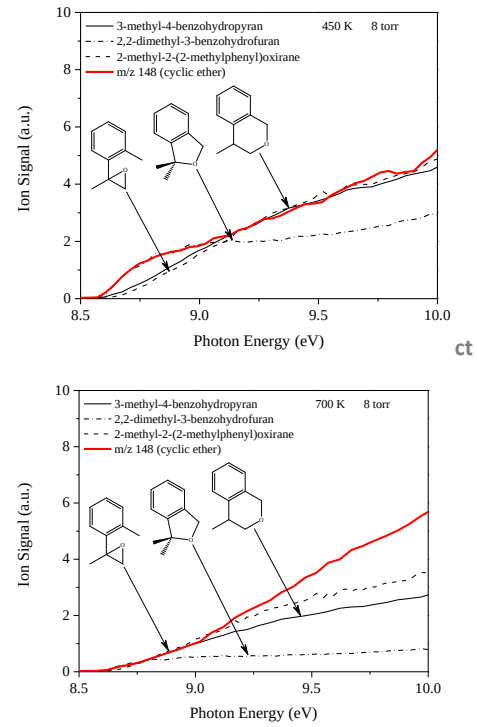


Figure 3. Photoionization spectra of products of o-cymene oxidation at 8 Torr (450 K, above, and 700 K, below) compared to reference spectra of the most-favorable cyclic ether products. The low-energy feature in the *m/z* 148 spectrum (red) disappears at 700 K due to the absence of 2,2,-dimethyl-3-benzohydrofuran, which arises only from reaction of resonance-stabilized o-cymenyl radicals

**Conference Presentations**

- "Analysis of OH and HO2 Time Histories Measured in Low-Temperature Oxidation of Hexene Isomers" B. Rotavera, H. Huang, I. O. Antonov, L. Sheps, J. Zádor, and C. A. Taatjes, 9th U. S. National Combustion Meeting
- Organized by the Central States Section of the Combustion Institute, May 17-20, 2015, Cincinnati, Ohio
- "Influence of Oxygenation in Cyclic Hydrocarbons on Chain-Termination Reactions from R + O2: Tetrahydropyran and Cyclohexane", B. Rotavera, J. D. Savee, I. O. Antonov, H. Huang, L. Sheps, J. Zádor, D. L. Osborn, and C. A. Taatjes, 9th International Conference on Chemical Kinetics, June 28-July 3, 2015, Ghent, Belgium.

# Chemical and Physical Models for Novel Fuels

***Cooperative Project***


## U.S. Research Team Lead

- Angela Violi, University of Michigan

## U.S. Partners

- University of Michigan
- Sandia National Laboratories
- Joint BioEnergy Institute

## China Research Team Lead

- Xin He, Tsinghua University

## China Partners

- Tsinghua University


## Research Objectives

The aim of this project is to develop kinetic mechanisms to predict the combustion behavior of various renewable fuels that can be used to replace current fossil fuels. Using a series of atomistic simulations, the project team is investigating the major reaction pathways of new bio-derived fuels, such as farnesane and bisabolane. A detailed analysis is carried out to relate fuel formulation with combustion by-products and efficiency of combustion.

## Technical Approach

- Investigate systems of interest: methyl butanoate (MB), n-butylcyclohexane (n-BCH), 2,5-dimethylhexane (2,5-DMH), 2,6-dimethylheptane (2,6-DMH), and farnesane
- Employ density functional theory to perform ab initio simulations of reactants, intermediates, and products present in various reaction pathways
- Utilize Rice-Ramsperger-Kassel Marcus/master equation simulation solvers such as Multiwell to compute pressure- and temperature-dependent rate constants
- Assemble the kinetic mechanisms and validate them with experimental data
- Identify discrepancies between the kinetic model and experiments and refine the model

## Significant Results

The main results of this project include developing the kinetic mechanisms, rate constants, and kinetic modeling of MB, n-BCH, 2,5-DMH, 2,6-DMH, and farnesane.

*2,5-DMH:* Figure 1 shows the new reaction pathways identified for the decomposition of 2,5-DMH.

In the high-temperature regimes, 2,5-DMH can decompose either through C-C bond fissions or through hydrogen migration reactions with bond breaking and forming, simultaneously. In low temperature oxidation, the fuel undergoes a hydrogen-elimination reaction followed by an oxidation reaction – creating a peroxy radical, ROO. The ROO radical undergoes hydrogen migration reactions creating QOOH radicals leading to alkenes and HOO species. Figure 2 provides an example of the rate calculation for ROO→QOOH reaction (TS1). We determined using the best method for calculating reaction rates was the MultiWell Suite.

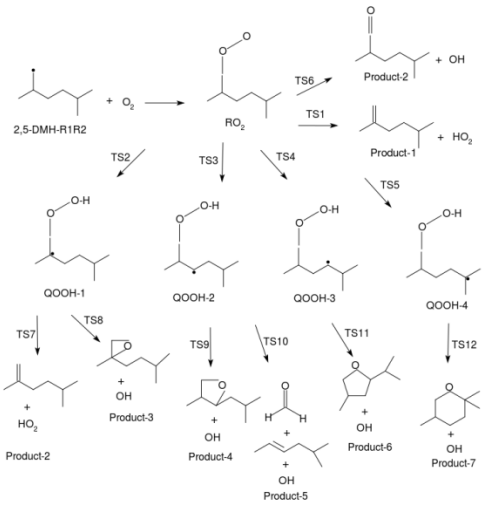


Figure 1: New pathways for the unimolecular decomposition of 2,5-dimethylhexane

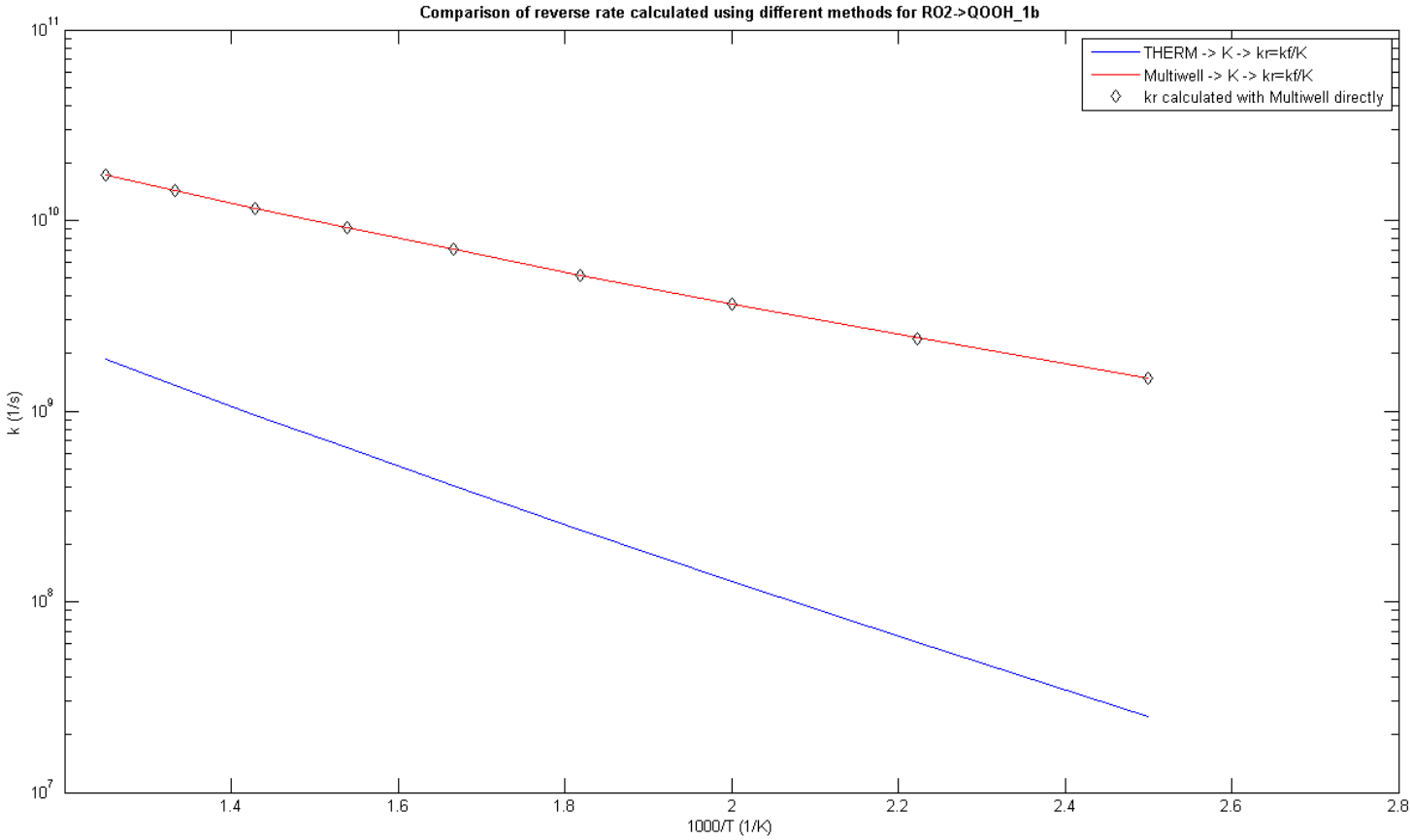


Figure 2: Reaction rate calculation comparison of methods. This led us to use Mutiwell for rate calculations.

The mechanism we developed was then used to model the oxidation of the fuel in a shock tube, specifically we were interested in the ignition delay properties of the fuel.

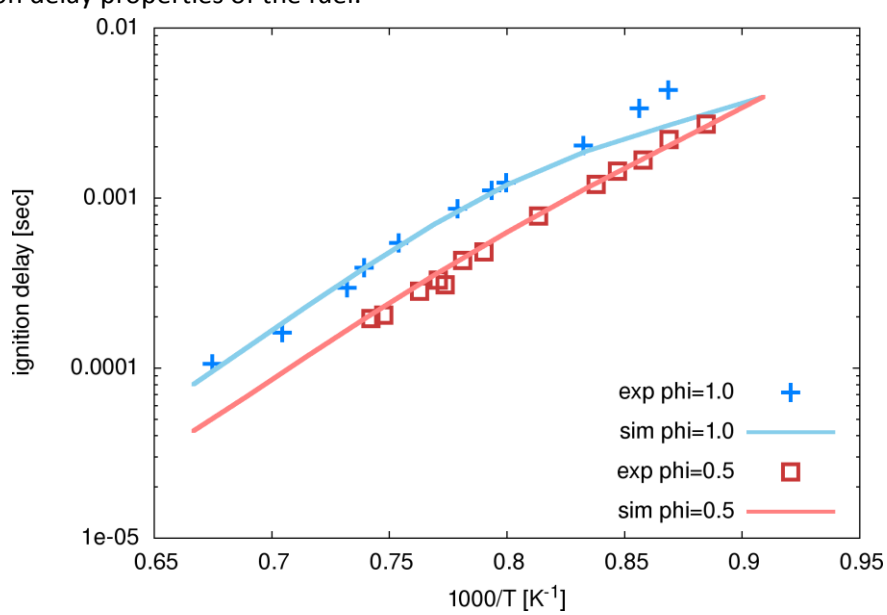


Figure 3: Comparison of the ignition delay property of 2,5-DMH with shock tube experiments.

This study also highlights, for the first time, the importance of entropic contributions during unimolecular decomposition of 2,5-DMH. The rate constants and branching ratio under different temperature ranges indicate that the main reaction pathway for thermal decomposition of 2,5-DMH is ROO→alkene+HOO (TS1), with less contribution from hydrogen migration channels.

**Low-temperature oxidation of 2,6-DMH:**

Dimethylheptyl radical (model compound of Farnesane), which leads to two major products; namely, alkene + $HO_2$ and cyclic ether + OH, as shown in Figure 4.

The focus is computation of potential energy surfaces of 2,6-dimethyheptyl radical + $O_2$ reaction. Using the results, the project team implements *ab initio* transition state theory based on the master equation calculation to determine pressure- and temperature-dependent rate constants.

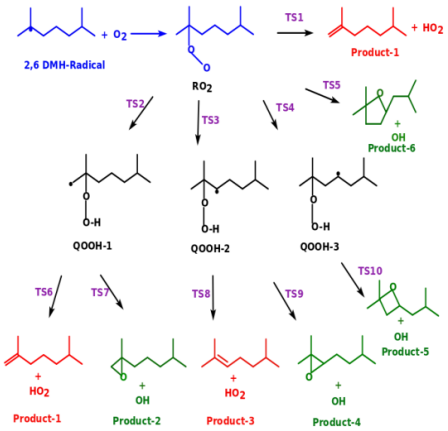


Figure 4: Reaction pathways for the oxidation of dimethylheptyl radical

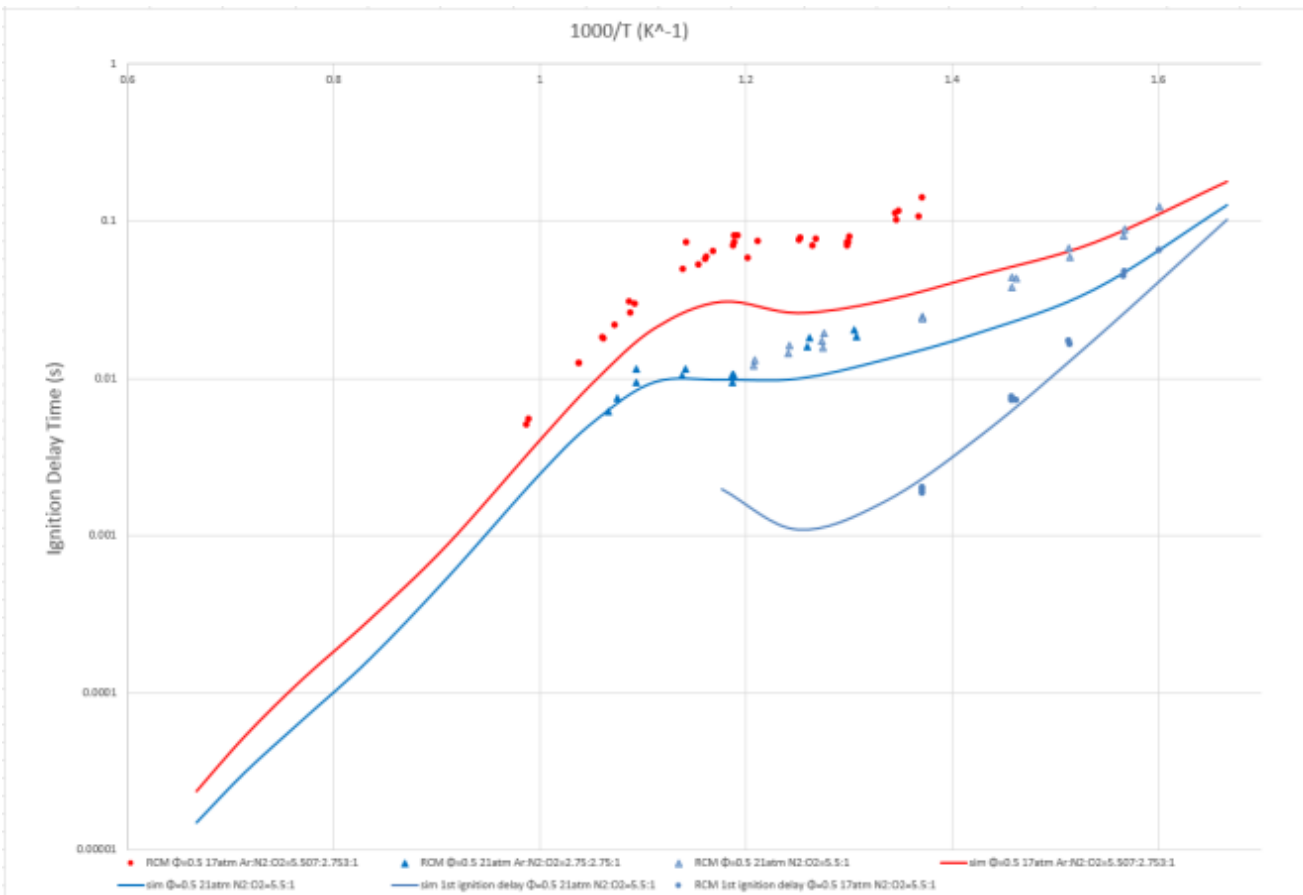


Figure 5: Comparison of the ignition delay property of 2,6-DMH with rapid compression machine experiments

The methods and validation studies of 2,6-DMH fuel were identical to those for the of 2,5-DMH study. Subsequent studies used the same techniques to produce low temperature chemistry and kinetic rates of the fuel decomposition pathways for MB, n-BCH, and farnesane.

## Expected Outcomes

- Fuel Decomposition pathways and kinetic rates for MB, n-BCH, 2,5-DMH, 2,6-DMH, and farnesane
- High fidelity kinetic reaction rate coefficients for all reactions not previously described in literature
- High fidelity gas-phase kinetic mechanisms for 2,5-DMH, 2,6-DMH, and farnesane
- Connected fundamental rate calculations to lab-scale experiments
- Produced validated chemistry and rates that are useful in combustion, fuel synthesis, and biofuel design

# Integrated Powertrain and Aftertreatment System Control for Clean Vehicles

***Joint Project***


**U.S. Research Team Lead**
- Junmin Wang, The Ohio State University

**U.S. Partners**
- The Ohio State University

**China Research Team Lead**
- Fuyuan Yang, Tsinghua University

**China Partners**
- Tsinghua University


## Research Objective

The objective of this project is to develop systematic and generalizable estimation and control methodologies for clean vehicle diesel powertrain systems. Such control systems will optimally coordinate fuel property estimation, advanced combustion modes, exhaust aftertreatment systems, and hybrid powertrains to enable maximization of the energy efficiency and emission reduction potentials for clean vehicles.

## Technical Approach

- Develop onboard fuel property estimation systems. Model-based onboard fuel property estimation and adaptive engine control algorithms, considering the sensing and actuation capabilities and limitations, will be developed
- Develop systematic, optimal, and generalizable control methodologies for clean vehicle powertrain systems. To conduct research on systematic and scalable control and management of diesel engine and aftertreatment systems

## Recent Progress

- Developed and validated stochastic optimal control methods for hybrid electric vehicles considering road grade preview and driver pedal behavior
- Devised methods for coordinated active thermal management and SCR control
- Further developed model predictive control methods for hybrid electric vehicles considering the aftertreatment systems and emissions requirements
- Devised methods for optimal and integrative control of hybrid electric vehicles with aftertreatment systems
- Researched on methods for optimal and integrative control of hybrid electric vehicles with aftertreatment systems.
- Developed control methods for hybrid electric vehicles considering the aftertreatment systems and emissions requirements.
- Developed stochastic control methods for hybrid electric vehicles considering road grade preview.

## Significant Results

- The project team has developed a method to estimate fuel properties using high-pressure common rail pressure signals for diesel engines. Figure 1 shows the simulated rail pressure signals of different fuels in the frequency domain, clearly demonstrating differences among different fuels
- Developed a control-oriented, multiphase combustion model applicable for diesel and biodiesel fuels in diesel engines. The premixed and mixing-controlled combustion is modeled by using two cascaded Wiebe functions. A set of Wiebe coefficients, which are partially physics-based, is found through a grey-box parameter identification approach
- Developed an ignition-delay correlation and CA50 prediction models applicable for diesel and biodiesel fuels. Figure 2 displays the comparison of model-predicted and measured CA50 for both B0 and B100 fuels. The model-predicted values match well with experimentally measured values

- An observer-based simultaneous air-fraction and biodiesel blend level estimation method has been derived and experimentally studied. Figure 3 and Figure 4 show the experimental results
- Mathematical models for describing the DOC and DPF temperature and oxygen dynamics have been produced for the integrated powertrain thermal management strategies. For example, Figure 5 displays the DOC-out gas temperature model validation results
- The characteristics of diesel and biodiesel post injections during active diesel particulate filter regenerations have been experimentally studied. For example, Figure 6 gives the influences of SOI timing on the engine-out THC and CO emissions

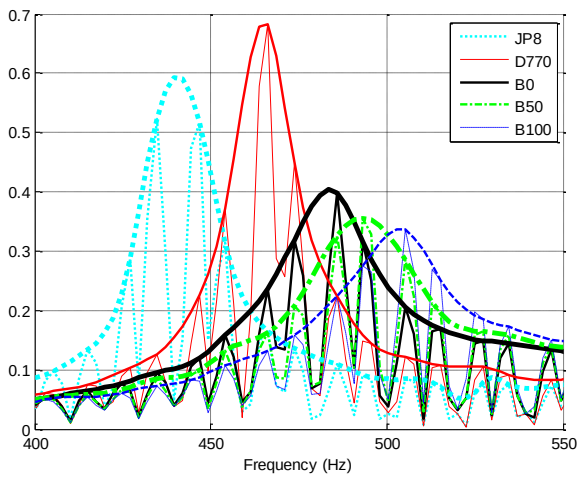


Figure 1. Simulated rail pressure signals and their envelopes for different fuels.

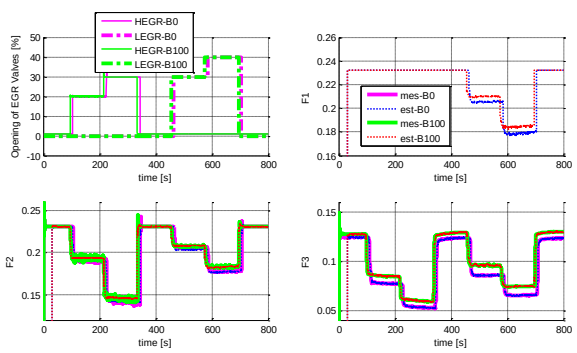


Figure 3. Experimental results of the air-fraction estimation method.

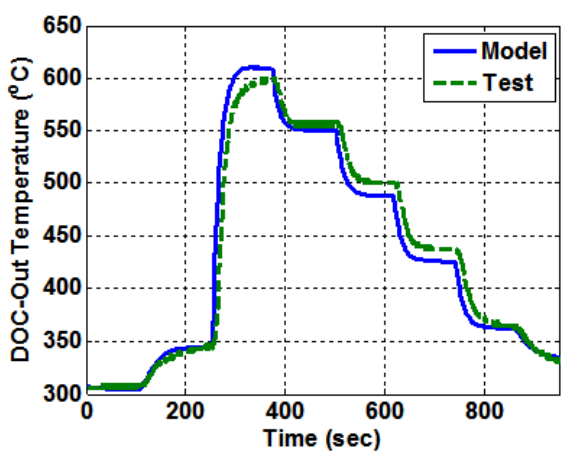


Figure 5. DOC-out gas temperature model validation.

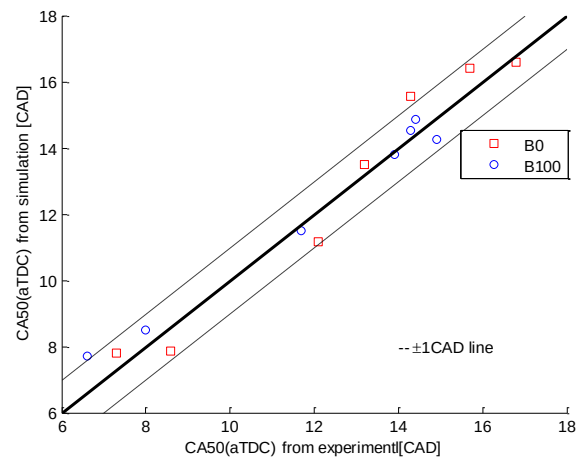


Figure 2. Comparison of model-predicted and measured CA50 for both B0 and B100 fuels (biodiesel fuel blends).

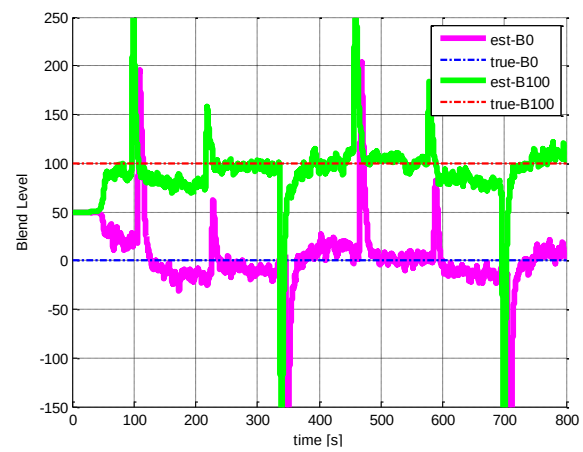


Figure 4. Experimental results of the biodiesel blend level estimation method.

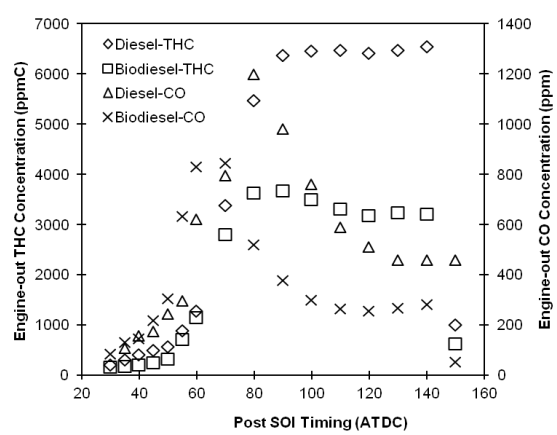


Figure 6. Influences of SOI timing on the engine-out THC and CO emissions.

## Collaboration

- Prof. Junmin Wang visited Tsinghua University again to discuss on the collaborations in August 2015
- The team discussed research collaborations with China partners at the CERC-CVC Annual Conference in August 2015, and through conference calls.

## Expected Outcomes

- Adaptive engine estimation and control methodologies for maintaining optimal engine performance with uncertainties in fuels
- A framework for integrated engine, aftertreatment, and hybrid powertrain system control method development with consideration of diesel/biodiesel blend ratio variation

## Recent Publications

The following 26 peer-reviewed papers (16 journals and 10 conferences) have been published, and several other manuscripts are under review.


1. Xiangrui Zeng and Junmin Wang, "A Parallel Hybrid Electric Vehicle Energy Management Strategy Using Stochastic Model Predictive Control with Road Grade Preview," IEEE Transactions on Control Systems Technology (in press), 2015 (DOI: 10.1109/TCST.2015.2409235).
2. Pingen Chen and Junmin Wang, "Coordinated Active Thermal Management and SCR Control for Simultaneous Fuel Economy Improvement and Emissions Reduction during Low-temperature Operations," ASME Transactions Journal of Dynamic Systems, Measurement and Control, Vol. 137, Issue. 12, 121001-1-11 (11 pages). 2015.
3. Pingen Chen and Junmin Wang, "Nonlinear Model Predictive Control of Integrated Diesel Engine and Selective Catalytic Reduction System for Simultaneous Fuel Economy Improvement and Emissions Reduction," ASME Transactions Journal of Dynamic Systems, Measurement and Control, Vol. 137, Issue 8, 081008-1-13, (13 pages), 2015.
4. Junfeng Zhao and Junmin Wang, "Integrated Model Predictive Control of Hybrid Electric Vehicles Coupled with Aftertreatment Systems," IEEE Transactions on Vehicular Technology (in press), 2015 (DOI: 10.1109/TVT.2015.2405918).
5. Junfeng Zhao, Pingen Chen, Umar Ibrahim, and Junmin Wang, "Comparative Study and Accommodation of Biodiesel in Diesel-electric Hybrid Vehicles Coupled with Aftertreatment Systems," Asian Journal of Control, Vol. 18, No. 3, pp. 1-13, May 2016 (DOI: 10.1002/asjc.1137)
6. Junfeng Zhao and Junmin Wang, "Adaptive Observer for Joint Estimation of Oxygen Fractions and Blend Level in Biodiesel Fueled Engines," IEEE Transactions on Control Systems Technology, Vol. 23, no. 1, pp. 80 - 90, 2015.
7. Pingen Chen, Umar Ibrahim, and Junmin Wang, "Experimental Investigation of Diesel and Biodiesel Post Injections during Active Diesel Particulate Filter Regenerations," Fuel, Vol. 130, pp. 286 - 295, 2014.
8. Pingen Chen and Junmin Wang, "Air-Fraction Modeling for Simultaneous Diesel Engine NOx and PM Emissions Control during Active DPF Regenerations," Applied Energy, Vol. 122, pp. 310 - 320, 2014.
9. Junfeng Zhao and Junmin Wang, "On-Board Fuel Property Identification Method Based on High-Pressure Common Rail Pressure Signal," ASME Transactions Journal of Dynamic Systems, Measurement, and Control, Vol. 136, No. 3, 031010 (9 pages), 2014.
10. Pingen Chen and Junmin Wang, "Control-Oriented Model for Integrated Diesel Engine and Aftertreatment Systems Thermal Management," Control Engineering Practice, Vol. 22, pp. 81 – 93, 2014.
11. Pingen Chen and Junmin Wang, "Nonlinear and Adaptive Control of NO/NO2 Ratio for Improving Selective Catalytic Reduction System Performance," Journal of The Franklin Institute, Vol. 350, Issue 8, pp. 1992 – 2012, 2013
12. Pingen Chen and Junmin Wang, "Observer-based Estimation of Air-Fractions for a Diesel Engine Coupled with Aftertreatment Systems," IEEE Transactions on Control Systems Technology, Vol. 21, No. 6, pp. 2239 - 2250, 2013
13. Junfeng Zhao and Junmin Wang, "Control-Oriented Multi-Phase Combustion Model for Biodiesel Fueled Engines," Applied Energy, Vol. 108, pp. 92 - 99, 2013.
14. Junfeng Zhao and Junmin Wang, "Effect of Exhaust Gas Recirculation on Biodiesel Blend Level Estimation in Diesel Engines," ASME Transactions Journal of Dynamic Systems, Measurements, and Control, Vol. 135, Issue 1, 011011, 2013.

15. Pingen Chen and Junmin Wang, "Oxygen Concentration Dynamic Model and Observer-Based Estimation through a Diesel Engine Aftertreatment System," ASME Transactions Journal of Dynamic Systems, Measurement, and Control, Vol. 134, Issue 3, 031008 (10 pages), 2012.
16. Pingen Chen and Junmin Wang, "Control-Oriented Modeling and Observer-based Estimation of Solid and Gas Temperatures for a Diesel Engine Aftertreatment System," ASME Transactions Journal of Dynamic Systems, Measurement and Control, Vol. 134, Issue 6, 061011 (12 pages), 2012.
17. Xiangrui Zeng and Junmin Wang, "Stochastic Optimal Control for Hybrid Electric Vehicles Running on Fixed Routes," Proceedings of the 2015 American Control Conference (Invited Paper), pp. 3273 – 3278, 2015.
18. Xiangrui Zeng and Junmin Wang, "A Stochastic Model Predictive Control Approach for Hybrid Electric Vehicle Energy Management with Road Grade Preview" Proceedings of the 2014 ASME Dynamic Systems and Control Conference (Invited Paper), 2014.
19. Junfeng Zhao and Junmin Wang, "Model Predictive Control of Integrated Hybrid Electric Powertrains Coupled with Aftertreatment Systems" Proceedings of the 2014 ASME Dynamic Systems and Control Conference, 2014.
20. Junfeng Zhao and Junmin Wang, "Engine Mass Airflow Sensor Fault Detection via an Adaptive Oxygen Fraction Observer," Proceedings of the 2014 American Control Conference (Invited Paper), pp. 1517 – 1522, 2014.
21. Junfeng Zhao and Junmin Wang, "Observer Based Oxygen Fraction Estimation for a Dual-Loop EGR Diesel Engine Fueled with Biodiesel Blends," Proceedings of the 2013 ASME Dynamic Systems and Control Conference (Invited Paper), pp. 365 - 371, 2013.
22. Pingen Chen and Junmin Wang, "Integrated Diesel Engine and Selective Catalytic Reduction System Active NOx Control for Fuel Economy Improvement," Proceedings of the 2013 American Control Conference, pp. 2199 - 2204, 2013
23. Junfeng Zhao and Junmin Wang, "On-Board Fuel Property Identification Method Based on Common Rail Pressure Signal," Proceedings of the 2012 ASME Dynamic Systems and Control Conference (Invited Paper), pp. 2238 – 2245, 2012.
24. Junfeng Zhao and Junmin Wang, "Energy-based and Oxygen-based Biodiesel Blend Level Estimation Methods for Diesel Engines," Proceedings of the 2012 American Control Conference (Invited Paper), pp.4975 – 4980, 2012.
25. Pingen Chen and Junmin Wang, "Control-Oriented Modeling of Thermal Behavior for a Diesel Oxidation Catalyst," Proceedings of the 2012 American Control Conference, pp. 4987 – 4992, 2012.
26. Pingen Chen and Junmin Wang, "Oxygen Concentration Dynamic Model through a Diesel Engine Aftertreatment System," Proceedings of the ASME Dynamic Systems and Control Conference (Invited Paper), pp. 867 – 874, 2011.

## Invention Disclosure

The following invention disclosure was filed through OSU

- Junfeng Zhao and Junmin Wang, "Engine onboard fuel property identification method using common rail pressure signal," Oct. 2012.

# Energy Conversion

*Joint Project*

## U.S. Research Team Lead

- Ctirad Uher, University of Michigan
- Rachel Goldman, University of Michigan
- Kevin Pipe, University of Michigan
- Joseph Heremans, The Ohio State University
- Hsin Wang, Oak Ridge National Laboratory
- Douglas Medlin, Sandia National Laboratories

## U.S. Partners

- University of Michigan
- The Ohio State University
- Oak Ridge National Laboratory
- Sandia National Laboratories

## China Research Team Lead

- Xinfeng Tang, Wuhan University of Technology
- Han Li, Wuhan University of Technology

## China Partners

- • Wuhan University of Technology

## Research Objectives

The objective of this project is to develop novel, highly efficient, and inexpensive nanocomposite thermoelectric materials with dimensionless figure of merit (ZT) ~ 1.5 to convert waste heat of cars and trucks into electricity. The project will also determine a Seebeck coefficient using scanning thermoelectric microscopy (SThEM) in conjunction with scanning tunneling microscopy to measure sample homogeneity on a nanometer scale.

## Technical Approach

- Seek a high Seebeck coefficient and high electrical conductivity while simultaneously aiming for as low a thermal conductivity as possible. To achieve this, we explore the formation of band-resonant states in nanocomposite materials such as CoSb3-based skutterudites and various forms of doping Mg2Si1-xSnx solid solutions.

## Significant Results

The main results of this project so far include the development of antimony (Sb)-doped n-type Mg2Si1-xSnx solid solutions with ZT = 1.35, the development of operational scanning Seebeck coefficient microscopy, and most recently, the development of a combustion synthesis known as the self-propagating-high-temperature-synthesis (SHS) for exceptionally rapid and economical fabrication of compound thermoelectric materials.

In addition, the research team has published several joint publications supported by the U.S.-China Clean Energy Research Center Clean Vehicles Consortium program

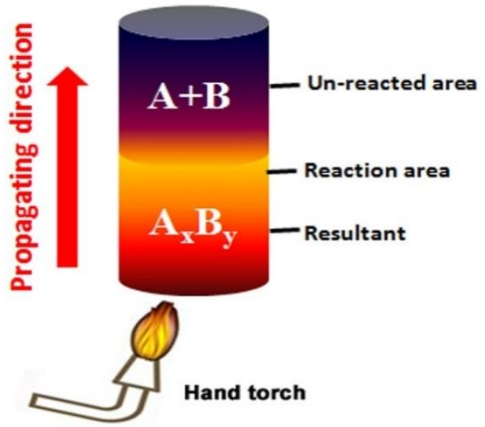


Figure 1: Schematic s of the combustion (SHS) synthesis.

## Future Plans

The initial attempt to form bond resonant states with tin (Sn) doping in CoSb3 will be followed with other prospective dopants to further improve the Seebeck coefficient of CoSb3-based skutterudites.

The research team will attempt to improve the performance of n-type Mg2Si1-xSnx solid solutions by doping with bismuth, which is a heavier element. A greater mass difference in comparison to antimony-doped structures should result in lower lattice thermal conductivity and thus higher ZT.

The research team will also focus on improving the performance of p-type Mg2Si1-xSnx solid solutions that, so far, lag far behind the n-type forms of the material.

Modifications will be made to a sample holder of the SThEM apparatus to allow measurements of thin-film samples.

## Expected Outcomes

- Development of high-performance p-type skutterudites for waste heat recovery
- Development of efficient and inexpensive n-type Mg2Si1-xSnx solid solutions
- Improvement of p-type forms of Mg2Si1-xSnx
- Development of low-resistance contacts to both forms of Mg2Si1-xSnx solid solutions
- Implementation of scanning Seebeck coefficient microscopy for nanometer-scale characterization of dopant distribution in thermoelectric materials
- Fine-tuning the SHS synthesis process for fabrication of skutterudites

## References/Publications


1. W. Liu, X. Tan, K. Yin, H. Liu, X. F. Tang, J. Shi, Q. Zhang, and C. Uher. "Convergence of Conduction Bands as a Means of Enhancing Thermoelectric Performance of N-type Mg2Si1-xSnx Solid Solutions." Physical Review Letters 108, 166601 (2012)
2. W. Liu, X. F. Tang, H. Li, K. Yin, J. Sharp, X. Zhou, and C. Uher. "Enhanced Thermoelectric Properties of N-type Mg2.16(Si0.4Sn0.6)1-ySby due to Nano-sized Sn-rich Precipitates and an Optimized Electron Concentration." Journal of Materials Chemistry 22, 13653 (2012)
3. X. J. Tan, W. Liu, H. J. Liu, J. Shi, X. F. Tang, and C. Uher. "Multiscale Calculations of Thermoelectric Properties of N-type Mg2Si1-xSnx Solid Solutions." Physical Review B 85, 205212 (2012)
4. W. Liu, K. Yin, X. Su, H. Li, Y. Gao, X. F. Tang, and C. Uher. "Enhanced Hole Concentration Through Ga Doping and Excess of Mg and Thermoelectric Properties of P-type Mg2(1+z)(Si0.3Sn0.7)1-yGay." Intermetallics 32, 352 (2013)
5. J. C. Walrath, Y. H. Lin, K. P. Pipe, and R. S. Goldman. "Quantifying the Local Seebeck Coefficient Using Scanning Thermoelectric Microscopy." Applied Physics Letters 103, 212101 (2013)
6. W. Liu, H. Chi, H. Sun, Q. Zhang, K. Yin, X. F. Tang, Q. Zhang, and C. Uher. "Advanced Thermoelectrics Governed by Single Parabolic Band: Mg2Si0.3Sn0.7, a Canonical Example." Physical Chemistry and Chemical Physics 16, 6893 (2014)
7. J. Zhang, H. J. Liu, L. Cheng, J. Wei, J. Shi, X. F. Tang, and C. Uher. "Enhanced Thermoelectric Performance of a Quintuple Layer of Bi2Te3." Journal of Applied Physics 116, 023706 (2014)
8. T. Liang, X. Su, Y. Yan, G. Zheng, Q. Zhang, H. Chi, X. F. Tang, and C. Uher. "Ultra-fast Synthesis and Thermoelectric Properties of Te-Doped Skutterudites." Journal of Materials Chemistry A 2, 17914 (2014)
9. X. Su, F. Fu, Y. Yan, G. Zheng, T. Liang, Q. Zhang, X. Cheng, D. Yang, H. Chi, X. F. Tang, Q. Zhang, and C. Uher. "Self-Propagating High-Temperature Synthesis for Compound Thermoelectrics and New Criterion for Combustion Processing." Nature Communications: DOI: 10.1038/ncomms5908, Sept. 2014.
10. Y. Li, V. A. Stoica, K. Sun, W. Liu, L. Endicott, J. C. Walrath, A. S. Chang, Y.-H. Lin, K. P. Pipe, R. S. Goldman, C. Uher, and R. Clarke, "Ordered Horizontal Sb2Te3 Nanowires Induced by Femtosecod Lasers", Applied Physics Letters 105, 201904 (2014).
11. Q. Zhang, Y. Zheng, X. Su, K. Yin, X. F. Tang, and C. Uher, "Enhanced Power Factor of Mg2Si0.3Sn0.7 Synthesized by a Non-equilibrium Rapid Solidification Method", Scripta Materialia 96, 1 (2015).
12. G. Zheng, X. Su, T. Liang, Q. Lu, Y. Yan, X. F. Tang, and C. Uher, "High Thermoelectric Performance of Mechanically Robust N-type Bi2Te3-xSex Prepared by Combustion Synthesis", Journal of Materials Chemistry A 3, 6603 (2015).

13. J. C. Walrath, Y.-H. Lin, S. Huang, and R. S. Goldman, “Profiling the Local Carrier Concentration Across Semicondutor Quantum Dot”, Applied Physics Letters 106, 192101 (2015).
14. K. Yin, Q. Zhang, Y. Zheng, X. Su, X. F. Tang, and C. Uher, “Thermal Stability of Mg2Si0.3Sn0.7 Under Different Heat Treatment Conditions”, Journal of Materials Chemistry C 3, 10381 (2015).
15. T. Liang, X. Su, X. Tan, G. Zheng, X. She, Y. Yan, X. F. Tang, and C. Uher, “Ultra-Fast Non-Equilibrium Synthesis and Phase Segregation in InxSn1-xTe Thermoelectrics by SHS-PAS Processing”, Journal of Materials Chemistry C 3, 8550 (2015).
16. K. Yin, X. Su, Y. Yan, C. Uher, and X. F. Tang, “In-situ Nanostructure Design Leading to a High Figure of Merit in an Eco-Friendly Stable Mg2Si0.3Sn0.7 Solid Solutions”, RSC Advances 6, 16824 (2016).
17. Q. Zhang, X. Su, Y. Yan, H. Xie, T. Liang, Y. You, X. F. Tang, and C. Uher, “Phase Segregation and Superior Thermoelectric Properties of Mg2Si1-xSnx (0 x 0.025)”, ACS Applied Materials & Interfaces 8, 3268 (2016).

# Electrical Variable Traction-Transmission (EVTT) System Based on DMP Machine

***Joint Project***


## U.S. Research Team Lead

- Longya Xu, The Ohio State University
- Haiwei Cai, The Ohio State University

## U.S. Partners

- The Ohio State University

## China Research Team Lead

- Wen Xuhui, Chinese Academy of Sciences
- Tao Fan, Chinese Academy of Sciences

## China Partners

- Chinese Academy of Sciences


## Research Objectives

This project seeks to develop a novel traction-transmission system that is capable of efficiently converting mechanical power from internal combustion engine to wheels. The proposed system reduces the overall system size by replacing the two electric machines and the planetary gear in an existing full HEV system by a compact electric machine without sacrificing the functions and benefits.

## Technical Approach

- Develop the equivalent circuit for Dual-Mechanical-Port (DMP) machine by both finite element analysis and circuit analysis methods,
- Develop control algorithm for both rotors of the DMP machine and verify it by simulation,
- Analyze the power flow and the multi-operational modes of DMP machine.
- Analyze a dual-clutch system for DMP machine to realize the system level simulation.

## Significant Results

The team has shown the capability the Electrical Variable Traction-Transmission (EVTT) system based on DMP machine for hybrid electric vehicle application.

A complete DMP machine model analysis has been studied. Based on the flux line distribution of the DMP machine, the analytical machine model and the equivalent circuit has been presented. A simplified machine model has been proposed for greater control.

The Field Oriented Control (FOC) algorithms for both rotors of the DMP machine have been analyzed, both with and without position sensors. Independent control of both rotors could be achieved via the FOC algorithms. Position sensorless control for the outer rotor has been achieved by high frequency injection and introduction of a sliding mode at low and high speeds, respectively. The effectiveness of the algorithms has been verified by simulations.

Based on the FOC algorithm, power flow and operational modes of the PMDMP machine were also analyzed. A dual clutch system is proposed as one practical approach to enable the flexibility of the EVTT in HEV application. A rule based control has been designed to meet some of the control objectives. The simulation results show that the EVTT with a rule based controller offers high fuel efficiency as compared to its conventional counterpart.

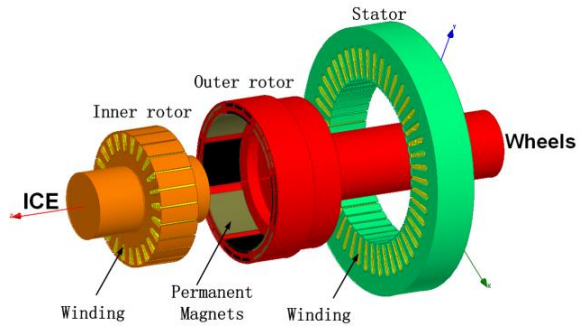


Figure 1: Structure of DMP Machine.

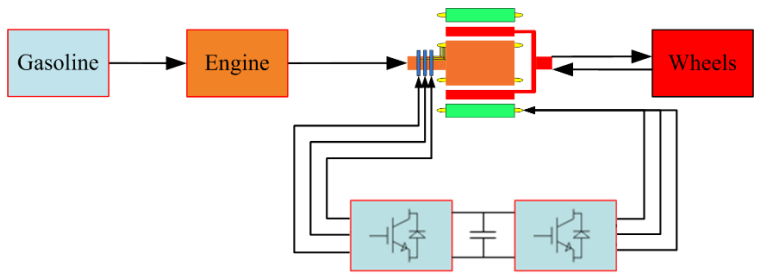


Figure 2: Structure of EVTT.

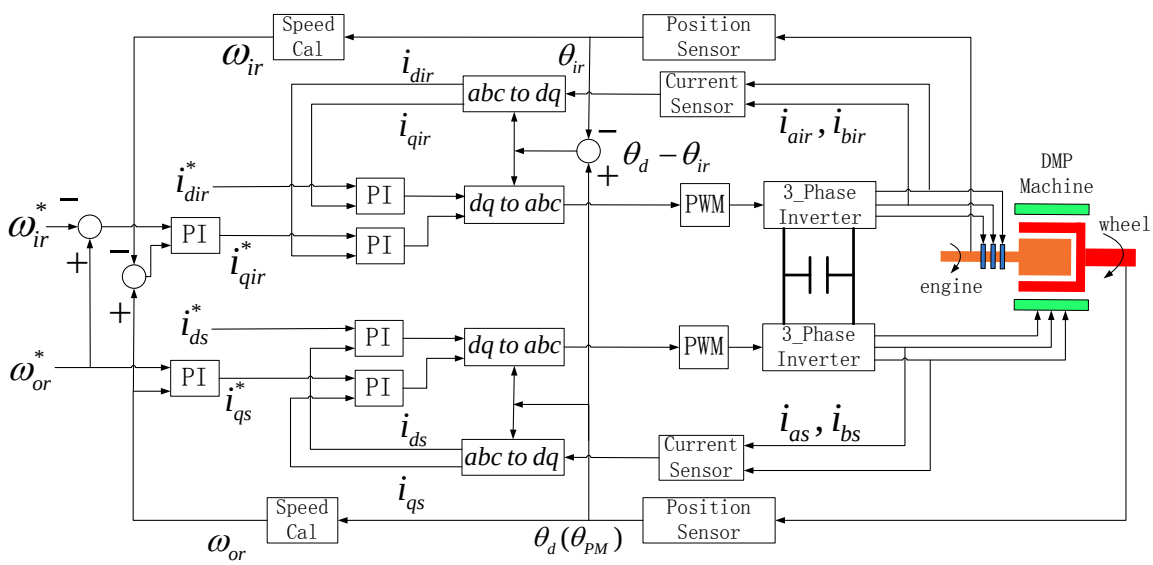


Figure 3: Field Oriented Control Block Diagram for DMP machine.

| | Driving cycle | Conventional vehicle | EVTT based on DMP machine | Improvement |
|---|---|---|---|---|
| Fuel Economy (MPG) | FUDS | 29.69 | 48.1 | 62.0% |
| | FHDS | 38.23 | 45.29 | 18.4% |
| | NEDC | 30.93 | 50.86 | 64.4% |

Figure 4: Simulation Result of Driving Cycles.

## Future Plans

The mechanical strength of the outer rotor and the heat dissipation of the inner rotor should be further studied. Because the outer rotor is sandwiched between airgaps and rotates at high speed, the mechanical strength of the outer rotor should be designed to meet the deformation requirement. Due to the fact that the inner rotor is placed inside the outer rotor, the heat generated by the inner rotor current must travel through two layers of airgaps to reach the stator core. The thermal resistance of this path is very high. Thermal analysis of the DMP machine should be done to provide an optimal solution. The finite element method should be used to complete the first stage of analysis.

## Expected Outcomes

- Optimal mechanical design for the outer rotor that will meet both electrical and mechanical requirements.
- Optimal thermal design for the inner rotor that will reduce the thermal stress on the inner rotor

## References/Publications


1. Q. Ahmed, H. Cai, G. Rizzoni and L. Xu, "Modeling and Control of a Novel Power Split Hybrid Electric Vehicle." ASME 2014 Dynamic Systems and Control Conference. American Society of Mechanical Engineers, 2014.

# Efficient and High Power Density Electric Powertrain

***Joint Project***


## U.S. Research Team Lead

- Heath Hofmann, University of Michigan
- Longya Xu, The Ohio State University

## U.S. Partners

- University of Michigan
- The Ohio State University
- Oak Ridge National Laboratory

## China Research Team Lead

- Wen Xuhui, Chinese Academy of Sciences
- Tao Fan, Chinese Academy of Sciences
- Ziyou Song, Tsinghua University

## China Partners

- Chinese Academy of Sciences
- Tsinghua University
- Jing-Jin Electric
- Hunan CSR Electric Vehicle Company


## Research Objective

This project seeks to develop innovative and optimized electric machines for electrified powertrains with significantly higher power density and efficiency. This will be achieved through the investigation of novel electric machine designs and the development of computationally efficient design tools.

## Technical Approach

- Develop computationally efficient steady-state analysis techniques for finite element models of electric machines to aid in high-fidelity loss calculations including skin- and proximity-effect
- Develop innovative electric machine topologies that are integrated with vehicle transmissions
- Reduce machine losses so that air cooling becomes feasible, dramatically increasing the power density of the overall system

## Recent Progress

An optimized power management strategy for battery/ultracapacitor energy storage systems was developed for the China Bus Driving Cycle using dynamic programming. This was compared to various control approaches that have been presented in the literature. It was determined that, under certain conditions, a rules-based control technique most closely fits the dynamic programming results. Different power electronic circuit topologies which interface the ultracapacitors and batteries were investigated. Finally, the sizing of the ultracapacitor and battery energy storage for an electric bus was optimized.

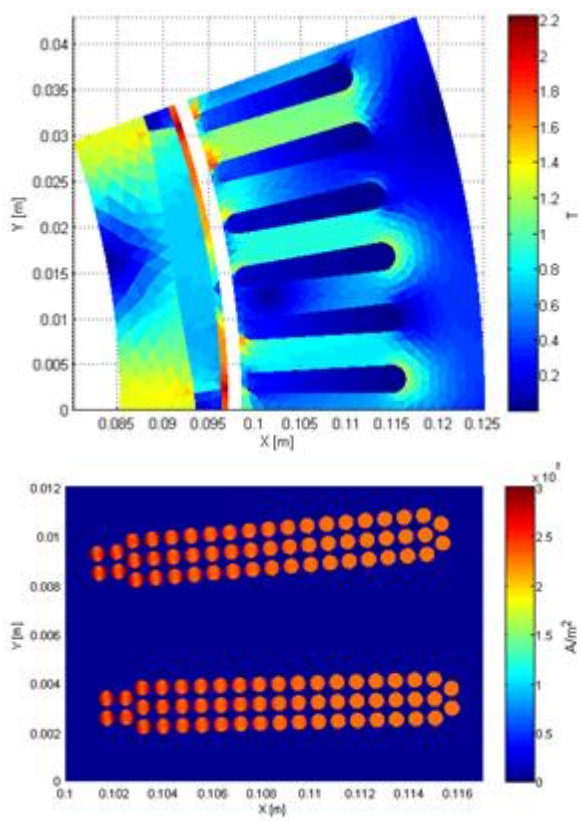


Figure 1. Top: Flux density distribution in a model of a UQM 145 surface mount permanent magnet machine. Bottom: Harmonic amplitude of the current density in two slots of the UQM 145 machine with stranded conductors demonstrating skin and proximity effect.

Recently completed implementing adaptive versions of our time-domain steady-state solvers.

A preconditioner was developed for a harmonic-balance-based steady-state FEA solver for electric machines. The preconditioner dramatically accelerates the convergence of harmonic balance, to the point where it becomes the fastest of all steady-state algorithms studied. An adaptive time-stepping procedure for harmonic balance was likewise developed.

Begun investigating how modeling of the B-H curve affects the convergence of the steady-state solution. Any model magnetization function whose Taylor series has a finite radius of convergence must implicitly limit the permissible step-size of a Runge-Kutta method. The differentiability of the solution also limits the maximum order of convergence achievable by the time-domain methods and prevents the harmonic balance method from achieving the optimal "spectral" convergence rate.

## Significant Results

Researchers at the University of Michigan have created and improved three steady-state analysis techniques for electric machines through the application of advanced numerical integration techniques and iterative algorithms that exploit the underlying structure of the electric machine simulation problem. A comparison of existing time-domain based methods was presented in a recent publication, demonstrating over an order of magnitude improvement in simulation time over conventional approaches. New insights into the structure of the frequency-domain formulation of the steady-state problem have resulted in a novel preconditioner that allows the simulation times for this problem to achieve parity with the time-domain formulations. On a fixed mesh size, the improved algorithms have demonstrated simulation times within a factor of 4 of the lower-bound represented by uniform current density static finite-element analysis.

Researchers at the Chinese Academy of Sciences have optimized the design of a permanent magnet machine with amorphous iron laminations. A prototype of this design was built and compared to a design with conventional silicon laminations. The high-frequency capability of the amorphous iron material allowed for a significant increase in efficiency (as much as five percentage points) over the conventional machine. The prototype machine is also significantly smaller than the conventional machine.

A recent achievement has been the determination that a rules-based power management strategy for battery/ultracapacitor energy storage systems can closely emulate an optimal strategy as determined by dynamic programming.

## Future Plans

Researchers at the University of Michigan are currently investigating the application of adaptive solution refinement to the steady-state simulation algorithms that they have previously developed. It is believed the simulation times of these algorithms can be further reduced by iteratively refining the solutions in an intelligent manner. In addition, adaptivity allows the solution accuracy to be controlled automatically, increasing confidence in the results and the ease of use of the simulation tool.

## Expected Outcomes

- Computationally efficient steady-state solvers for synchronous machines with time-domain adaptivity for automatically controlling solution accuracy
- High-efficiency machine designs that will eliminate the need for liquid cooling, thereby dramatically increasing power density and reliability

## Collaboration

A prototype in-wheel electric motor that was designed using our custom FEA codes has been constructed as part of a separate project sponsored by DENSO.

## Recent Publications


1. J. Pries and H. Hofmann. "Steady-State Algorithms for Nonlinear Time-Periodic Magnetic Diffusion Problems using Diagonally-Implicit Runge-Kutta Methods," accepted for publication in *IEEE Transactions on Magnetics*
2. Q. Li, T. Fan, and X. Wen. "Armature-Reaction Magnetic Field Analysis for Interior Permanent Magnet Motor Based on Winding Function Theory." *IEEE Transactions on Magnetics* 49(3) (March 2013): 1193–1201

3. T. Fan, Q. Li, and X. Wen. “Development of a High Power Density Motor Made of Amorphous Alloy Cores,” *IEEE Transactions on Industrial Electronics*, 61 (9) (September 2014): 4510–4518
4. Z. Song, H. Hofmann, J. Li, X. Han, M. Ouyang. “Optimization for a hybrid energy storage system in electric vehicles using dynamic programing approach”, Applied Energy Vol. 139, Feb. 2015, pp. 151-162 (note: available online).
5. Z. Song, H. Hofmann, J. Li, X. Han, X. Zhang, M. Ouyang. “A Comparison Study of Different Semi-Active Hybrid Energy Storage System Topologies for Electric Vehicles”, Journal of Power Sources, Vol. 274, Jan. 2015, pp. 400-411. (note: available online)
6. Z. Song, J. Li, X. Han, L. Xu, L. Lu, M. Ouyang, H. Hofmann, “Multi-objective optimization of a semi-active battery/supercapacitor energy storage system for electric vehicles”, Applied Energy, Vol. 135, Dec. 2014, pp. 212-224.
7. Z. Song, H. Hofmann, J. Li, J. Hou, O. Xuebing. “Energy management strategies comparison for electric vehicles with hybrid energy storage system”, Applied Energy, Vol. 134, Dec. 2014, pp. 321-331.

# Rapid System Integration through Modular Configuration

***Joint Project***


## U.S. Research Team Lead

- Huei Peng, University of Michigan
- Jing Sun, University of Michigan
- Giorgio Rizzoni, The Ohio State University

## U.S. Partners

- University of Michigan
- The Ohio State University

## China Research Team Lead

- Jianqiu Li, Tsinghua University
- Chengliang Yin, Shanghai Jiao Tong University

## China Partners

- Tsinghua University
- Shanghai Jiao Tong University


## Research Objective

To develop key techniques for the modeling, analysis, design, and control of power-split hybrid vehicles.

## Technical Approach

- Perform analysis and automated modeling of all configurations of power-split hybrid vehicles with multiple operating modes
  - Study powertrains that use a single planetary gear
  - Expand to powertrains using two planetary gears
- Develop modeling and optimization methods that enable rapid computation of control algorithms for powertrains with multiple modes
- Focus on specific applications to accelerate technology transfer

## Recent Progress

Over the last three years, we developed the automatic modeling, screening and mode classification methodology for hybrid vehicles powertrains with multiple planetary gear and clutches. In addition, we further developed a novel power-based algorithm which can be used to rapidly compute the optimal input of the powertrain component to achieve the best acceleration performance. Optimal mode selection is included in the decision process.

Over the last quarter, we have developed a theory to categorize mode shift and included physical mode shift constraint into the design process. By imposing physical mode shift hard constraint into the previously developed near-optimal control algorithm (PEARS+ algorithm), all mode shifts are guaranteed to be physically feasible and the optimization results become more realistic.

When a mode shift between Mode A and Mode B can be executed without stopping the vehicle, such mode shift is defined as feasible mode shift. All feasible mode shift can be categorized as in Figure 1: A direct mode shift is defined as a mode shift from A to B that the speeds of components do not change from the first clutch operation to the end of the last clutch operation. In other words, with the assumption that the clutch operation is instantaneous, a direct mode shift can happen instantaneously. A direct mode shift can be categorized into two classes: unconditional and conditional direct mode shift. In an unconditional direct mode shift, the mode shift can happen at any component speed combination (i.e., there are only clutch disengagement(s) during the mode shift); In a conditional direct mode shift, the mode shift can only be initiated when certain speed constrains are satisfied (i.e., clutch engagement(s) are involved).

Two theories have been developed to differentiate direct mode shift classes, when assuming that the node speed of each side of each clutch is controllable, which is generally true when assuming two MGs, one engine and one output shaft in a double PG system.

Theory 1: ∀ two different Mode A and Mode B, and their engaged clutches (including fixed connection) set are CSA and CSB. If CSB⊂CSA, then the mode shift from Mode A to Mode B is an unconditional direct mode shift (UCM), and Mode shift from Mode B to Mode A is a conditional direct mode shift (CM).

Theory 2: ∀ two different Mode A and Mode B, and their engaged clutches (including fixed connection) set are CSA and CSB. If ∃ a Mode C, whose engaged clutches set is CSC, such that CSA⊂CSC and CSB⊂CSC. Then the mode shift between Mode A and Mode B is a conditional direct mode shift.

The Volt Gen 2 design has been used to benchmark the performance when the physical mode shift constraint is added to the PEARS+ algorithm. The four operating modes of the Volt Gen 2 and its clutch states are shown in Figure 2 and Table 1.

The state trajectories optimized by PEARS+ with/without physical mode shift hard constraints are shown as in Figure 3. It can be found that the physically infeasible mode shift such as around 290s and 1350s in the previous PEARS has disappeared in the new result, while the overall fuel economy for FUDS only changes a little bit: From 64.5 mpg to 64.3 mpg.

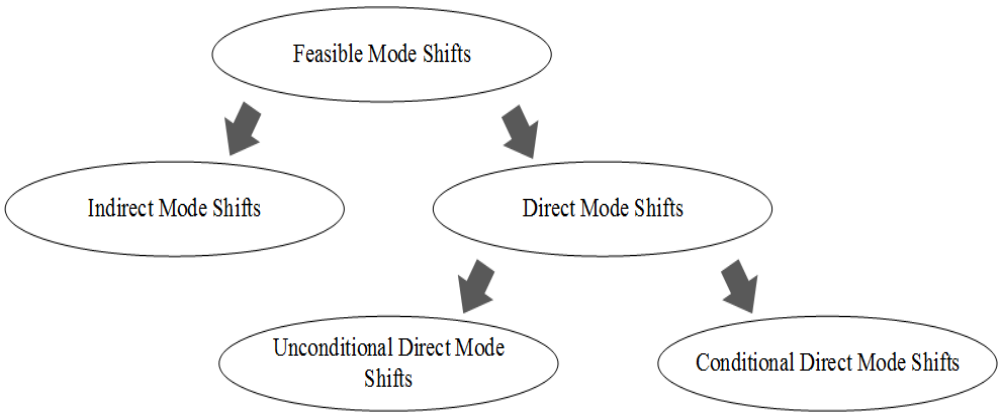


Figure 1: General Mode Shift Category

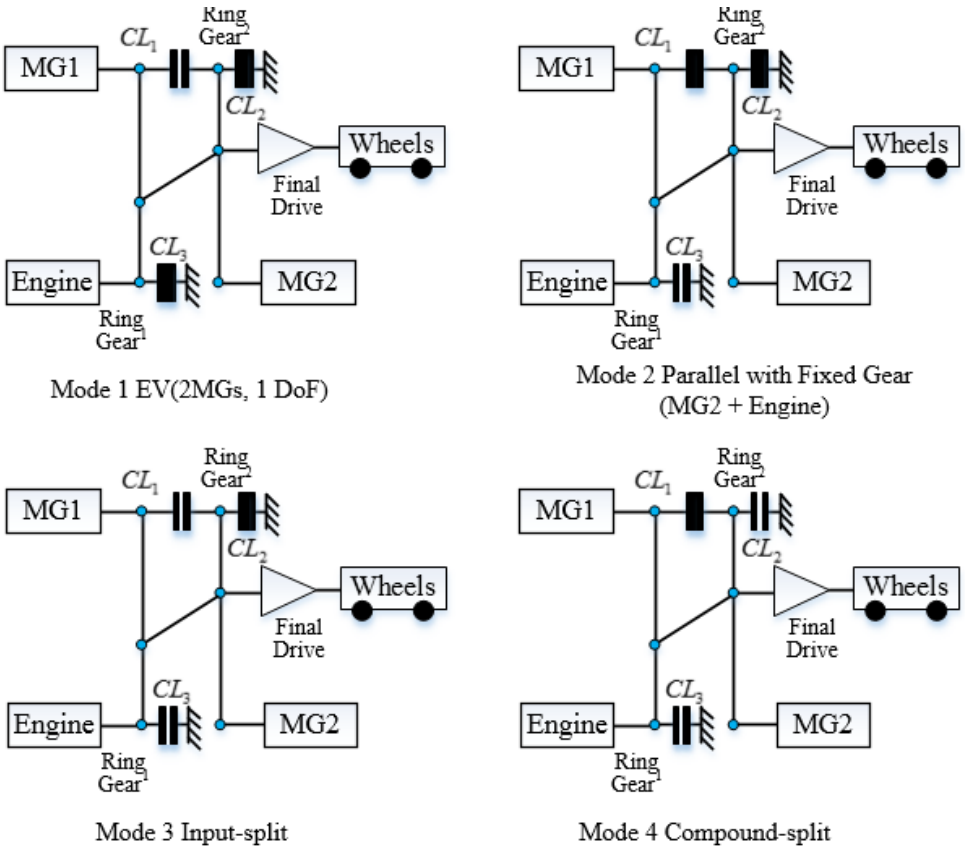


Figure 2: Four operating modes of the Volt Gen 2 (MY2016)

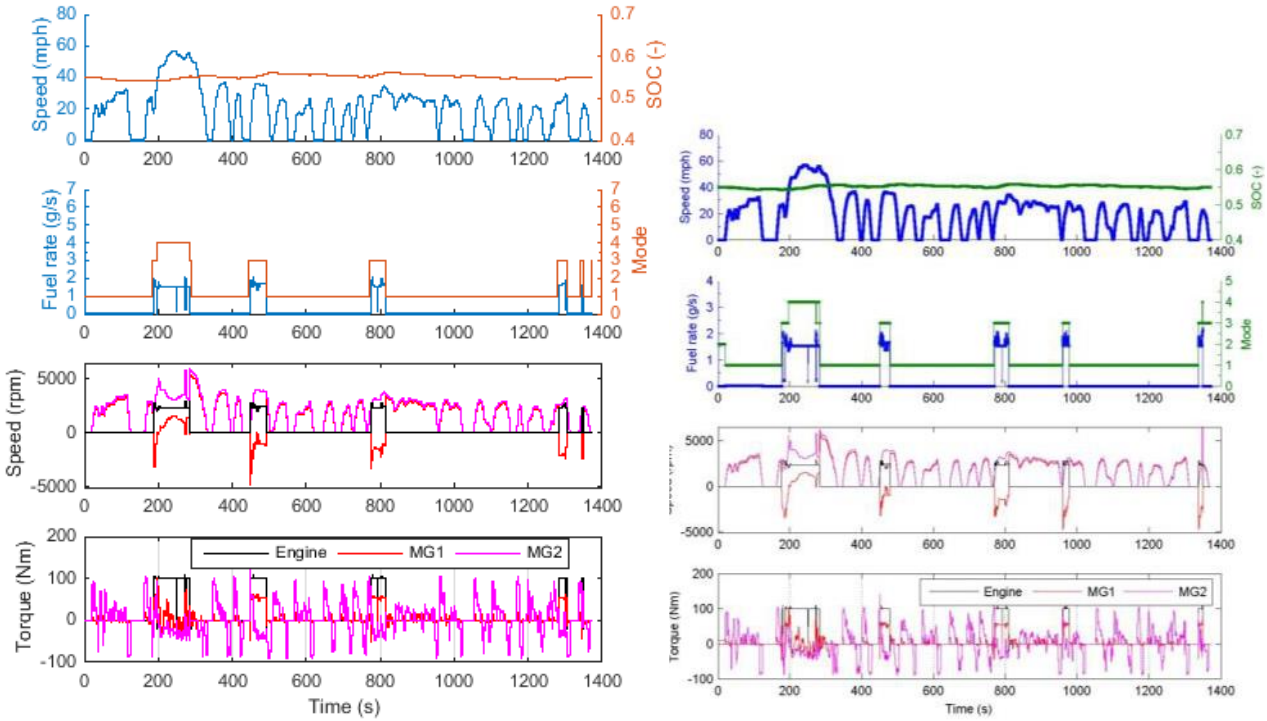


a) without physical mode shift constraint

b) With physical mode shift constraint

Figure 3. States and control trajectories of the PEARS+ for Volt Gen 2 in FUDS cycle with/without physical mode shift constraint

## Significant Results

The team has extended the automated modeling and screening method to power-split powertrains that use two planetary gears and clutches. One of the key challenges in the modeling process arises from the fact that when a clutch is engaged, typically the degree of freedom of the dynamic system changes. This means the state matrix that describes the motion of the vehicle changes, as well as the state vector. It is then necessary to develop executable rules that enable automated model reduction and subsequent screening schemes to eliminate infeasible or redundant dynamic systems. In addition, when multiple modes are available, identifying the best mode to use is not trivial, because the large discrepancy between engine efficiency and electric motor efficiency. To address these issues, a near-optimal control method was developed that is 3–4 orders of magnitude faster than a traditional optimization method such as dynamic programming.

In order to study the effectiveness of the proposed design and near-optimal control strategy, we started from the two-planetary gear powertrain shown in Figure 4, which is the powertrain design used in current model year of Toyota Prius and Camry hybrid vehicles. This powertrain has no clutch and only has a single mode. Inspired by the analysis results of our previous research, a Prius 2010++ design (also in Figure 4) is also analyzed. Both designs shown in Figure 4 serve as benchmarks of our new results. After detailed analysis, we found that up to 16 clutches can be added (see Figure 5). We analyzed the so-called "Utopian Prius" design in which all 16 clutches are assumed to be available for use, which enables 101 different modes. This design apparently is too complicated and costly to be commercialized. However, it serves as the theoretical upper bound of possible performance of our subsequent designs.

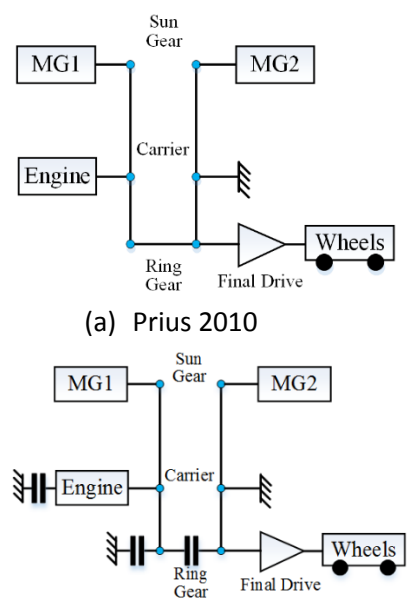


(a) Prius 2010

(b) Prius 2010++

Figure 4. The original input-split configuration used in the Toyota Prius model year 2010–2014 (top) and the conceptual Prius 2010++ design (bottom)—not used commercially. Both serve as benchmarks of our design study.

We conducted an exhaustive design search using the developed automated modeling and near-optimal control method, and we searched through all possible designs that use only three clutches and a permanent connection. These connections can be any 4 of the 16 potential locations shown in Figure 5, and a total of more than 7,000 designs are possible. By limiting the number of clutches to three, the resulting designs are more likely to be practical (Chevy Volts, for example, use three clutches). Among the more than 7,000 design candidates, 181 were found to achieve both better launching performance and fuel economy, compared with the original Prius 2010 design in simulations (see Figure 6). We selected one design on the Pareto front, highlighted by the green donut symbol in Figure 6 as the "optimal design." This design achieves 4.1% better fuel economy on combined urban/highway cycle driving, and the 0 to 60 mph launching performance is 32.7% better.

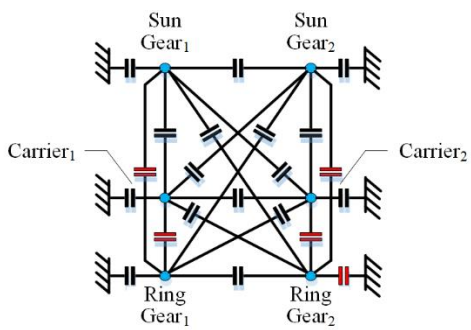


**Figure 5. For power-split hybrid powertrains using two planetary gears, up to 16 clutches can be added (shown in black color). This is obtained after eliminating redundant clutches (shown in red color).**

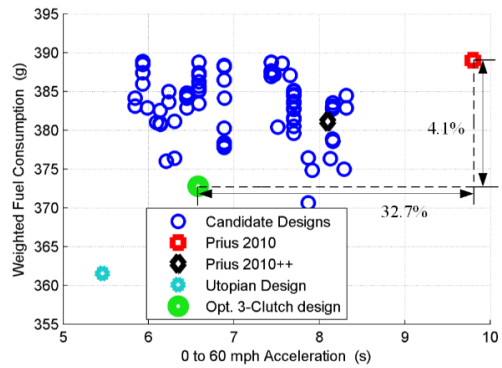


**Figure 6. Among more than 7,000 possible 3-clutch designs, 181 were found to achieve better fuel economy and better launching performance than the Prius2010 benchmark, when the same engine/motor/generator are used.**

## Future Plans

Hybrid vehicles have secured about 3.5% of the light-duty vehicle market share in the United States; we believe what is needed is a systematic design procedure to enable fast design for heavier vehicles, including full-size passenger cars, light trucks, and sport utility vehicles (SUVs). Some of these new target segments require more emphasis on attributes that are "beyond fuel economy," such as towing and acceleration performance. The proposed methodology will be applied to study these vehicles, including light trucks and SUVs, with practical performance requirements, in consultation with CERC member researchers.

## Expected Outcomes

- Comprehensive modeling, analysis, and control tools for design and simulation of power-split vehicles using one or two planetary gears; two-planetary-gear designs are especially suitable for heavy-duty applications such as light trucks, SUVs, and trucks up to Class 6
- A complete study of the benefits and challenges in deploying clutches to enable multiple modes
- In-depth analysis of several powertrain designs for next-generation CV applications
- Technology transfer to U.S. industrial partners

# Intelligent Fault Diagnosis and Prognosis

***Joint Project***


## U.S. Research Team Lead

- Prof. Giorgio Rizzoni, The Ohio State University

## U.S. Partners

- The Ohio State University

## China Research Team Lead

- Prof. Hongmei Li, HFUT
- Prof. Hongwen He, BIT
- Prof. Qi Chen, HFUT

## China Partners

- Hefei University of Technology (HFUT)
- Beijing Institute of Technology (BIT)


## Research Objectives

The objective of this project is to develop methods, algorithms, and software tools for electrified vehicle diagnosis and prognosis to guarantee functional safety and longer life cycle of electrified vehicles.

## Technical Approach

- Conduct hazard analysis (HA) including fault tree analysis (FTA) and design failure modes and effects analysis (FMEA) for electrified powertrains
- Develop fault and aging models, including a novel aging propagation modeling approach for interconnected systems.
- Develop simulators that incorporate fault and aging models at the component level, and simulate the effects of faults on the overall system
- Develop fault detection and isolation schemes for electric drive system, battery pack system and transmissions using structural approaches
- Develop system-level model-based state-of-health assessment and prognostics schemes for lifecycle management.
- Develop life extension strategies and algorithms for the battery system
- Develop fault diagnosis and fault mitigation strategies for torque security of electrified vehicles
- Translate the proposed methodology into a process that implements ISO26262 or some aspects thereof as part of the standard rapid prototyping software tool chain(Simulink/Matlab/dSpace)

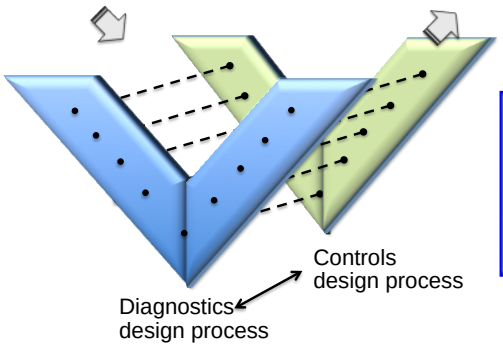


Figure 1: A "V-like" model for Fail-safe architectures, fault tolerant control and limp-home operation

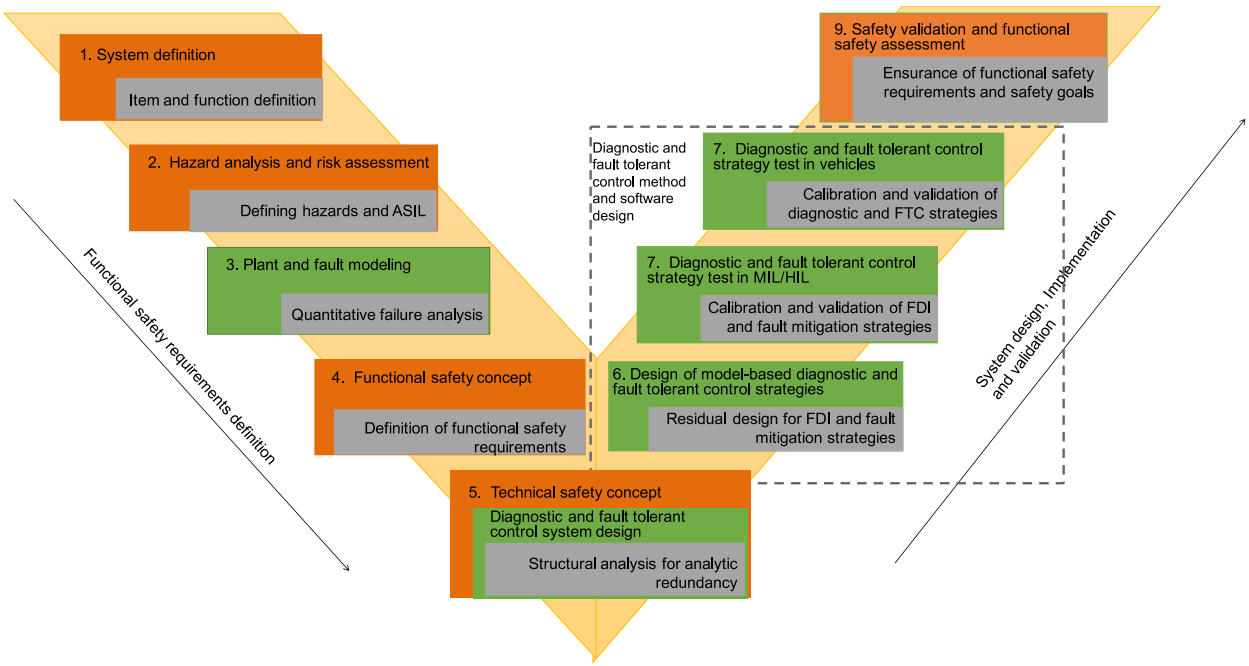


Figure 2: A systematic process for the design of model-based diagnosis and fault tolerant control that implements functional safety requirements

## Significant Results

***Structural Analysis for FDI:***

The project team has successfully applied structural approaches for fault diagnosis of electric drive system (Jiyu Zhang), battery systems (Andrea Cordoba Zhentong Liu), as well as automated manual transmissions, AMT (Dr. Qi Chen). Structural analysis methods for diagnosis analyze the structure of the system's mathematical model, with the aim of finding system redundancy in the system's structural model, and of constructing diagnostic tests through minimum structurally over-determined sets (Figure 3).

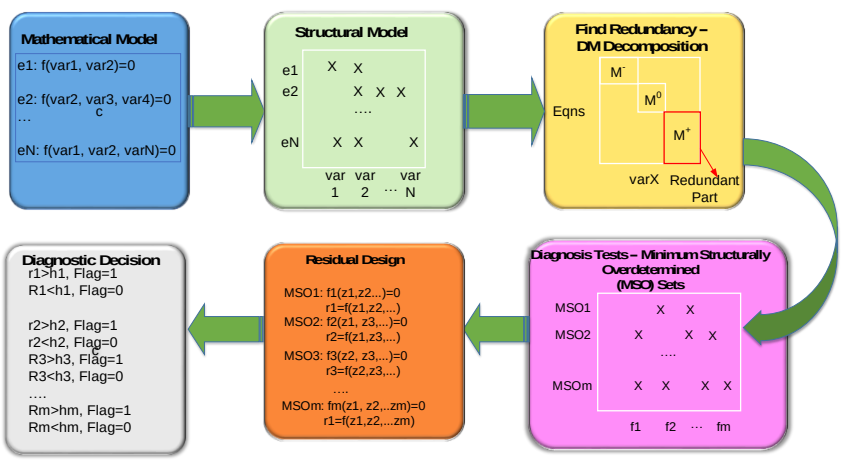


Figure 3: Structural analysis for FDI design

The team has used structural analysis approach to analyze the detectability and isolability of various faults in electric drives, battery systems and AMTs. In particular, a sensor placement study has performed to improve the isolation of faults for AMT systems. The team used MSO sets for diagnosis tests design and derived realizable sequential residual generators for each of the MSO set to achieve detection and isolation of various faults. The residual generators were validated through software-in-the-loop methods using Matlab/Simulink.

***PMSM drive systems:*** A FDI scheme was proposed using the structural analysis approach for various sensor faults . In particular, a set of diagnosis tests and sequential residual generators were selected to enable effective FDI of major faults in PMSM drives (Figure 4, Table 1).

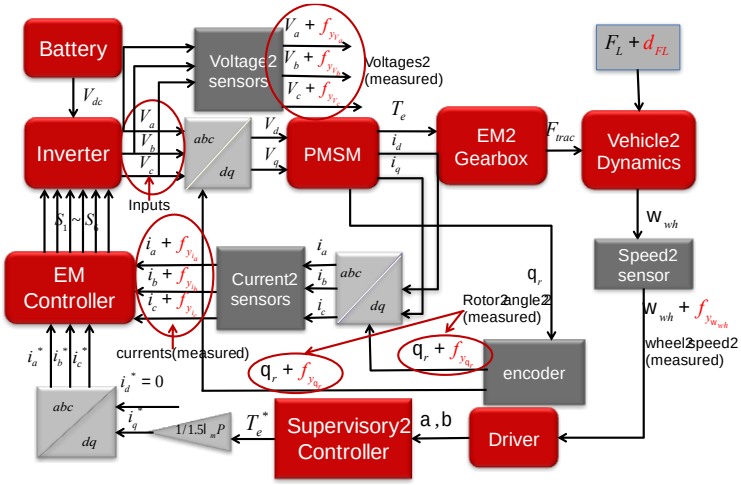


Figure 4: PMSM drive system architecture and fault locations

Table 1: Diagnosis tests selection for FDI of sensor faults in PMSM drive systems

| | $f_{Va}$ | $f_{Vb}$ | $f_{Vc}$ | $f_{ia}$ | $f_{ib}$ | $f_{ic}$ | $f_{\vartheta}$ | $f_{wh}$ |
|---|---|---|---|---|---|---|---|---|
| ***MSO1*** | | | | | | | X | X |
| ***MSO2*** | | X | X | X | X | | X | |
| ***MSO3*** | X | | X | X | X | | X | |
| ***MSO4*** | X | X | | X | X | | X | |
| ***MSO5*** | X | X | X | X | | | X | |
| ***MSO6*** | X | X | X | | X | | X | |
| ***MSO7*** | X | X | X | | | X | X | |

***Lithium-Ion Battery Systems****:* A model-based FDI scheme was also developed using structural analysis for battery systems. This scheme can successfully detect and isolate current, voltage and temperature sensor faults, as well as cooling system faults. The proposed FDI scheme is applied to a single cell as well as to a 2P2S battery module and experimental data were used for validation (Figure 5).

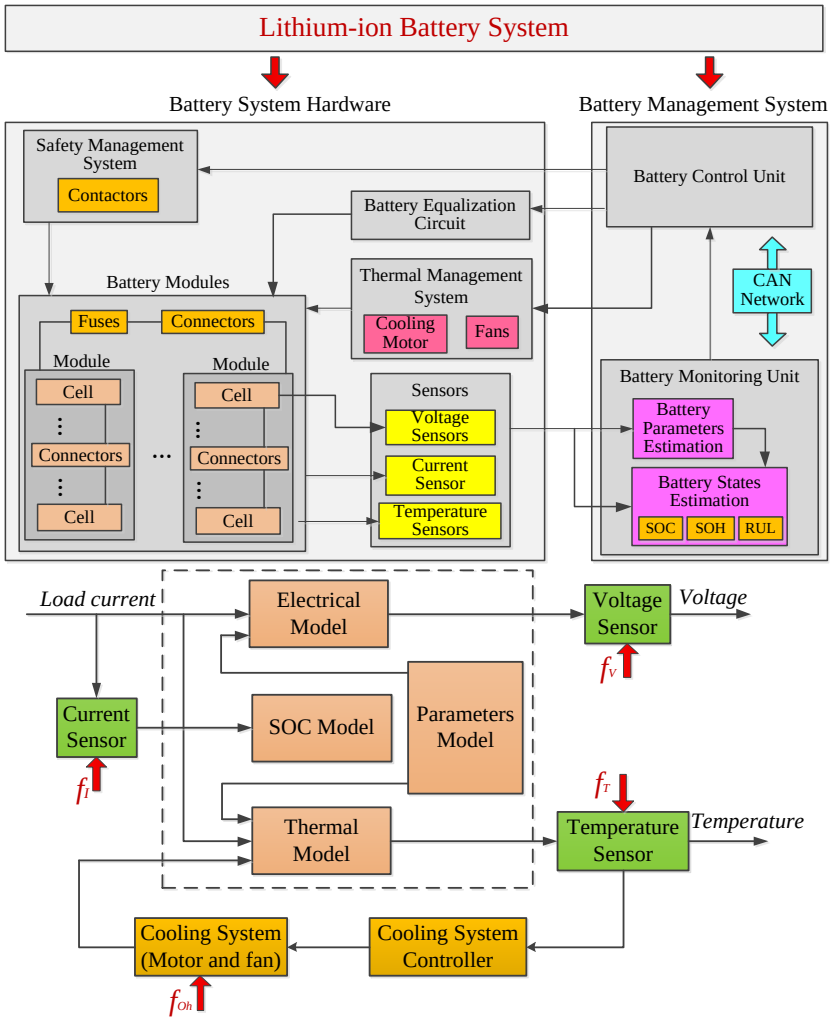


Figure 5: Lithium battery system architecture, modeling and fault locations

***AMT***: A systematic methodology based on structural analysis was proposed to classify the sensor placements to maximize the Fault Detection and Isolation utilizing the concept of Structural Analysis to the AMT. The team also developed a software tool (Matlab GUI) to conduct structural FDI easily and visually (Figures 6, 7).

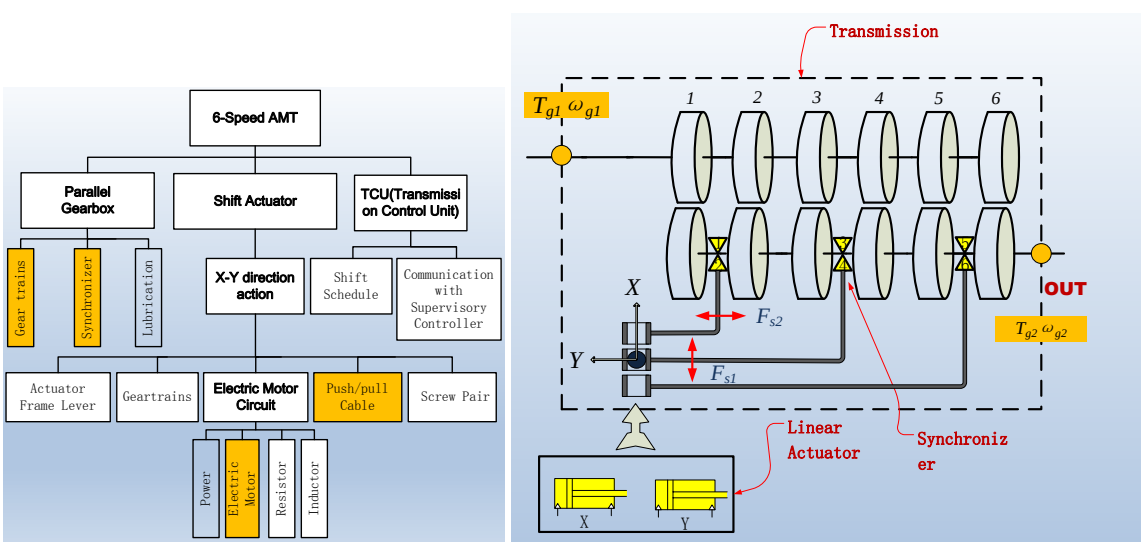


Figure 6: Configurations of a six-speed AMT

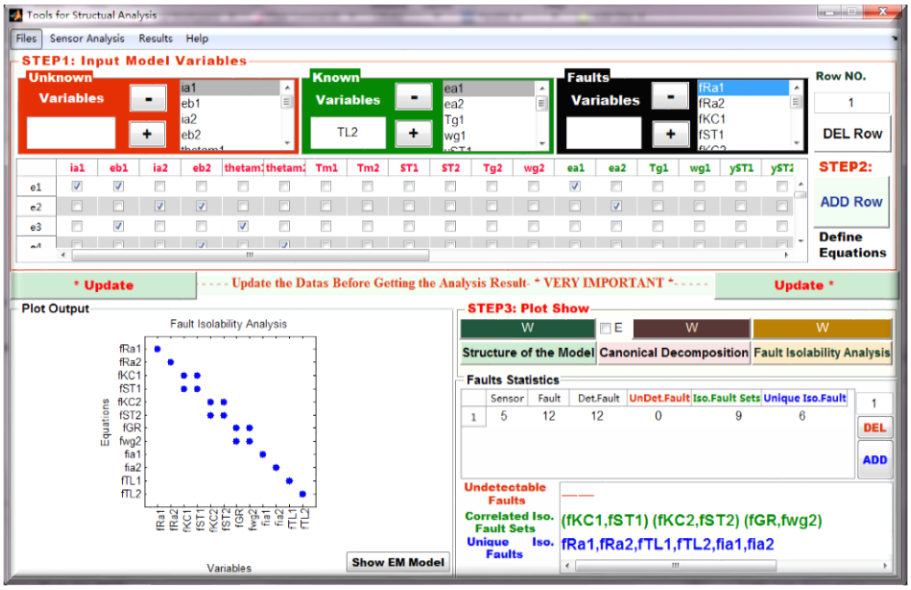


Figure 7: A Matlab GUI to enable using structural approaches for detectability, isolability analysis and sensor placement studies

**Demonstration project: Diagnosis for electrified vehicle torque security**

- The team conducted a hazard analysis using FMEA for electrified vehicle torque security problems (unintended acceleration) to identify the failure modes that could contribute to unintended acceleration problems.
- The team developed a fault diagnostic and fault mitigation strategy to deal with faults related to torque security problem, with focus on pedal stiction and pedal position sensor faults.

The team used the EcoCAR2 vehicle as a case study and demonstrated the effectiveness of the proposed strategy using MIL/HIL and in vehicle tests. To summarize these accomplishments, the team created a video for demonstration of the diagnostics and mitigation strategies through HIL experiments.

## Future Plans

The project team will conduct a more complete and systematic model-based fault diagnosis and prognosis methods and procedures for EV powertrains. The team also plans to take advantage of the fault diagnosis techniques to assist control development. The methods and tools will be demonstrated on an experimental vehicle, in collaboration with industrial partners. OSU is currently collaborating with Ford on a related project.

## Expected Outcomes

- A systematic methodology for the design of system-level solutions for EV state-of-health assessment, diagnosis, and prognosis for ensuring functional safety
- Methods, algorithms, and software tools for EV powertrain key systems life cycle management
- Fault-tolerant control methods for limp-home and life-extending operation of electrified powertrains
- Collaboration with U.S. and Chinese industry partners in validating these methods experimentally.

## References/Publications


1. Cordoba-Arenas, Andrea. “Aging Propagation Modeling and State-of-Health Assessment in Advanced Battery Systems”. Ph.D. Dissertation, The Ohio State University, 2013. Advisor: Prof. Giorgio. Rizzoni (currently employed at Ford R&A)
2. Liu, Zhentong “Model-Based Fault Diagnosis of Electrified Driven Powertrains in Pure Electric Vehicles”, Ph.D. dissertation, Beijing Institute of Technology, Spring 2016. Advisor: Prof. Hongwen He, co-Advisor: Prof. Giorgio Rizzoni
3. Zhang, Jiyu “Functional safety of electrified vehicles by model based fault diagnosis and fault tolerant control”, Ph.D. Dissertation, The Ohio State University, December 2016. Advisor: Prof. Giorgio Rizzoni

4. Hua Y., Cordoba-Arenas A., Warner N., Rizzoni. G. “A multi time-scale state-of-charge and state-of-health estimation framework using nonlinear predictive filter for lithium-ion battery pack with passive balance control”. Journal of Power Sources, Volume 280, 15 April 2015, Pages 293-312. (IF = 4.908)
5. Cordoba-Arenas, A., Onori,S., Rizzoni, G. A control-oriented lithium-ion battery pack model for plug-in hybrid electric vehicle cycle-life studies and system design with consideration of health management. Journal of Power Sources, Volume 279, 15 April 2015, Pages 1-18. (IF = 4.908)
6. Cordoba-Arenas, A., Onori,S., Guezennec Y., Rizzoni, G. “ Capacity and power fade cycle-life model for plug-in hybrid electric vehicle lithium-ion battery cells containing blended spinel and layered-oxide positive electrodes”. Journal of Power Sources, Volume 278, 15 March 2015, Pages 473-483. (IF = 4.908)
7. Jiyu Zhang, Giorgio Rizzoni, “Functional Safety of Electric Traction Drive Through Model-Based Fault Diagnosis ”. IEEE Transactions on Vehicular Technology. Accepted in 2015.
8. Jiyu Zhang, Andrea Cordoba-Arenas, Alessandro Amodio, Bilin Aksun-Guvenc, Giorgio Rizzoni, “A Model-Based Approach for Functional Safety of EV Powertrain, with a Case Study on Torque Security”, Control Engineering Practice, in review.
9. Zhentong Liu, Qadeer Ahmed, Giorgio Rizzoni, Hongwen He. “Structural analysis based sensors fault detection and isolation of cylindrical lithium-ion batteries in automotive applications”. Control Engineering Practice, in review.
10. Zhentong Liu, Andrea Cordoba-Arenas, Qadeer Ahmed, Giorgio Rizzoni, Hongwen He. “Hierarchical Sensors Fault Diagnosis for a Lithium-Ion Battery Pack in Electric Vehicles.” IEEE Transactions on Industrial Electronics, in review.
11. Chen, Q., Ahmed, Q., Rizzoni, G., Qiu, M., “Design and Evaluation of Model-based Health Monitoring Scheme for Automated Manual Transmission”. ASME Journal of Dynamic Systems Measurement and Control, in review.
12. Jiyu Zhang, Alessandro Amodio, Bilin Aksun-Guvenc, Giorgio Rizzoni, Pierluigi Pisu (2015), “Investigation of Torque Security Problems In Electrified Vehicles”. ASME 2015 Proceedings of Dynamic System and Control Conference, October 26-28, Columbus, OH, USA
13. Jiyu Zhang, Giorgio Rizzoni (2015), “Diagnosability and Control Reconfigurability Analysis for PMSM drive system”. Proceedings of the 9th IFAC SafeProcess, September 2-4, 2015, Paris, France.
14. Zhentong Liu, Hongwen He, Qadeer Ahmed, Giorgio Rizzoni (2015). “Structural Analysis Based Fault Detection and Isolation Applied for A Lithium-Ion Battery Pack”. Proceedings of the 9th IFAC Symposium on Fault Detection, Supervision and Safety for Technical Processes, September 2-4, 2015, Paris, France.
15. Qi Chen, Qadeer Ahmed, Giorgio Rizzoni, etc. (2015). “Model-Based Fault Diagnosis of an Automated Manual Transmission Shifting Actuator”. Proceedings of the IFAC 9th IFAC Symposium on Fault Detection, Supervision and Safety for Technical Processes, September 2-4, 2015, Paris, France.
16. Jiyu Zhang, Giorgio Rizzoni, “Functional Safety of Electrified Vehicles Through Model-Based Fault Diagnosis”. Proceedings of IFAC 2015workshop on Engine, Powertrain Control, Simulation and Modeling (E-COSM’15), August 23-26, 2015, Columbus, OH, USA.
17. Jiyu Zhang, Andrea Cordoba-Arenas, Giorgio Rizzoni (2014), “Fault Diagnosis for PMSM Drive System in Electric Vehicle”. Proceedings of the 2014 ASME Dynamic System and Control Conference, October 22-24, 2014, San Antonio, TX, USA.
18. Zhentong Liu, Qadeer Ahmed, Giorgio Rizzoni, Hongwen He (2014), “Fault Detection And Isolation For Lithium-Ion Battery System Using Structural Analysis And Sequential Residual Generation”, Proceedings of the ASME 2014 Dynamic System and Control Conference, October 22-24, 2014, San Antonio, TX, USA.
19. Qi Chen, Qadeer Ahmed, Giorgio Rizzoni (2014). “Sensor Placement Analysis for Fault Detectability and Isolability of an Automated Manual Transmission”. In Proceedings of the ASME 2014 Dynamic Systems and Control Conference (DSCC2014), San Antonio, TX, USA.
20. Jiyu Zhang, Giorgio Rizzoni, “Structural Analysis for FDI of PMSM Drive System in Electric Vehicles”. In Transportation Electrification Asia-Pacific (ITEC Asia-Pacific), 2014 IEEE Conference and Exp, Aug. 31, 2014 – Sept. 3, 2014
21. Jiyu Zhang, Giorgio Rizzoni, Qadeer Ahmed (2013), “ Fault Modeling For Hierarchical Fault Diagnosis And Prognosis”, Proceedings of the ASME 2013 Dynamic Systems and Control Conference, October 22-24, 2014, San Antonio, TX, USA.

22. Cordoba-Arenas, A., Onori,S., Rizzoni. G., Fan, G. (2013) “Aging Propagation in Interconnected Systems with an Application to Advanced Automotive Battery Packs”. Proceeding of the 7th IFAC Symposium on Advances in Automatic Control, Tokyo, September 2013.
23. Andrea Cordoba-Arenas, Jiyu Zhang, Giorgio Rizzoni (2013), “Diagnostics and Prognostics Needs and Requirements for Electrified Vehicles Powertrains”. Proceedings of 7th IFAC Symposium on Advances in Automotive Control, The International Federation of Automatic Control, September 4-7, 2013, Tokyo, Japan.
24. Onori, S., Rizzoni, G., Cordoba-Arenas, A. (2012) “A Prognostic Methodology for Interconnected Systems”. Proceedings of the 8th IFAC International Symposium on Fault Detection, Supervision and Safety of Technical Processes (SAFEPROCESS 2012), Mexico City, Mexico, 2012.

# Adaptive Battery Management System On and Off the Grid

***Joint Project***


## U.S. Research Team Lead

- Jing Sun, University of Michigan
- Huei Peng, University of Michigan

## U.S. Partners

- University of Michigan

## China Research Team Lead

- Minggao Ouyang, Tsinghua University
- Jianqiu Li, Tsinghua University
- Lifang Wang, Chinese Academy of Science
- Chengliang Yin, Shanghai Jiaotong University
- Li Chen, Shanghai Jiaotong University

## China Partners

- Tsinghua University
- Chinese Academy of Science
- Shanghai Jiao Tong University


## Research Objective

This project seeks to develop intelligent monitoring (while driving), diagnosis/prognosis, and conditioning (while connected with the grid) strategies to improve the reliability, performance, and life cycle of battery systems on electrified vehicles. The current research objectives are directed toward the development of suitable models for battery system aging characterization and real-time adaptation, and the development of design framework and computational algorithms to perform robust battery system identification and diagnosis with onboard sensor and communication constraints.

## Technical Approach

- Develop phenomenological models that can represent battery aging data while explaining underlying physical behavior
- Improve understanding of the aging and environmental effects on batteries' cycle performance
- Identify real-time and onboard battery system adaptation requirements and limitations
- Develop energy management algorithms and strategies to maintain optimal and robust performance for battery systems with changing characteristics

## Recent Progress

**Q3 2015**

The team continued the efforts on characterization of the relation between battery module degradation and the cell non-uniformities within the module. In particular, we are looking at how the differences in cell capacity and resistance would affect the battery module in terms of long term aging performance. The research results could help to determine how cell should be arranged when there are unavoidable cell-to-cell variations due to manufacture errors.

The research activities have been focused on the following two aspects: (a) Perform aging simulation of battery modules with non-uniformly aged cells. (b) Experimental design and set up to explore the long-term influence of cell non-uniformity on battery module and pack degradation.

For part (a), simulations on battery module degradation due to cell resistance and capacity difference are performed respectively. It is shown that the types of non-uniformity would result in different module aging results. The battery modules that consist of cells with resistance difference could age a lot faster than modules with uniform cells, whereas the non-uniformity of cell capacities does not influence the module aging significantly. The validity of the simulation results are going to be verified by experiments.

The work of part (b) is focused on the design and set up of the test for battery module aging study. The objective is to understand how the initial cell non-uniformity could affect the long turn aging performance of a multi-cell module/pack, as well as identify the influential factors that might accelerate or slow down the aging process. The tests consist of two different designs. One is to test the modules that have parallel connected cells directly and the other is to test individual cells with current profiles that emulate the current distribution in an actual module. The second test set up is adopted in order to allow individual cell current monitoring. The information on cell current could further validate the battery aging model that is being investigated.

The team will continue on the experiments for the long term aging study of battery modules that has cells connected in parallel. 24 cells with different characteristics have been selected and will be tested using the two different designs mentioned above. The experimental results will be used to validate the aging simulation of battery modules as well as improve the accuracy of cell aging model.

**Q2 2015**

For the second quarter of 2015, the team continued the research effort on developing effective and robust system identification algorithms for on-line detection of battery state of health for real-time monitoring, diagnosis, and prognosis purposes. Extensive study on the sensitivity of ICA based SOH monitoring technique with respect to cell non-uniformity in parallel-connected battery modules and packs were performed. Both simulation and experimental results were used to show the robustness of the proposed SOH monitoring framework under different cell non-uniformity conditions.

Our research activities in the second quarter of 2015 have been focused on the following two aspects: (a) Sensitivity study of ICA results with respect to cell non-uniformity in 2-cell battery modules using a simulation model that considers the battery aging mechanism. (b) Experimental design to validate existing battery capacity aging models and investigate the long-turn influence of cell non-uniformity on battery module and pack performance degradation.

For part (a), the simulations were performed using a battery module model that has two cells connected in parallel. The dynamics of each individual cell was represented using a 1st order equivalent circuit model and an open circuit voltage function that could emulate the aging behavior at both cathode and anode. The 2-cell module is picked for the convenience of results visualization. However, regardless of the cell numbers, the simulation results should reflect the relationship between the accuracy of ICA with respect to cell capacity and resistance variation in a module. In this part of the study, the reference module which had two identical cells was used as the benchmark, whereas the modules made up of two cells with varied capacity and resistance were used to reflect the non-uniformity. The simulated modules had the same total capacity as the reference module. The results of the sensitivity study are shown in Fig.1. The variation in the IC peak is defined by comparing: $\Delta IC = ICref - ICvarICref$

where ICref and ICvar are the IC peak values of the reference module and the modules with varied cell non-uniformity respectively.

The work of part (b) is focused on the design of test plan for battery module/pack aging study. The objective is to understand how the initial cell non-uniformity could affect the long turn aging performance of a multi-cell module/pack, as well as identify the influential factors that might accelerate or slow down the aging process. As part of this study, literature review on various empirical and electrochemical aging models has been performed. The accuracy of those models will also be investigated using the experimental results.

In the next quarter, the team continue the effort in characterizing the aging process of battery modules, specifically the effects of non-uniformity of cells with in the module. In parallel, we will start to focus on experimental design and set-up for the long term aging study of battery modules that has cells connected in parallel. Cells with various characteristics will be combined to build 2-cell modules with different non-uniformity. The quantitative relationship between cell capacity and resistance difference and the overall battery module aging performance will be explored.

**Q1 2015**

For the first quarter of 2015, the team continued the research effort on developing effective and robust system identification algorithms for on-line detection of battery state of health for real-time monitoring, diagnosis, and prognosis purposes. Analytical and numerical analysis on the application of ICA framework to battery pack data are performed. A theoretical foundation is being established to explain why and how the ICA technique can be used to monitoring the SOH of a battery pack with multiple cells connected in parallel.

Our research activities in the first quarter of 2015 have been focused on the following three aspects: (a) Mathematical analysis of ICA's applicability to battery packs. (b) Robustness study of ICA with respect to resistance and capacity non-uniformity.

For part (a), a simplified equivalent circuit model for battery pack is used for the analysis. The IC value of the battery pack, which is evaluated based on its terminal measurements, can be expressed as the sum of the IC values of each individual cell. Therefore, when the battery cells have uniform characteristics, performing ICA over battery pack data is the same as evaluating the single cells. Consequently, the battery capacity estimation model derived from single cell data could be directly extended to battery pack data. However, non-uniformity of battery cells exist in practice and it's necessary to study the robustness of ICA method when applied to pack, and assess its sensitivity with respect to different degree of cell variations.

The work of part (b) is focused on the use of both analytical and simulation tools to study the sensitivity of IC values. Due to cell non-uniformity, the currents during charging and discharging are distributed unevenly and this uneven distribution results in an imbalance in the cell SOC levels. Consequently, the individual cells in a battery pack would reach their voltage plateaus at different timing. The gap between the peaks causes the pack IC value to deviate from the value that would reflect the pack capacity correctly. The understanding of this SOC imbalance helps us to estimate and quantify the influence of cell non-uniformity on the ICA based SOH monitoring framework.

In the next quarter, the team will continue to focus on the model based analysis for battery packs SOH monitoring. The robustness study will be finalized. On the other hand, we will also explore how the SOH monitoring results can utilized for on-board energy management and optimization of battery operation.

**Q4 2014**

The CERC team continued the research effort on developing effective and robust system identification algorithms for on-line detection of battery state of health for real-time monitoring, diagnosis, and prognosis purposes. More experimental works were performed to solidify our previous results on ICA's application to battery pack capacity estimation. The results show that, the total capacity loss of a battery pack (with cells connected in parallel) could also be correlated with the IC curve peaks of the pack, and the correlation is quantitatively the same as the single cell case. The findings suggest that the ICA based SOH monitoring framework developed for single cells can be applied to battery packs.

Our research activities in the fourth quarter of 2014 have been focused on the following three aspects: (a) performing battery pack tests with various cell combinations; (b) Identifying the correlation between battery pack capacity and IC peak values; (c) Investigation of ICA's robustness with respect to different battery chemistry, charging/discharging rates and temperature.

For part (a) and (b), battery packs consisting of 3 and 7 cells were constructed for the tests. For a total number of 30 cells in our test cell inventory, the distribution of the cell capacity and resistance are plotted in Fig. 1. The inventory allowed us to build packs with different total capacity and resistance to reflect different aging status as well as different cell variations. The packs used in the experiments were formed by selecting aged cells from the inventory and connecting them in parallel. The battery packs (total of 26, 20 with 3 cells connected in parallel, and the rest with 7 cells connected in parallel) were charged/discharged using constant current rate and ICA was applied.

To quantify the correlation between capacity and the corresponding IC peak values, a fitted curve, i.e., a model, (dashed line in Fig. 2) was obtained using the single cell test data. This model provides us a quantitative analysis tool to estimate the battery capacity based on the IC peak values identified from the test data. To extend this estimation method with battery pack data, normalization was performed first. Both capacity and IC peak values obtained from the data are divided by the nominal capacity values. After normalization, we could plot the ICA results of the battery packs together with the correlation identified using the single cell data, as shown in Fig. 2. The maximum deviation between fitted correlation and the battery pack data is about 2%. Therefore, although the estimation model is built based on the single cell data, it is directly applicable to 3-cell and 7-cell pack data. This result implies that, the correlation identified using single cell data is generalizable to battery packs with various numbers of cells, and could be used as a battery pack degradation model for capacity estimation.

For part (c), charging/discharging data of batteries with different chemistries were processed using ICA with SVR. The aging signature could be extracted by the approach for most batteries. The influences of current rate and environmental temperature on the IC curves were also investigated and tests were conducted.

In the next quarter, the team will start to focus on the model based aging analysis for battery packs. Several theoretical battery aging models will be considered. The influence of cell non-uniformity on the aging of battery packs will be explored.

## Significant Results

Efforts have been focused on characterization and identification of battery state of health (SOH) for electrified vehicles. The team has built a large database of battery aging cycles over the past two years. The data sets have been analyzed to develop/validate new models and SOH identification algorithms. The main results achieved so far include the design of an effective identification framework for onboard battery SOH monitoring and degradation diagnosis and the development of a unified battery open-circuit-voltage (OCV) model for state of charge (SOC) and SOH estimation.

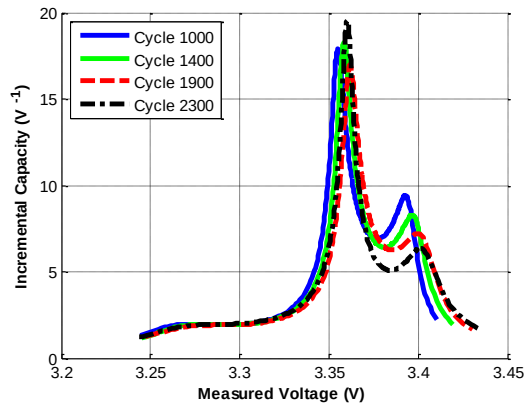


Figure 1. IC curves of data at different aging stages.

The incremental capacity analysis (ICA) leverages the lithium-ion battery staging phenomenon during the intercalation process at the graphite anode side. This analysis exploits the sensitivity of the battery charged capacity (Q) with respect to the terminal voltage (V) and transforms voltage plateaus on the V-Q curve into clearly identifiable peaks on the dQ/dV curve. While it is known that the peaks on the incremental capacity (IC) curve are associated with battery electrochemical properties and aging status under quasi-equilibrium conditions, this project focuses on the investigation of the IC signature and its utility under normal charging conditions. Through extensive analysis of the aging data, a strong correlation is established between the IC peak at higher SOC range and the SOH for data collected under normal charging conditions (1/2 C rate).

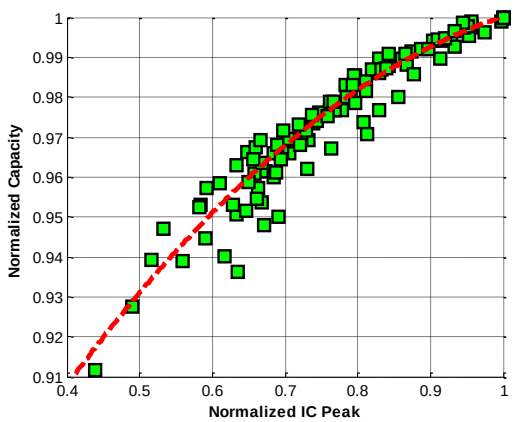


Figure 2. Correlation between normalized battery capacities and IC peaks.

Extracting the IC aging signatures from the battery charging/discharging data is challenging, as the flatness of the curve and the noise sensitivity make it infeasible to directly differentiate measured Q-V data. The team has explored both parametric and non-parametric approaches, developed and evaluated several algorithms, and validated the algorithms with battery aging data sets. The use of support vector regression (SVR) is shown to provide the most promising features for real-time applications, because the SVR model is able to extract the IC peak information and predict the capacity fade within a 1% error bound more than 90% of the time, as validated on data collected for eight different A123 $LiFePO_4$ cells with up to 2,800 aging cycles.

Furthermore, the established ICA-based battery SOH monitoring framework has been extended from single cells to battery packs. The applicability of ICA to battery packs was investigated through both model simulations and experimental tests. A battery pack model incorporating cell dynamic behavior and aging mechanism was built for the study. For the experiments, multiple battery packs consisting of cells with various aging conditions are built and tested. A cell inventory of about 30 A123 $LiFePO_4$ cells is established. The cells in the inventory were cycled with different loading profiles before the pack tests. The cells are then combined into multi-cells packs and processed with

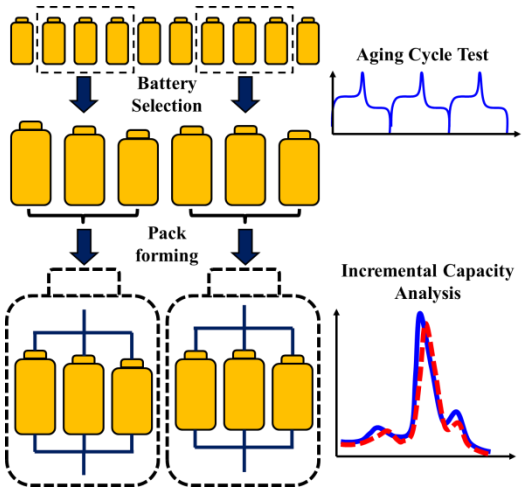


Figure 3. Battery Pack Formulation and Characterization Tests.

characterization profiles. The preliminary test results (with three-cell packs) show that the IC behaviors of battery packs are consistent with those of cells. The ICA-based SOH monitoring framework is applicable to battery packs.

## Future Plans

Future research activities include the following: (1) extend the SOH monitoring framework to battery packs with different number of cells and various chemistries; (2) investigate the sensitivity of the ICA-based SOH monitoring to environmental and operational parameters (such as temperature and cell non-uniformity); (3) develop adaptive power management strategies incorporating battery SOH information; and (4) implement the framework in electric vehicle applications.

## Expected Outcomes

- Algorithms and methodologies for online battery system identification and adaptation
- Battery pack model for aging and degradation analysis
- Design and validation of an integrated adaptive battery power management strategy
- Recommendations on battery system prognosis and diagnosis strategy

## Recent Publications

- A paper was presented IFAC E-COSM workshop.
- Four journal papers have been published, including two with joint authorship of University of Michigan and Tsinghua University.
- One paper has been recently accepted by the IEEE Transactions on Vehicular Technology
- Two joint papers have been submitted to Applied Energy, and the Journal of Power Sources respectively.

# Data-Based Techniques for Battery-Health Prediction

***Joint Project***


## U.S. Research Team Lead

- Jeffrey Stein, University of Michigan
- Dennis Bernstein, University of Michigan
- Tulga Ersal, University of Michigan
- Xin Zhou, University of Michigan

## U.S. Partners

- • University of Michigan

## China Research Team Lead

- • Languang Lu, Tsinghua University

## China Partners

- Tsinghua University


## Research Objectives

The objective of this project is to develop and demonstrate non-invasive methods to estimate health-relevant variables of a battery and thus monitor battery state of health (SOH).

## Technical Approach

- Use three health-relevant electrochemical variables, the solid-electrolyte-interphase (SEI) film resistance, the side reaction current density, and the number of cyclable lithium-ions, as three alternatives for indicators of the SOH.
- For estimation of the SEI film resistance, adopt Retrospective-Cost Subsystem Identification (RCSI) to identify the inaccessible battery health subsystem and estimate the SEI film resistance as the output of the subsystem.
- For estimation of the side reaction current density, use both Retrospective-Cost Subsystem Identification (RCSI) and its modification, the two-step filter (TSF), to identify the inaccessible battery health subsystem and estimate the SEI film resistance as the output of the subsystem.
- For estimation of the number of cyclable Li-ions, adopt the extended Kalman filter to estimate the number of cyclable Li-ions as a parameter in the nonlinear battery model.
- Examine the robustness of the aforementioned three approaches under various non-ideal conditions such as measurement noise, state of charge (SOC) estimation errors, and modeling errors.
- Conduct simulations and laboratory experiments to validate the most effective and robust approach and evaluate its performance.

## Significant Results

The team has explored estimating three different health-related electrochemical variables for two different battery chemistries to expand the scope and stretch the limit of using electrochemical variables to monitor battery SOH. We demonstrated in simulation approaches of estimating the three variables by using high-fidelity models for battery dynamics under ideal conditions, that is, without measurement noise, SOC estimation error, and modeling error. The robustness of these approaches has also been examined in simulation under various non-ideal conditions such as measurement noise, SOC estimation error, and modeling errors to predict the expect performance in practice.

Initially, we explored SOH monitoring of $LiFePO_4$ (LFP) battery, which demonstrated great potential for electric vehicle (EV)/hybrid electric vehicle (HEV) batteries. Degradation of LFP is mainly caused by electrochemical degradation mechanisms that consume cyclable Li-ions, especially the SEI-film-formation mechanism.

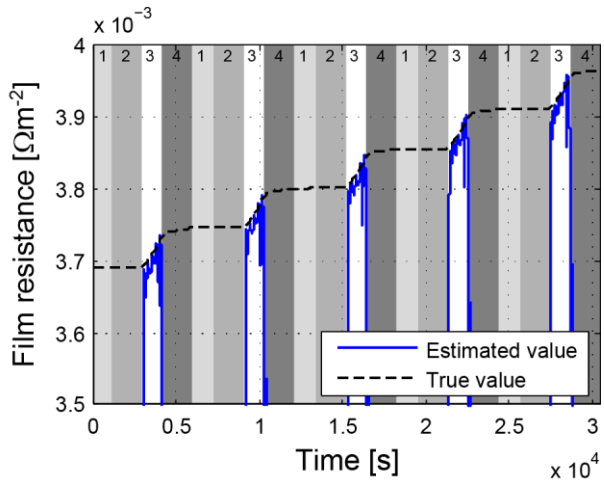


**Figure 1: Estimate of the SEI film resistance using Retrospective-Cost Subsystem Identification during constant current constant voltage (CCCV) cycles under ideal conditions. The regions numbered 1, 2, 3, and 4 indicate the constant current charge mode, constant voltage charge mode, constant current discharge mode, and constant voltage discharge mode, respectively. Simulations show that the estimate can track the true value of the SEI film resistance during the constant current charge mode when degradation rate is significant.**

In the initial stage of the project, we focused on estimating the SEI film resistance, which is an indicator for SOH under the SEI-film-formation degradation mechanism. Figure 1 shows the simulation results for estimating the SEI film resistance in LFP batteries under ideal conditions during five consecutive constant current constant voltage (CCCV) cycles. Every cycle is formed with four modes: constant current charge (CCC), constant voltage charge (CVC), constant current discharge (CCD), and constant voltage discharge (CVD). Simulations show that the estimate can track the true value of the SEI film resistance during the CCC mode. This is due to the fact that degradation is the most significant and therefore the subsystem that generates the SEI film resistance is the most identifiable during the CCC mode. In contrast, during the other three modes, degradation is negligible, and thus the subsystem is under-excited, resulting in the unidentifiability of the SEI film [1].

In light of the limitation of the SEI film resistance that indicates SOH only under the SEI-film-formation mechanism, we introduced a new SOH indicator, the side reaction current density, which indicates SOH under all degradation mechanisms that consume cyclable Li-ions. Figure 2 presents the estimation results of the side reaction current density in LFP batteries under ideal conditions during the (a) 1-C constant current charge and discharge (CCCD) cycle, (b) 10-C CCCD cycle, and (c) urban dynamometer driving schedule (UDDS). These three scenarios are carefully chosen to represent the operation range of electric vehicles. The estimation accuracy is measured with the relative estimation error, which is the normalized error between the true value and the estimated value. Simulations show that the relative estimation error is bounded within $\pm 2 \times 10^{-4}\%$, $\pm 1\%$, and $\pm 0.3\%$ for the 1-C CCCD cycle, 10-C CCCD cycle, and the UDDS cycle, respectively. This result shows that the side reaction current density can be accurately estimated for all three tested scenarios under ideal conditions. During the discharge modes in (a) and (b) as well as the high-C discharge period or low SOC period in (c), the estimated value diverges from the true value, which is also due to the weak identifiability caused by insignificant degradation under these situations [3, 5]. This divergence can be attenuated by shutting down the estimation algorithm in the unidentifiable region.

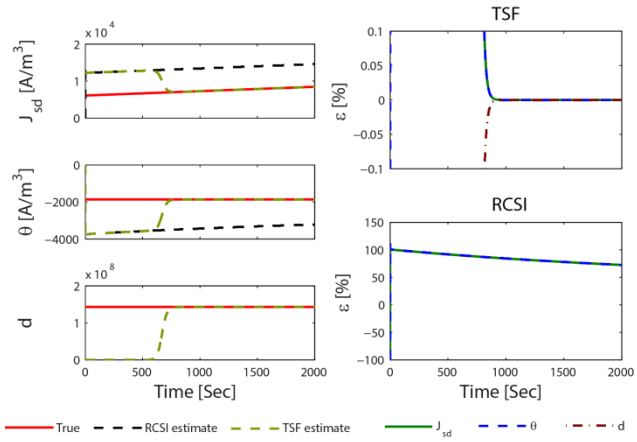


**Figure 2: Estimate and relative estimation error ($\epsilon$) of the side reaction current density ($J_{sd}$) under ideal conditions during the (a) 1-C constant current charge and discharge (CCCD) cycle, (b) 10-C CCCD cycle, and (c) urban dynamometer driving schedule (UDDS). The relative estimation error is bounded within $\pm 2 \times 10^{-4}\%$, $\pm 1\%$, and $\pm 0.3\%$ for the 1-C CCCD cycle, 10-C CCCD cycle, and the UDDS cycle, respectively. This result shows that the side reaction current density can be accurately estimated for all three tested scenarios under ideal conditions.**

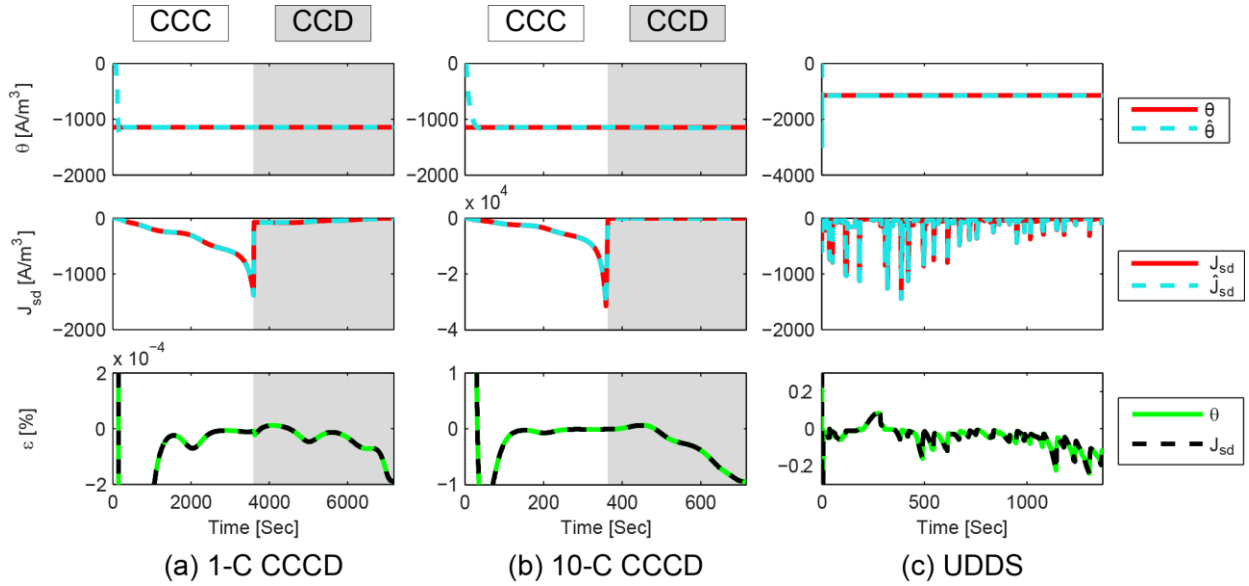


**Figure 3: Comparison between the estimation results of the side reaction current density under the existence of state of charge estimation error during the 1-C constant current charge mode using two estimation algorithms: retrospective-cost subsystem identification (RCSI) and the two-step filter (TSF). J_sd, θ, and d denotes the side reaction current density, the health subsystem parameter, and the SOC estimation error, respectively. TSF estimate shows great improvement in terms of estimation accuracy compared with RCSI.**

For estimating the side reaction current density under the existence of SOC estimation error, we developed a new estimation algorithm, the two-step filter (TSF), which is a modification of RCSI. The TSF can estimate not only the side reaction current density and the health subsystem parameter as RCSI, but also the SOC estimation error. Figure 3 shows the comparison between the estimation results of the side reaction current density during the 1-C constant current charge mode under the existence of state of charge estimation error using RCSI and TSF. While the relative estimation errors of the side reaction current density and the health subsystem parameter using RCSI remains above 60%, the relative estimation errors of the side reaction current density, the health subsystem parameter, and the SOC estimation error are converging to 0% with TSF. This result shows that TSF (1) improves estimation accuracy greatly compared with RCSI and (2) can also be used to correct SOC estimation.

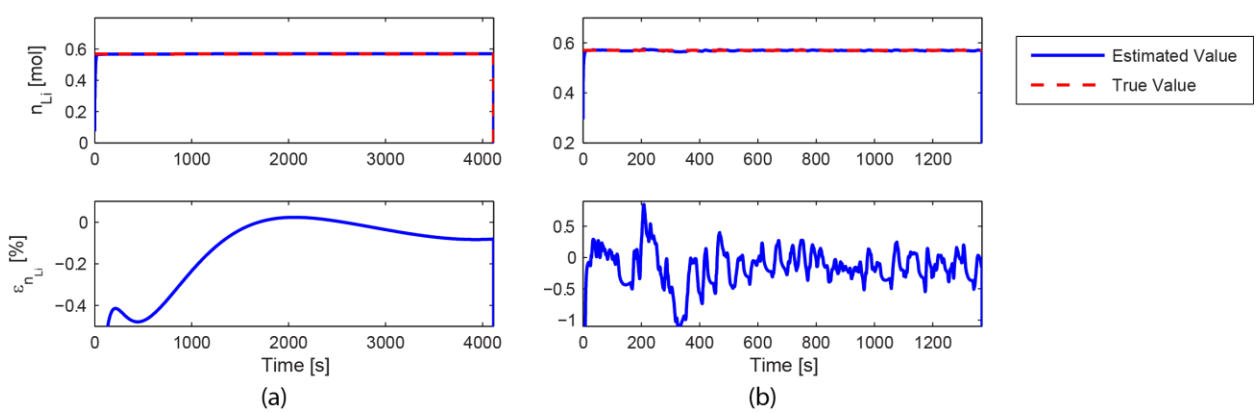


**Figure 4: Estimate and relative estimation error (ϵ_(n_Li )) of the number of cyclable Li-ions (n_Li) under ideal conditions during the (a) 1-C constant current charge (CCC) mode and (b) urban dynamometer driving schedule (UDDS). The relative estimation error is bounded within [-0.5,0.1]% and [-1.1,0.9]% for the 1-C CCC and UDDS modes, respectively. This result shows that the number of cyclable Li-ions can be accurately estimated for both tested scenarios under ideal conditions.**

With the side reaction current density being sensitive to non-ideal conditions, we further explored another SOH indicator, the number of cyclable Li-ions, which is more robust to non-ideal conditions. We also expanded our research to explore one of the currently most popular EV/HEV battery chemistries, namely, $LiMn_2O_4$ (LMO) mixed with other Li-compounds. This new battery chemistry also benefits estimation of the number of cyclable Li-ions by improving its identifiability. Figure 4 shows the estimation results of the number of cyclable Li-ions in LMO-mixture batteries under ideal conditions during the (a) 1-C CCC mode and (b) urban dynamometer driving schedule (UDDS). The relative estimation error

is bounded within $[-0.5, 0.1]\%$ and $[-1.1, 0.9]\%$ for the 1-C CCC and UDDS modes, respectively. This result shows that the number of cyclable Li-ions can be accurately estimated for both the tested scenarios under ideal conditions.

The above results show the simulation results of estimating all three electrochemical variables under ideal conditions. Results have also been obtained under various non-ideal conditions such as measurement noise, SOC estimation errors, and modeling errors. For brevity, the results under non-ideal conditions are not included in this report. Details about these results can be found in [2] and [5].

## Future Plans

Use the developed algorithm with laboratory cycling data.

## Expected Outcomes

- A battery SOH monitoring algorithm that works with noninvasive measurements and can be applied to monitor battery SOH as the battery is in use
- Analyses of robustness of the algorithm and techniques for the algorithm to work under non-ideal conditions
- Experimental validation of the algorithm

## References/Publications


1. A. D'Amato, J. Forman, T. Ersal, A. A. Ali, J. L. Stein, H. Peng, et al., "Noninvasive battery-health diagnostics using retrospective-cost identification of inaccessible subsystems," Proceedings of ASME Dynamic Systems and Control Conference, pp. 299-307, Fort Lauderdale, FL, 2012.
2. X. Zhou, T. Ersal, J. L. Stein, and D. S. Bernstein, "Battery health diagnostics using retrospective-cost system identification: Sensitivity to noise and initialization errors," Proceedings of ASME Dynamic Systems and Control Conference, pp. V003T42A004 (10 pages), Palo Alto, CA, 2013. (Best Student Paper Finalist)
3. X. Zhou, T. Ersal, J. L. Stein, and D. S. Bernstein, "Battery State of Health Monitoring by Side Reaction Current Density Estimation via Retrospective-Cost Subsystem Identification," Proceedings of ASME Dynamic Systems and Control Conference, pp. V001T19A002 (10 pages), San Antonio, TX, 2014. (Best Student Paper Finalist)
4. X. Zhou, T. Ersal, J. L. Stein, and D. S. Bernstein, "A subsystem identification technique towards battery state of health monitoring under state of charge estimation errors," Proceedings of the American Control Conference, pp. 1812-1817, Chicago, IL, 2015.
5. X. Zhou, D. S. Bernstein, J. L. Stein, and T. Ersal, "Battery state of health monitoring by side reaction current density estimation via retrospective - cost subsystem identification", Journal of Dynamic Systems, Measurement, and Control (in review).
6. X. Zhou, J. L. Stein, and T. Ersal, "Battery state of health monitoring by estimation of the number of cyclable Li-ions," Proceedings of ASME Dynamic Systems and Control Conference, Minneapolis, MN, 2016 (in review).
7. Publications in Preparation
8. X. Zhou, D. S. Bernstein, J. L. Stein, and T. Ersal, "A subsystem identification technique for battery state of health monitoring under state of charge estimation errors," in preparation.
9. This paper is the journal version of [4]. Instead of the linearized battery model that is used in [4], [7] uses a nonlinear battery model to simulate the true battery.
10. X. Zhou, J. L. Stein, and T. Ersal, "Battery state of health monitoring by estimation of the number of cyclable Li-ions," in preparation.


This paper is the journal version of [6] with the following improvements: (1) a higher fidelity battery model is used to better capture battery charge and discharge dynamics; and (2) the parameterization of the battery model is included to examine the influence of different parameter sets on estimation accuracy.

# Cost-Effective Lightweight Materials

***Cooperative Project (U.S.)***


## U.S. Research Team Lead

- Jose M. Castro, The Ohio State University
- Rebecca Dupaix, The Ohio State University
- Ziwei Zhao, The Ohio State University

## U.S. Partners

- The Ohio State University
- Nano Materials Innovation

## China Research Team Lead

- • Languang Lu, Tsinghua University

## China Partners

- Tsinghua University


## Research Objective

The objective of this project is to develop cost-effective, lightweight structures for next-generation vehicles. A key barrier is the balance of processability and performance of the new composites. This project will shift focus from the previous research of nano-enhanced FRPC's to the application of the new composites to a new hybrid structural joining method. The hybrid joining method will be incorporated with the previous nanoparticle research results to a number of prototype structural joints.

## Technical Approach

- Use spray with vacuum to spray CNF–acetone solution into glass fiber preforms to enhance their bulk properties; use preform to fabricate CNF-enhanced FRPCs in the vacuum-assisted resin transfer molding (VARTM) process; adding CNFs in composites increases their mechanical performance
- Use vacuum filtration with water as an environmentally friendly alternative approach to the acetone base approach
- Fabricate nanopapers using functionalized nanoparticles (Polyaniline); use the nanopapers with the VARTM process for improvement of surface properties
- Measure mechanical properties, electromagnetic interference (EMI) shielding effectiveness, and surface sand abrasion resistance to evaluate their performance
- Measure the permeability of glass fiber with/without CNFs to evaluate the processability; measure permeability of nanopapers

## Recent Progress

Discussions were begun with Dr. Farhang Pourboghrat regarding the manufacturing of the joint bodies using compression molding techniques. Work on fundamental aspects of the joining system is continuing. Preliminary gateway tests of the adhesive system have been completed and have led to appropriate bounds for a number of the system factors under test. Results have been applied to a DOE model to generate new test matrix to investigate all relevant factor interactions in order to finish testing of the adhesive system.

Baseline work on fundamental aspects of the joining system is continuing. Further discussions with Dr. Soheil Soghrati resulted in the development of a set of adhesive tests in order to provide data necessary to develop a higher level FE model. The new data will also support the development of a 3D model. We have designed a test protocol to identify the best silane based coupling agent in order to increase the adhesion between the epoxy and glass spacer beads. We have started the process to investigate the effects of various atmospheric plasma treatments for improved adhesion. Surface analysis using XPS and AFM will be used to quantify the effects of plasma treatments. Completion of additional tests will end the preliminary research into the adhesive system.

The team:

- Completed the gateway adhesive testing program.
- Designed a final test matrix using Design of Experiments principles to complete the research in the adhesive system.
- Baseline tests of fundamental joint strength were completed along with tests of volume % of glass beads in standard double lap shear coupons.

## Significant Results

- Mechanical properties of nano-enhanced glass reinforced composites were measured; tensile strength increased about 20% (Figure 1)
- The permeability of fiber preform with nanoparticles was measured (Figure 2)
- EMI shielding effectiveness of nanopaper and CNF spray on glass (Figure 3)
- Permeability of CNF nanopaper (Figure 4)
- Mechanical and fatigue properties of nanopaper-enhanced composites (Figure 5)
- Two journal papers (*Polymer Composites*) and several conference presentations

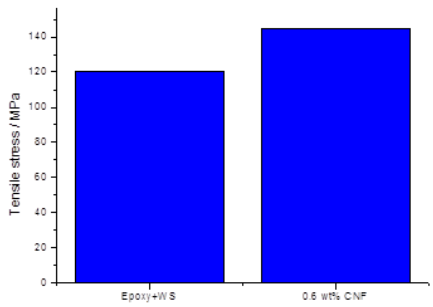


**Figure 1. Tensile strength increase of glass fiber composites with/ without CNFs.**

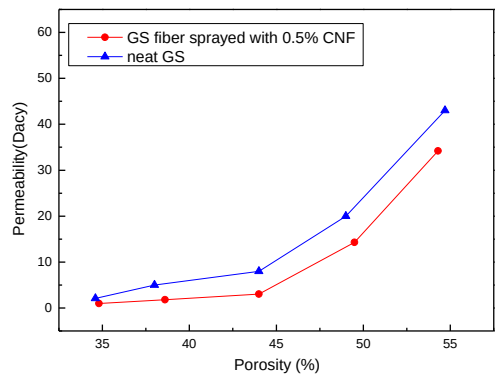


**Figure 2. Permeablity decreases of glass fiber with/without CNFs.**

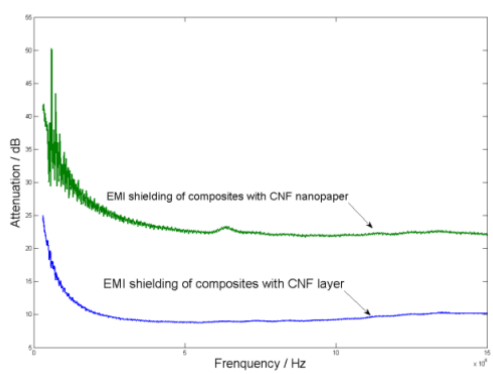


**Figure 3. EMI shielding effectiveness of composites with nanopaper and CNF layer.**

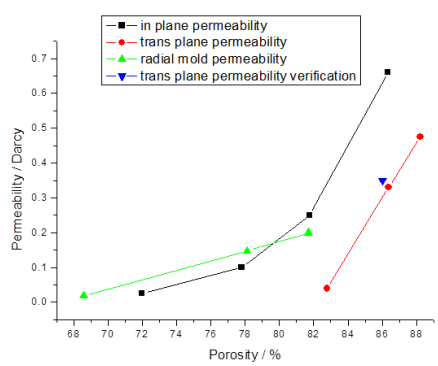


**Figure 4. Permeability results of CNF nanopaper.**

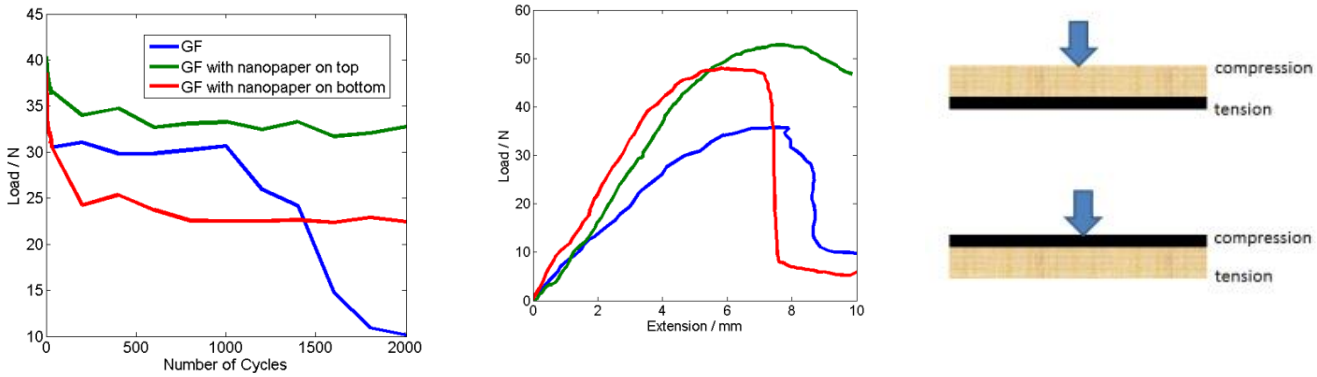


**Figure 5. Effect of nanopaper on fatigue and flexural properties.**

# Joining Multi-Material Structures – Vaporizing Foil Actuator Approach

***Cooperative Project (U.S.)***


## U.S. Research Team Lead

- Glenn S. Daehn, The Ohio State University
- Steven Hansen, The Ohio State University

## U.S. Partners

- The Ohio State University
- General Motors
- University of Michigan
- Oak Ridge National Laboratory


## Research Objective

This project uses an integrated experimentation and modeling approach to establish a new method of developing very high pressures and speeds in sheet metal to provide to several manufacturing operations, including developing flyer speeds high enough for collision welding of aluminum and steel sheets with few to no heat-affected zones. Such a joint morphology could help produce multi-material structures with reduced weight and improved crash resistance; stiffness; and noise, vibration, and harshness characteristics.

Electrically vaporized foil actuators (VFA) are capable of producing a strong pressure pulse that can be harnessed for rapid metalworking applications such as solid-state joining and high-velocity forming. Our method has proven applicable for the sizes of material relevant to automotive construction, being able to accelerate millimeter-scale sheet metal to over 1 km/s within a few millimeters.

The team has been investigating the parameters of the VFA process that affect the magnitude and distribution of the pressure pulse resulting from vaporization. These include varying energy input characteristics as well as varying foil dimensions from ~10 mm to over 200 mm in length.

## Technical Approach

- Electrically vaporized thin metal conductors have been used to drive aluminum sheets on the scale of 1 mm for the purpose of small-scale, lab- and industry-safe collision welding. The process uses the pressure pulse from the sudden expansion of the vaporized metal to controllably drive aluminum to velocities in excess of those needed to collision weld. The project has made 1.5 cm wide joints in lengths from 1.5 cm to over 15 cm
- Instrumented experiments including velocity measurement are used to determine the predictability and repeatability of this method for use as a joining tool
- Key variables to control are the velocity and collision angle, which must vary depending on the material pair and their thicknesses. Control of these parameters is essential to produce a strong joint free of voids or intermetallic layers

## Recent Progress

**Q3 2015**

The energy deposition into the foil relative to the energy necessary for sublimation of the foil's mass is linearly proportional to the magnitude of the pressure pulse. Recently, experiments were performed showing that a fast current rise time is critical to increasing the pressure pulse from vaporization. By using identical foil actuators on two capacitor banks having different current rise times, charged to the same energy, it was seen that more than double the energy was

deposited into the foil on the faster bank compared to the slower bank. The resulting velocity of a driven flyer plate was 50% higher for the faster bank.

- Experiments forming 1 mm thick 6061-T6 sheets into perforated steel plates (perforations of ~1/32”) have been performed to show that the pressure distribution and magnitude depends on the energy deposited relative to that necessary to sublimate the mass of the foil, as well the distribution of that mass. Given the same input energy, a larger vaporized mass of foil not only produces lower pressure over its surface area, but also less evenly distributed pressure when the energy deposited is lower than that energy necessary to sublimate the total foil mass. More even pressure distribution is reached at greater foil lengths by tailoring the foil cross-section to reduce vaporizing mass.
- Team is prepared to create standardized joints to compare to the other methods put forward in this thrust area, pending selection of the materials and geometry of the joint.

**Q2 2015**

VFA impact welds and interference joints have been successfully demonstrated ranging from 12 mm diameter circular welds analogous to a spot weld, to longer continuous sheet-to-sheet solid-state welds, up to 150 mm long, mostly using AA6061-T6 and DP980 steel in addition to AA6061-T4 and AA3003. However, impact welds approaching 150 mm have not been successful to date with 6061-T6, likely indicating that the energy input possible with this setup is not sufficient to give the flyer high enough velocity. Alternate foil thicknesses and configurations are being assessed.

- Experiments driving 6061-T6 sheets into perforated steel plates (perforations of ~1/32”) show that the pressure distribution over the 150 mm length foils appears largely uniform, with localized higher pressure at the electron source side. The team has access to PVDF sensors also, which will allow us to observe the development and magnitude of pressure over different areas around the foil.

**Q1 2015**

The VFA joining-by-forming method was tested using AA6061-T6 as the driven workpiece and DP980 steel as the stationary workpiece. Successful joints were made spanning 115 mm.

- An iteration on the spot-type VFAW technique is being developed, in which the standoff distance necessary for flyer travel is formed into the flyer sheet as a raised feature. The result is a cleaner-looking joint in which no standoff material is trapped and in which the bulk of the flyer and target sheets are in contact.
- Using the longer VFA fixture, seam joints up to 15 cm have been created between various aluminum alloys, primarily using AA6061. New geometries for longer foils were investigated with partial success using AA6061-T6 flyers and targets; however, more development is needed. Multi-channel velocimetry is possible in the smaller VFA fixture, but still must be implemented in the longer VFA fixture in order to understand the uniformity of pressure generation across varied foil lengths.
- Coach-peel testing of AA6061-T6/AA5052 patch welds universally showed failure outside the joint in the weaker 5052 parent sheet. Microhardness traverses indicated that no heat-affected zones were present in the material surrounding the weld interface.

**Q42014**

- Experiments using VFA to produce spot weld-like joints were successful, creating clean-looking joints, even at an early experimental stage. Longer patch-shaped welds were produced at various input energies using the same material stock for comparison. Coach-peel type tests of all samples failed outside the joint in the 5052 parent sheet. Microhardness traverses indicated that no heat-affected zones were present in the material surrounding the weld interface.
- Using the longer VFA fixture, seam joints up to 15 cm have been created between various aluminum alloys, primarily using AA6061. However, the joints at the longest length attempted (15 cm) were inconsistently bonded along the length of the interface. Therefore, some refinement of the method is necessary. Going forward, multi-channel velocimetry will be used to understand the uniformity of pressure generation across varied VFA lengths.

## Significant Results

This project established many important elements.

- The VFA approach has been shown to be very reproducible, and a scientific basis is being developed for understanding this
- Key experiments are focused on developing an understanding of the size of weld that can be developed
- Similar and dissimilar metal sheets can be joined with overlapping joints strong enough to break in the weaker parent material. Because of the nature of collision welding, heat-affected zones and resulting brittle intermetallic compounds can be minimized or eliminated, and the properties of age-hardened material can be maintained
- Experiments using velocity-measurement probes showed that the movement of the workpiece can be predictably controlled via input energy, allowing for high-quality joints to be made reproducibly

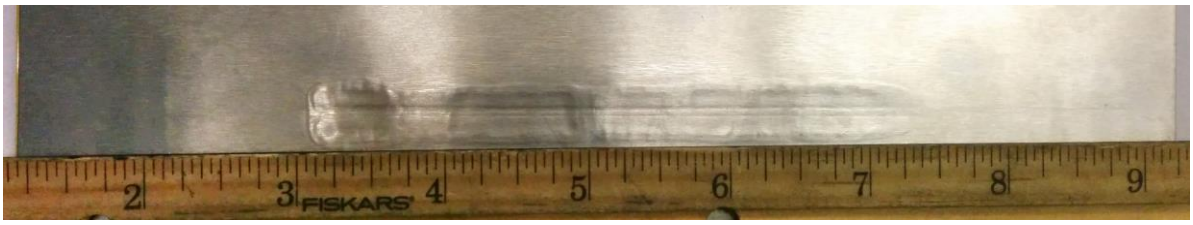


Figure 1. Experimental joint over 10 cm using 0.5 mm thick AA6061-T6.

## Future Plans

This method (termed "vaporizing foil actuator welding" or VFAW) shows promise as a new tool for impulse metalworking, including the formation of strong dissimilar-metal joints in lightweight structures. If and when specific geometric locations in automotive structures that will make use of these methods to join dissimilar metals are identified, focused research can be carried out to validate this for the particular joint configuration and set of materials of interest.

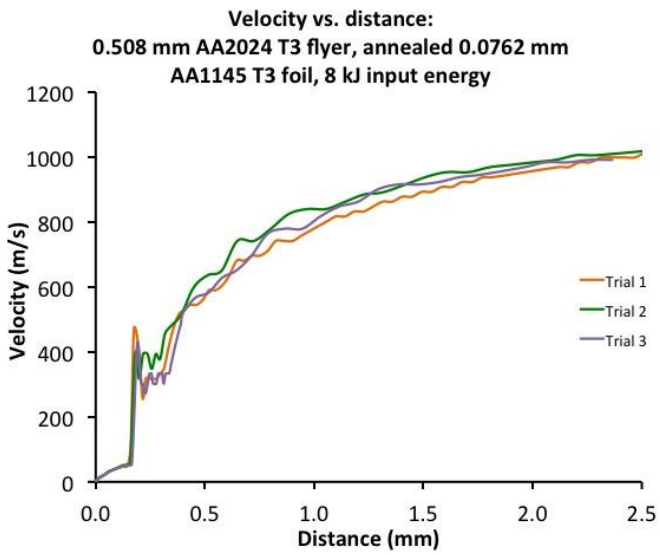


Figure 2. Velocity in repeated experiments using 0.508 mm AA2024-T3 sheets.

## Recent Publications and Patents

- ASME Journal of Manufacturing Science and Engineering: "Impact Welding of Aluminum Alloys 6061 and 5052 by Vaporizing Foil Actuators: Heat-Affected Zone Size and Peel Strength."
- Xun Liu, Shuhuai Lan, Jun Ni, 'Thermal mechanical modelling of the plunge stage during friction stir welding of dissimilar Al 6061 to TRIP 780 steel', Journal of Manufacturing Science and Engineering, under review.
- Patent: U of M Ref. No. 5675; HDP Ref. No. 2115-005675-US, Hybrid Friction Stir Welding for Dissimilar Materials Through Electro-Plastic Effect, Xun Liu, Shuhuai Lan, Jun Ni, application filed

# Electrically Assisted Friction Stir Welding for Joining Dissimilar Materials

***Joint Project***


## U.S. Research Team Lead

- Jun Ni, University of Michigan

## U.S. Partners

- University of Michigan

## China Research Team Lead

- Xinmin Lai, Shanghai Jiao Tong University

## China Partners

- Shanghai Jiao Tong University


## Research Objectives

The objective of this project is to develop high-quality and economical joining processes between dissimilar lightweight materials, especially for aluminum alloys and Advanced High Strength Steels. Electro-Plastic Effect (EPE) is incorporated into traditional Friction Stir Welding (FSW) process for reducing mechanical welding force, enlarging process window as well as improving joint quality.

## Technical Approach

- Study of Electro-Plasticity and evaluate its effectiveness on TRIP steel
- Experimental study on Friction Stir Welding (FSW) process of Al 6061 to TRIP steel
- Thermo-mechanical modeling on dissimilar FSW process
- Development of electrically assisted FSW experimental system
- Study of electrically assisted FSW process for joining dissimilar materials

## Significant Results

Figure 1 shows the stress-strain curves of the TRIP steel under different pulse conditions. At each pulse, the flow stress will reduce and then return back to the original stress-strain curve after the pulse is stopped. The current density in Figure 1(b) is twice that of current density in Figure 1(a) while the pulse length is ¼. The highest temperature measured in the two conditions are therefore the same. A higher stress drop in the larger current density condition shows that the electrical current can directly soften the TRIP steel in addition to the thermal effect, which means the electro-plastic effect exists on this type of advanced high strength steel. Further microstructure analysis showed the electrical pulses can retard the martensitic phase transformation process involved in plastic deformation of TRIP steel.

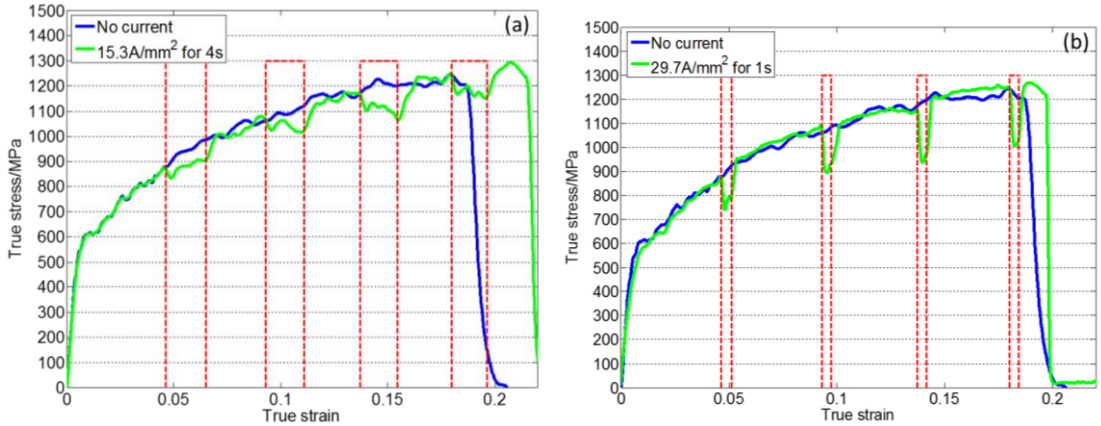


Figure 1: True stress and true strain curves under different test conditions: (a) 15.3 A/mm$^2$ with 4s (b) 29.7 A/mm$^2$ with 1s

Friction stir welding is then performed on Al 6061 to TRIP steel under different process conditions. Three failure modes were identified during tensile tests of weld specimen, as shown in Figure 2. The maximum joint strength in the necking condition can reach 85% of the base aluminum alloy.

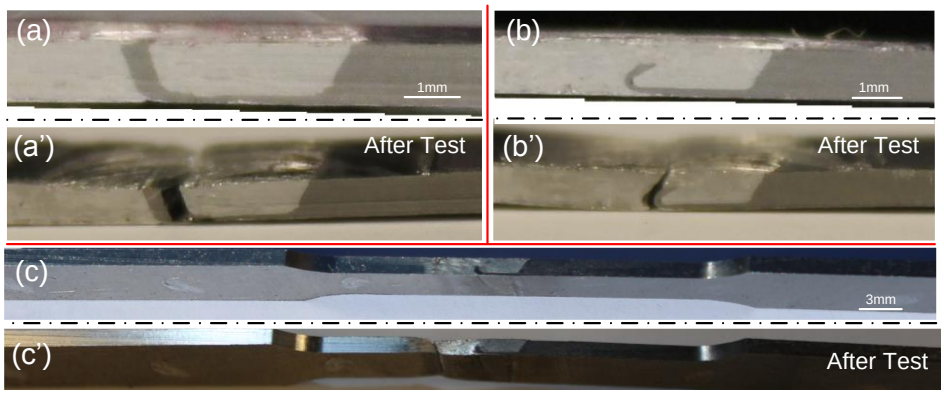


**Figure 2: Three failure modes: (a) Cracks at the inside boundary of steel strip; (b) Cracks at the outside boundary steel strip; (c) Failure in the aluminum heat affected zone**

Joint strength and microstructure are related to the measured mechanical welding force and temperature distribution. Higher rotating speed and larger tool offset can elevate the overall temperature in the weld and reduce the required axial and lateral welding force, which accordingly influence the composition of the formed IMC layer in the advancing side. Under a low rotational speed and small tool offset, FeAl is formed instead of $Fe_3Al$, which is formed under all other conditions. Welding speed in the studied range has an insignificant effect on mechanical welding force, temperature distribution or material strain rate and is not a sensitive factor for the IMC layer composition. However, higher welding speed can reduce the thermal cycle length and the interlayer thickness. Microstructure along the Al-Fe interface at the weld cross section is shown in Figure 3.

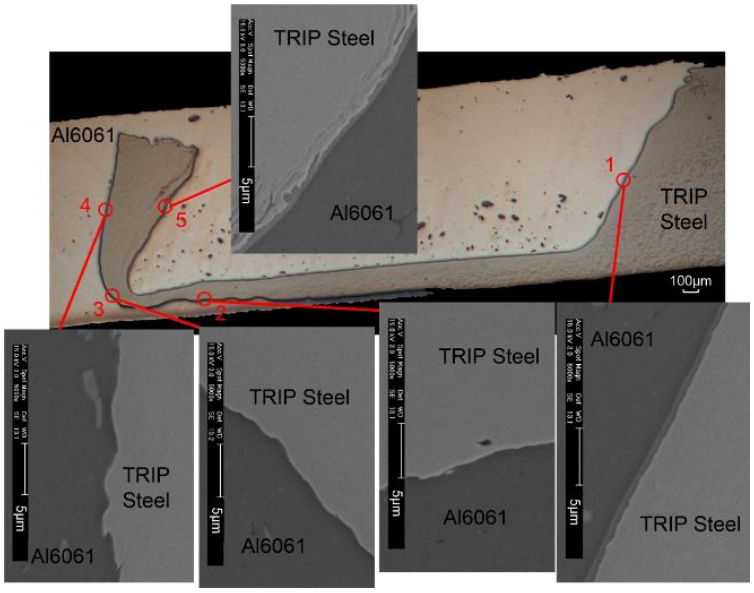


**Figure 3: Al-Fe interface of the joint section with fracture path along the outside boundary of steel strip**

In order to further understand the mechanisms and process physics involved in friction stir welding of Al 6061 to TRIP steel, both analytical and numerical models are developed. For the plunge stage modeling, the field variable was introduced to identify the regions of steel and aluminum and define the generalized material properties. A separate set of governing equations were also developed at the two materials interface to account for discontinuities. The corresponding numerical analysis was performed in the FEA software ABAQUS. Overall the calculated axial force and material distribution correlated well with experimental results, as shown in Figure 4. The model can also capture the material distribution at different plunge depths, as shown in Figure 5 for the condition with the tool offset of 1.03mm.

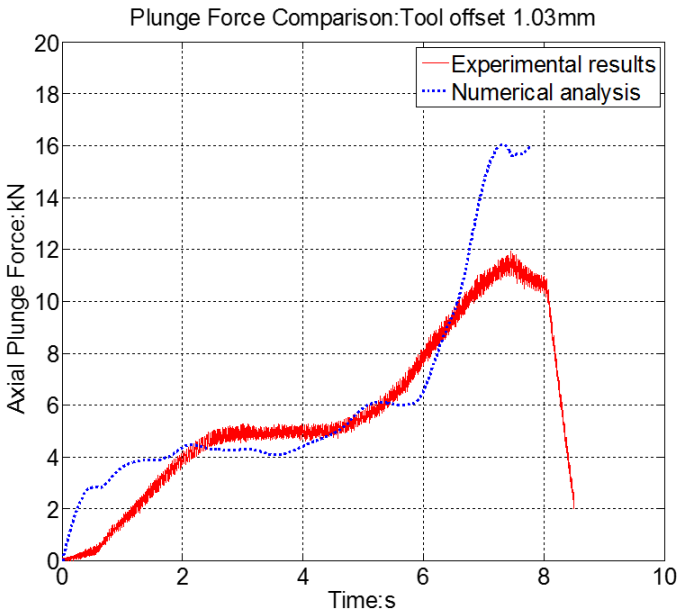


Figure 4: Comparison of axial plunge force between experimental and numerical results with tool offset of 1.03mm

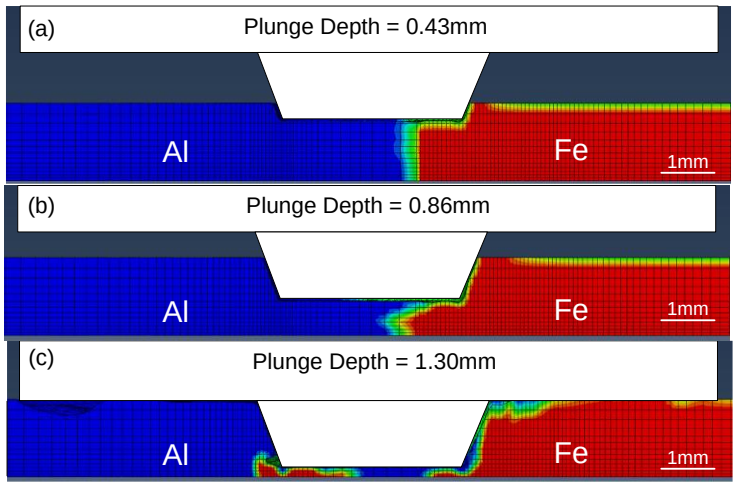


Figure 5: Material distribution at different plunge depths under tool offset of 1.03mm

The stable welding stage was modeled based on Eulerian formulation. Multiple phase flow theories with volume of fluid method were used for deriving analytical formulations, which were further implemented into the FLUENT software for numerical analysis. At the tool-workpiece contact interface, a frictional shear stress boundary yielded a much more reasonable material distribution compared with the velocity boundary condition. The model can capture the macrostructure feature of embedded steel strip in aluminum side, as shown in Figure 6. On the tool contact region, the calculated material velocity was significantly smaller than that of the tool, which indicated a prevailing slipping boundary condition. The predicted temperature profile and thermal history curves generally agreed well with experimental results under different weld conditions, as shown in Figure 7.

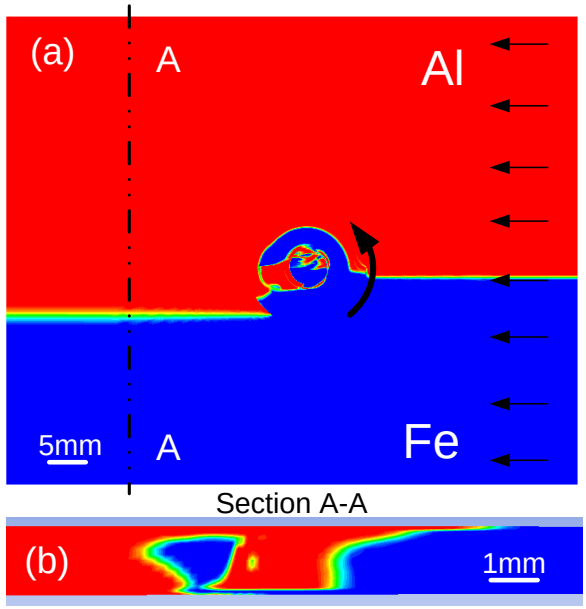


Figure 6: Material distribution in the condition of a smaller tool offset 1.03mm: (a) Workpiece top surface; (b) A-A section perpendicular to weldline

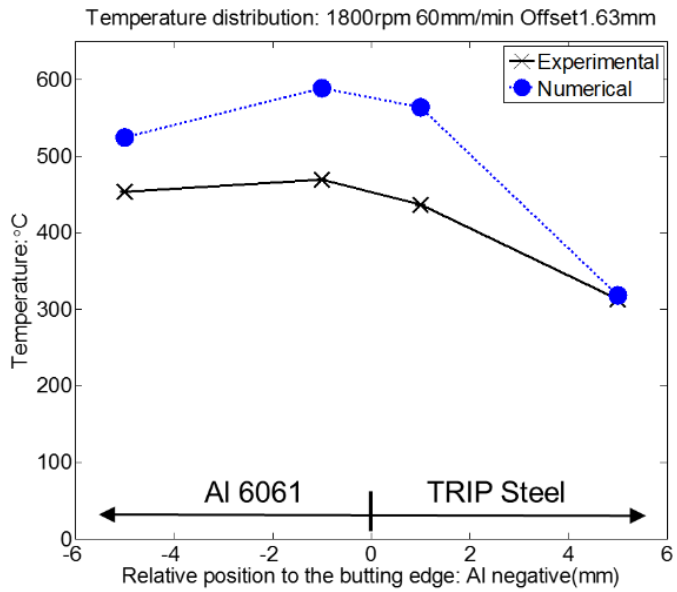


Figure 7: Validation of temperature distribution on bottom surface

Finally an electrically assisted friction stir welding system is designed and developed, as shown in Figure 8. The FSW tool is only passively involved in the electrical circuit and the system can be applied to thin sheet metals of various sizes. Based on this experimental system, plunge stage of FSW was studied for both aluminum alloy Al 6061 and TRIP 780 steel respectively. An effective reduction of the axial welding force is obtained with a good repeatability. Associated Joule heating effect for steel is considered from an additional preheating test. Apart from the thermal softening, approximately 2/3 of the force reduction can be attributed to the direct softening from electro-plastic effect, as shown in Figure 9. The electrical current is then applied to the entire welding process for Al 6061 to TRIP steel. The axial welding force was consistently reduced under various weld conditions, as shown in Figure 10. Based on the temperature measurements, the force reduction came from synergic effects of electro-plasticity and Joule heating. The first factor was more significant when the rotating speed was small or the tool was less shifted to aluminum. Regarding the joint strength, the Al-Fe interface of the welds is examined with SEM and the electrical current shows to enhance the formation of the thin intermetallic layer and micro-interlock features.

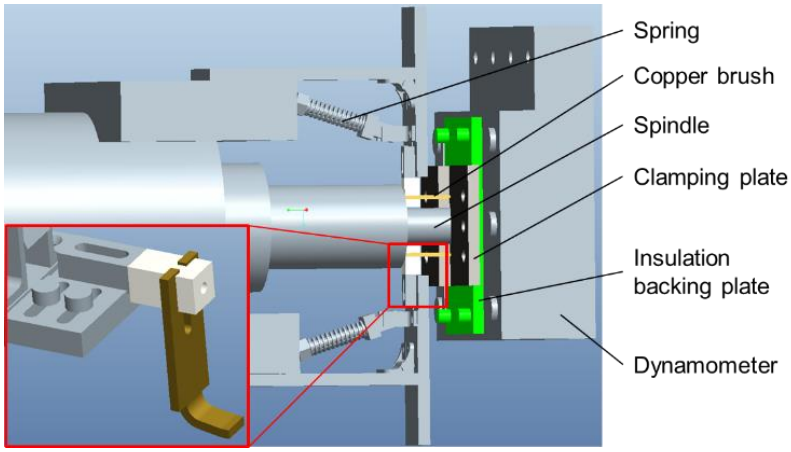


Figure 8: CAD design of the electrically assisted friction stir welding system

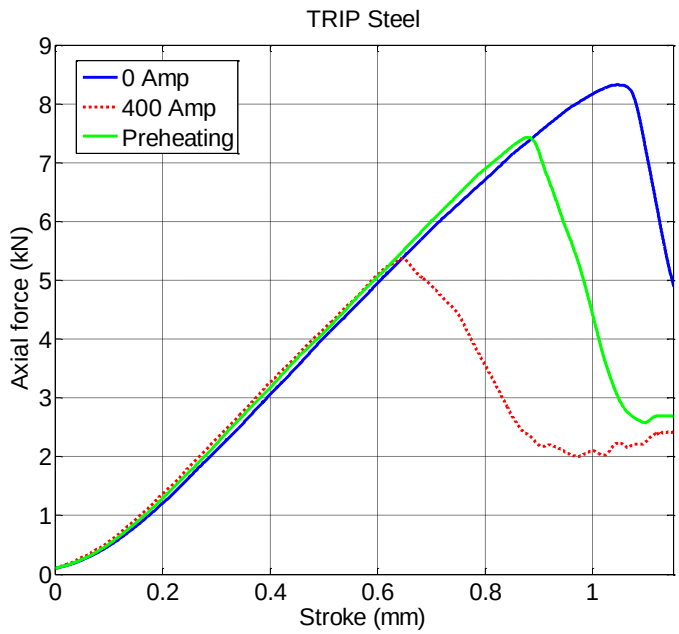


Figure 9: Comparison of axial force for TRIP 780 steel considering the thermal effect

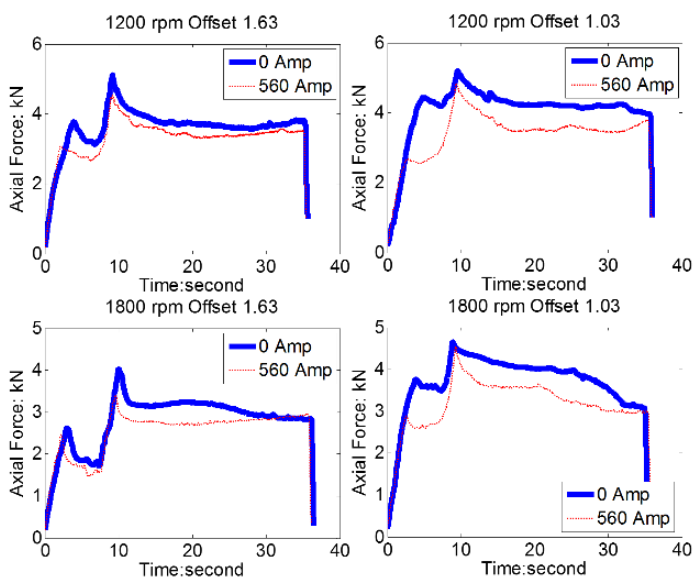


Figure 10: Axial force comparison under various processing conditions

## Future Plans

- Design and improve friction stir welding tool to eliminate the stirred over steel strip as shown in the joint cross sections
- Study interfacial structure for dissimilar material joint strength
- Investigate the corrosive issue of Al-Fe joint

## Expected Outcomes

- The electro-plastic effect is observed on one type of advanced high strength steel, TRIP 780/800
- Successful joints between Al 6061 alloy and TRIP steel are able to be achieved from friction stir welding process and the highest joint strength reaches 85% of the base aluminum alloy and the tensile specimen failed at the heat affected zone of aluminum; A thin intermetallic layer with the thickness of around 1 µm is formed at the Al-Fe interface in the advancing side
- Thermo-mechanical models are developed for the dissimilar FSW process and the models can capture welding force, material and temperature distribution
- The developed electrically assisted friction stir welding system is shown to be capable of applying high density electrical current into the FSW process. The axial welding force is consistently reduced under various weld conditions

# Hybrid Materials Interface Increased Strength Method and Modeling

***Cooperative Project (U.S.)***


## U.S. Research Team Lead

- Michael Thouless, University of Michigan

## U.S. Partners

- Peter Fritz (Eaton Corporation)

## China Research Team Lead

- • Languang Lu, Tsinghua University

## China Partners

- Tsinghua University


## Research Objective

The objectives are as follows:

- To demonstrate a methodology for modeling the bonding of hybrid materials, such as composites and metals, with a focus on demonstrating its capability for design and capturing the effects of surface modification
- To work with industry to implement an approach to evaluate and design hybrid joints for lightweight materials

## Technical Approach

- Identification of appropriate thermoset composites and metals and adhesives for bonding, and surface treatments
- Identification of suitable bonded hybrid geometries to measure cohesive parameters in Mode-I and Mode-II conditions
- Use of these cohesive parameters in a finite element model (FEM) to predict the behavior of validation geometries, and to compare these predictions to observations

## Recent Progress

**Q3 2015**

CERC researcher determined an accurate way to measure the elastic modulus and Poisson's ratio of the substrate materials using DIC. This was unexpectedly challenging for stiff materials, and was eventually resolved by using 3-D DIC.

Additional tests have been run of the symmetric steel double-cantilever beam (DCB), asymmetric DCB (with equal beam thicknesses), the “more symmetric” asymmetric DCB (with the composite beam twice as thick as the steel beam), and stubby-armed short lap-shear joints. The DCB tests were run again to find determine the adhesive’s variability. The previous lap-shear experiments had long arms that stored enough strain energy to cause catastrophic interface failure which did not allow for the measurement of the mode-II traction-separation law. Coupling the use of stubby-armed lap-shear specimens and slowing down the displacement rate of the tests allowed for the softening portion of the mode-II traction-separation to be measured. The experiments are currently being analyzed.

**Q2 2015**

The team is measuring the elastic properties of the composite which are required to analyze the experiments and to do accurate FEM calculations. Unfortunately, measuring simple tensile properties of steel using DIC turned out to be less easy than expected.

The team has continued analyzing results for hybrid system, including a second DCB geometry with a different thickness of composite arm.

One result of particular interest was to use our mode-I and mode-II cohesive laws to back out the phase angle (measure of mode-mixedness) as a function of distance from the crack tip. This has never been done before. Interestingly, it showed the trend predicted some years ago of an asymptotic value as the crack tip is approached. Furthermore, this was the first time that the phase angle has been measured directly for a bi-material system. It has only been inferred before. The team

made these measurements for two different versions of the DCB, showing how a geometry change affected the measured phase angle.

A fundamental problem with LEFM is that a useful definition of a phase angle is not possible with bi-material systems, except under the very special case where one of the Dundurs' parameters (⍰) is 0. No one has ever compared the predictions between this approximation from LEFM and the actual measurements. Here it was interesting to note that the first DCB geometry had a phase angle of 30±2º, compared to an LEFM result of 29.6º, whereas the second geometry has a phase angle of 13±2º, compared with an LEFM prediction of 7.3º. There is no reason why agreement should be expected, so it is interesting that they were reasonably close here. It was also of interest to observe that there might have been a small change in the phase angle with loading. This has been predicted as a possibility, and will need to be explored further.

Still to be done is a numerical analysis of these phase angles using the measured cohesive laws.

**Q1 2015**

In this period of time, we have identified and resolved many of the problems associated with using DIC to back out cohesive laws, allowing us to start get meaningful results for two geometries. More generally, we have developed an understanding for the limitations of the optical techniques we are using, and are now getting high-quality data with about 1 micron of resolution. We have also developed techniques to correct for rigid-body rotations, which are of significance for these problems.

Using a symmetric steel double-cantilever beam (DCB) system, the mode-I traction-separation law was backed out for a new adhesive (Betamate) using beam rotation and crack-tip measurements from digital image correlation (DIC). This was determined by plotting J vs. the crack-tip opening displacement and then differentiating. Implementing this traction-separation law into a FEA code, consistent agreement was found between the experimental results and the numerical calculations. There was also a general consistency between all the results obtained for this model system, indicated a good reliability of the data.

A second purpose for analyzing the symmetric DCB system was to verify the program developed by the Daly group (UM) to evaluate J-integrals ina fracture problem. Even though we had excellent displacement data, and a well-controlled system, multiple trials using the script did not generate consistent results. This indicates a problem with the program which we will try to address at a later date.

Asymmetric lap-shear joints with a very short ligament were produced using steel and G-10 Garolite composite and the Betamate adhesive. DIC was used to verify uniform shear displacements across the bonded interface, which then allowed for direct measurement of a portion of the mode-II traction-separation law.

Asymmetric DCB samples (using steel and G-10 Garolite composite) were also produced from analysis using the Betamate adhesive. These are mixed-mode geometries, from which we verified we could extract JI by subtracting the mode-II component from the total value of J determined from the loads and remote rotations. We verified that the resultant values of JI were consistent with the pure-mode-I results

**Q4 2014**

Asymmetric double-cantilever beam and single lap-shear joint samples using the old adhesive (SpaBond) were analyzed using digital image correlation (DIC). Along with the low toughness of the adhesive, the uncertainty is determining the crack-tip location caused a low confidence in the determined mode-I traction-separation law. The presupposed material properties of the composite were also questioned when theoretical calculations did not match experimental data. Samples have been made to begin testing the composite's material properties. Thin tensile samples were also made using the old adhesive. However, since testing has moved on to a tougher adhesive, the analysis of this data has been put on hold. These thin tensile samples may be revisited in the future as a way to directly measure the mode-I traction-separation law.

As a first step towards verifying the J-integral script (it calculates the energy release rate from DIC) from the Daly group (UM), a homogenous steel/steel bonded DCB system was tested using a tougher adhesive. The tougher adhesive is important, because there was a concern that the initial testing with a more brittle adhesive was resulting in low strains that data was indistinguishable with noise. The DCB system was chosen because it has a known, analytical for the J-integral. Additionally, the symmetric DCB has also provided the opportunity for troubleshooting the experimental setup. During the analysis, it was determined that data became unsynchronized. This could explain some of the difficulty in analyzing previous asymmetric DCB and lap-shear joint specimens.

Samples using the new adhesive (Loctite) have been made and tested. The data will be passed along to Eaton once it has been analyzed.

## Significant Results

We have established a procedure to use digital-image correlation (DIC) to measure shear and normal displacements along adhesively bonded interfaces.

We have made two different types of bonded geometries with which to study the Mode-I and Mode-II traction-separation laws: the double-cantilever-beam (DCB) and lap-shear (LS) geometry.

The traction-separation law can be found by measuring the crack-opening displacements as a function of the *J*-integral. For the DCB geometry, this is done by monitoring the load and rotation of the load point. For the LS geometry, this is done by evaluating the *J*-integral for the geometry as a function of load by FEM. The cohesive tractions are found by differentiating the *J*-integral with respect to the crack opening. An alternative approach is to measure the traction-separation curves directly. This requires knowledge that the adhesive layer is being loaded uniformly, which can be validated with DIC measurements.

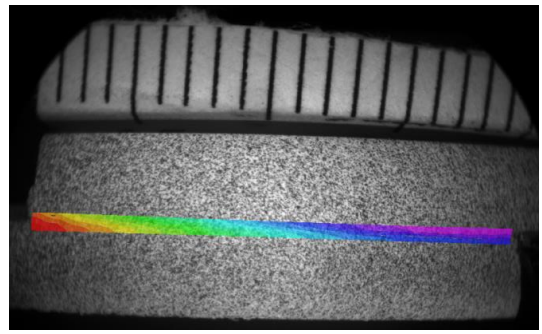

Figure 1. DIC image of interface, showing the speckle pattern used. The color gradient shows the (uniform) shear displacements across the lap-shear's interface.

The Mode-I and Mode-II traction-separation laws for the steel/ composite bonded hybrid system identified by Eaton is shown in Figure 2.

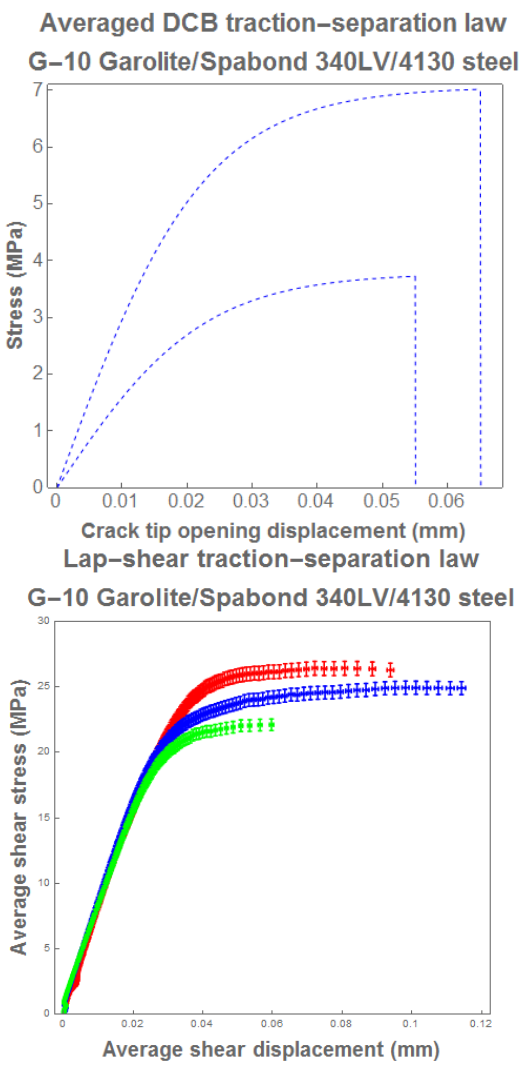


Figure 2. Mode-I and Mode-II traction-separation laws for a steel-Garolite composite system bonded by Spabond. The Mode-I toughness is 150-350 J/m² with a peak stress of 5±2 MPa. The Mode-II peak stress was determined to be 24±2 MPa. The variability of the critical displacement results in a large range of Mode-II toughness values between 900 and 2100 J/m².

## Future Plans

Unfortunately, the bonding protocol identified by the industrial sponsor, and used to produce the data above, did not produce uniform bonds. We have, therefore, had to modify this protocol to include glass beads to ensure a uniform bond. The techniques developed in 2013–2014 will be used to obtain new values for the adhesive, and for some new adhesives identified by the industrial sponsor.

Owing to the mode-mixedness of this system, we still need to determine the critical shear displacement required for the Mode-II traction-separation law. We plan to determine this by running lap-shear tests with longer ligaments, which are expected to have a smaller opening component at the crack-tip, thereby giving us a better lower bound of the critical shear displacement.

The team will validate these values by incorporating them in an FEM model of some laboratory test geometries, and then use the values to predict the behavior of a hybrid system, such as the gear-shaft assembly shown in Figure 3.

The team also plans to explore whether DIC approaches can be used to make direct measurements of the *J*-integral at the tip of a bonded crack, in geometries that would otherwise be difficult to evaluate.

- Expected Outcomes
- Demonstration of an effective numerical modeling method for hybrid lightweight structures

- A methodology for determining suitable test configurations to evaluate different bonding/surface treatments for hybrid systems such as steel/thermoset composite structures

## Presentations

- Presented a paper on the use of DIC to identify cohesive zones in hybrid systems at the ASME Mechanics of Materials Conference in Seattle (June 29, 2015): M. D. Thouless and J. A Gorman, Use of DIC to investigate cohesive zones in adhesive joints.

**Figure 3. Bonded hybrid gear-shaft assembly that will be analyzed as part of the validation approach.**

# Multi-Material Lightweight Body Subsystem and Vehicle Optimization

***Joint Project***


## U.S. Research Team Lead

- • Kazuhiro Saitou, University of Michigan

## U.S. Partners

- University of Michigan

## China Research Team Lead

- Qing Zhou, Tsinghua University
- Dafeng Jin, Tsinghua University
- Xinmin Lai, Shanghai Jiao Tong University
- Zhigang Yang, Tongji University

## China Partners

- Tsinghua University
- Shanghai Jiao Tong University
- Tongji University


## Research Objectives

The project is developing a methodology for economically integrating components made of lightweight materials in vehicle body structure with maximum weight reduction benefit. The materials under consideration are aluminum, magnesium, high-strength steels (HSSs) and ultra-high-strength steels (UHSSs), and composites.

## Technical Approach

- Determine deformation control and failure prevention strategy; exploration of innovative load paths, crash modes, and component layouts (Tsinghua University)
- Predict assembly dimensional variations: modeling of lightweight material process variations (Shanghai Jiao Tong University)
- Establish evaluation criteria for ease of manufacture and assembly: modeling of constraints for lightweight material processes (forming and joining) on part and joint geometry (University of Michigan)
- Enable multi-material optimization of vehicle body (sub)systems: a simplified body-in-white of a mini electric vehicle (EV) and an extended A-pillar of a midsize vehicle (all partners)

## Significant Results

The project team from Tsinghua University built a small electric vehicle (EV) model for crash analysis (see Figure 1) and studied influence of battery and occupant mass distribution on crash responses. The result showed that the change of center of gravity location had great influence on vehicle pitch direction. They also analyzed the influence of lightweight materials on vehicle crash safety.

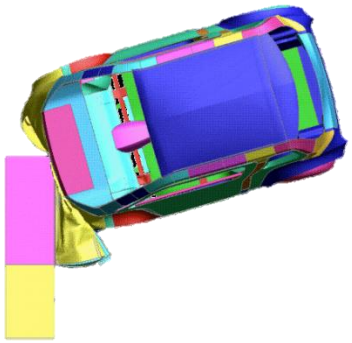

Figure 1: Crash simulation of small electric vehicle body using finite element analysis

Researchers from University of Michigan applied the computational data mining approach to identify and model manufacturing constraints for lightweight material forming/joining processes. For example, from the massive process simulation data, they computationally identified two critical failure modes for stretch-bending of advanced high strength steel, one of which is comparable with the quality index (R/t ratio) of shear fracture investigated previously through laboratory experiment by the Shanghai Jiao Tong team (see Figure 2 - left). The other computationally identified failure mode, side wall accumulated fracture (see Figure 2 - right), is in nature difficult to be captured empirically but identified computationally through data mining.

They also developed a gradient-based multi-component structural topology optimization synthesis to incorporate the identified manufacturing constraints into the system-level structural topology designs. Figure 3 - top shows a multi-component topology design considering the stamping die cost manufacturing constraint. As opposed to the classic topology optimization monolithic (single-piece) design (see Figure 3 - bottom), the multi-component design achieved much better component manufacturability with little sacrifice in structural performance due to the introduction of slightly weaker joints. Compared with the state-of-the-art multi-component topology optimization method, the proposed continuous relaxation formulation accomplished more than 1000-folds computational efficiency improvement.

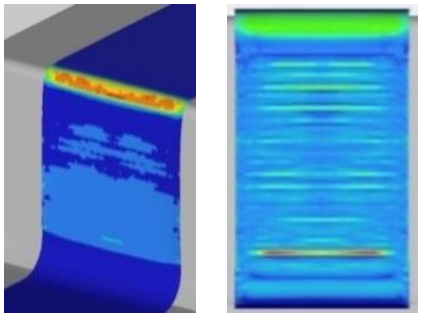

**Figure 2: Computationally identified critical failure modes for stretch-bending process. Left: shear fracture on the tight radii. Right: accumulated side wall fracture.**

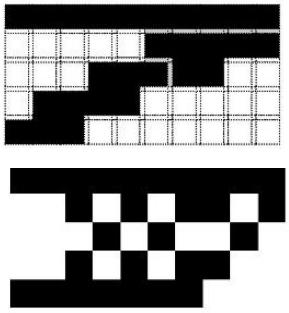

**Figure 3: Top: multi-component topology optimization design considering stamping die cost; Bottom: classic monolithic (single-piece) topology optimization without manufacturability considerations.**

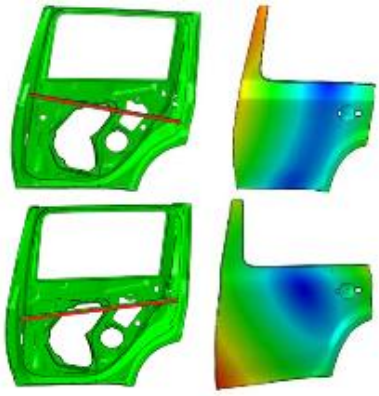

**Figure 4: Impact of vehicle door guard beam position on the deformation under different temperature**

To study the thermal deformation on lightweight vehicle bodies, researchers showed that car door made of dissimilar materials caused a greater deformation with the temperature variation and the door guard beam position had great impact on the deformation under different temperature (see Figure 4).

## Expected Outcomes

- Optimized material selection strategy of mini-EV frontal frame for crash safety,
- Guidelines to reduce dimensional variations of multi-material assemblies due to the variations in fixture, joints, and environmental temperature
- Optimization method for multi-material vehicle body subsystems, incorporating manufacturability criteria.

# Vehicle–Grid System Modeling for Technology Deployment

***Joint Project***


## U.S. Research Team Lead

- **Ramteen Sioshansi, The Ohio State University**

## U.S. Partners

- **The Ohio State University**
- **University of Michigan**
- **Eaton Corporation**
- **PJM Interconnection**

## China Research Team Lead

- **Hongbin Sun, Tsinghua University**

## China Partners

- **Tsinghua University**
- **Beijing Institute of Technology**


## Research Objective

The objective of this project is to assess the impact on the electric grid of a large-scale deployment of plug-in electric vehicles (PEVs). The project team will also develop a technology roadmap and policy recommendations for accelerating PEV deployment in the United States and China.

## Technical Approach

- Develop a comprehensive suite of PEV technology adoption, PEV driving, PEV charger location, PEV charging, and power system unit commitment and economic dispatch models
- Use these models in an integrated fashion to examine how PEV adoption and use can affect power system economics, operations, reliability, and capacity planning
- Capture demographic, socioeconomic, and spatial and social network impacts and associated clustering of PEVs and charging loads using the PEV technology adoption model
- Use simulation techniques to model PEV driving and grid-connection behavior
- Combine simulated PEV driving and charging demand profiles with power system operation models to study interactions between PEVs and the power system, the use of control, and other techniques and technologies to mitigate adverse effects
- Use results of these modeling efforts to develop technology and policy roadmaps that are specially tailored to vehicle and power system markets in the United States and China

## Recent Progress

- Paper focusing on numerical case studies demonstrating benefits of controlled PEV charging on providing storage-like benefits submitted for review for publication in Journal of Modern Power Systems and Clean Energy
- Preparing paper on spatial effects on PEV adoption within the state of Ohio for publication in Spatial Economic Analysis
- Beginning more spatially detailed modeling of central Ohio at the street address level
- Received research grant from Google to geocode state of Ohio vehicle registration data
- Modeled distribution-level effects of level-3 fast PEV charging stations
- Modeling effects of level-3 fast PEV charging stations co-located with big-box retailers on aging of existing transformers
- Developed stochastic linear program model to use distributed generation and controlled charging to relieve transformer loading due to level-3 fast PEV charging
- Developed Monte Carlo sampling-based procedure to solve stochastic linear programming model for PEV charge scheduling

- Conducting case studies to examine benefits of distributed generation and controlled PEV charging to relieve transformer loading due to level-3 fast PEV charging
- Developed stochastic variant of transformer aging simulation to provide more robust assessments of effects level-3 fast PEV charging on distribution infrastructure
- Preparing paper detailing stochastic flow catching EV charging station location model for publication in an archival journal
- Determined optimal charging station locations in northeastern Ohio based on interested from FirstEnergy (an industrial partner)

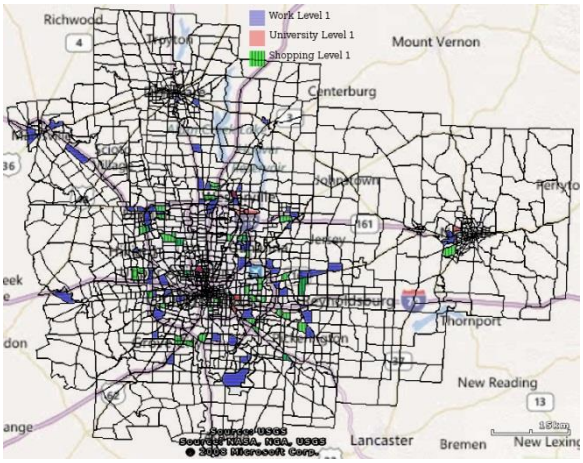


Figure 1. PEV charging infrastructure location optimization model results for central Ohio.

## Significant Results

Work on this project is proceeding in four main areas. First, the project has developed a comprehensive optimization/simulation model to locate public PEV charging infrastructure within a metropolitan area. This provides useful decision-making tools for public entities and private enterprises planning PEV charging station deployments. This model accounts for actual driving behavior and its inherent randomness and determines where best to locate charging stations with fixed resource constraints. A case study, based on the central Ohio region, demonstrates the flexibility of this framework to capture different optimization criteria. The U.S. and China teams are collaborating to expand this work to endogenously capture PEV destination decision making based on charging station availability.

Second, researchers are using actual vehicle adoption data to develop and calibrate spatial econometric models of PEV adoption. Given the relatively small penetration of pure PEVs, other advanced-technology vehicles (e.g., turbodiesels) and hybrid electric vehicles (HEVs) are being used as proxies for PEV adoption. Testing using census tract-level HEV adoption data for the state of Ohio shows strong spatial correlation in adoption patterns. Modeling and predicting the location of PEV owners is important for utility distribution infrastructure planning, given the new loads that these vehicles impose on distribution feeders and transformers. These models can also be useful to firms marketing PEVs and other advanced vehicle technologies.

Third, the project team is exploring the use of price-based schemes to control PEV charging in a decentralized manner. The purpose of these control schemes is to coordinate PEV charging with power system operations. PEV economics can be substantively improved if PEVs charge at the “correct” time, when excess generating capacity is available. Moreover, PEVs can also provide an added source of demand flexibility to aid the integration of variable renewable resources, such as wind and solar. This work focuses on using iterative price-update schemes to efficiently guide PEV owners and load aggregators to charge vehicles at times that are mutually beneficial to the power system and PEV owners. These control schemes will also be refined to ensure algorithmic efficiency (i.e., PEVs converge to a desirable charging profile with minimal communication overhead required between vehicle owners and the electric utility).

Finally, the project team is studying the impacts of high-power public charging infrastructure (e.g., DC fast charging) on the distribution system. This includes the effects of spatially and temporally clustered PEV charging loads on transformers and other electrical equipment. This work will also study the use of control techniques and distributed resources, including distributed generation and storage, to mitigate the negative distribution-level impacts of high-power PEV charging.

## Future Plans

Future work will focus on developing PEV swarm models to fully simulate the distribution- and bulk-power-system-level impacts of large PEV fleets. These models will highlight benefits and potential risks of large-scale PEV adoption. Based on these findings, technology and policy recommendations to mitigate any adverse impacts will be made. Policy recommendations will also be made for development and deployment of PEV technologies and related infrastructures in the United States and China.

## Expected Outcomes

- A flexible model to optimize the location of public charging infrastructure in different regions and with different optimization criteria and resource constraints
- PEV adoption models that capture the effects of demographics, socioeconomics, and social and geographic spatial networks
- Models and tools to analyze PEV impacts on the electric grid, at both the local distribution and bulk power system levels
- Models and tools to study the benefits of different techniques and technologies in reducing the negative power system impacts of PEV charging
- Policy recommendations for cohesive development and deployment of PEV technologies and related infrastructure in the United States and China
- Optimized control strategies for vehicle–electric grid interactions, including centralized and market-based approaches

## Collaboration

- AEP and FirstEnergy are active industry partners, with regular input on research being provided at semi-annual SMART@CAR meetings at The Ohio State University's Center for Automotive Research
- AEP and FirstEnergy are actively involved in helping to explore power system and distribution-level effects of level-3 charging
- Conducted an analysis of optimal charging station locations in northeast Ohio based on interest from FirstEnergy
- AEP providing load and transformer rating data for level-3 charging station modeling
- Eaton has expressed interest in charging infrastructure design optimization model, and we are engaged in discussions with them centering around the EVTown project
- Monthly webinars with Chinese counterparts continue to further establish joint research

## Recent Publications


- X. Xi and R. Sioshansi, "Wind Integration Benefits of Plug-in Electric Vehicles," submitted for review for publication in *Journal of Modern Power Systems and Clean Energy*
- X. Liu, M. C. Roberts, and R. Sioshansi, "Spatial Effects on HEV Adoption," under preparation for submission for publication in *Spatial Economic Analysis*

# Control Strategies for Vehicle-Grid Integration

***Cooperative Project (U.S.)***


## U.S. Research Team Lead

- Ian Hiskens, University of Michigan

## U.S. Partners

- Ian Hiskens, University of Michigan

## China Research Team Lead

- Hongbin Sun, Tsinghua University
- Qinglai Guo, Tsinghua University

## China Partners

- Tsinghua University


## Research Objective

The project seeks to develop control strategies that mitigate distribution-level issues associated with high penetration of plug-in electric vehicles (PEVs) and that allow PEVs to provide operational services to the wider grid. A range of operational services are being considered, including peak reduction, regulation, spinning reserve, and the use of load to track variability in renewable generation.

## Technical Approach

- Define expected impact of PEV population charging at the distribution level
- Extend distributed control strategies previously used in network congestion control to solve PEV overcharging challenges
- Simulate a distribution grid environment and test the ability of algorithms to mitigate detrimental impacts of PEV charging

## Recent Progress

- Developed a constrained-communication based charging scheme, in which the PEV controller has limited input to the system
- Investigated a model-predictive control based approach, in which the controller makes cost-function related decisions at every timestep
- Compared this PEV controller to previous design iterations
- Reformulated PEV charging problem as bi-level, hierarchical control strategy, and developed an average consensus control algorithm for the higher level
- Developed analytical tools to predict performance tradeoffs in a PEV fleet employing this control architecture, and used simulation results to confirm expectations
- Demonstrated through simulation the ability of the new charging algorithm to prioritize either reference tracking or vehicle battery charge sufficiency

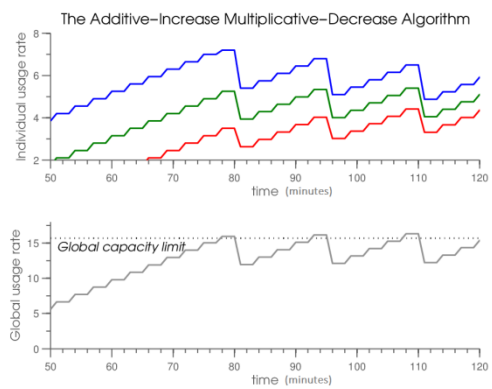


**Figure 1. The additive-increase multiplicative-decrease algorithm, one of several distributed control methodologies used to manage PEV charging.**

## Significant Results

Previous work focused on developing distributed control algorithms to manage total PEV charging load at the distribution level, as well as the design and construction of a testbed utilizing wireless communication to physically verify these results. Since then, efforts have focused primarily on defining an accurate distribution system environment, and analyzing the broader voltage and current effects that PEVs have within this network.

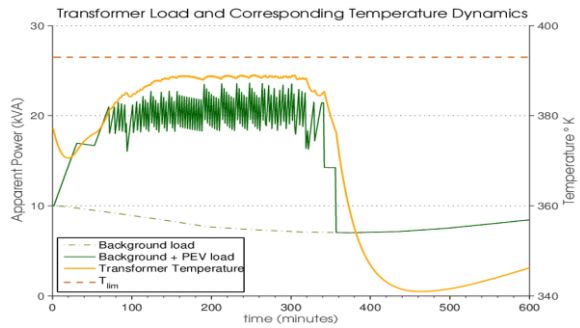


Figure 2. Transformer temperature, PEV load, and background load. The AIMD algorithm successfully maintains a temperature with acceptable levels, while the background load retains uninterrupted service.

Central to this thrust was the design of a distribution grid based on the IEEE-34 node network, which models a long, lightly-loaded feeder. The simulated circuit features a full three-phase power flow based on the DistFlow equations, and models individual pole-top transformers as 25 kVA units, each servicing a randomized portion of the total load at each node. PEVs are attached to the transformers and charge in a manner typical of commuter driving patterns. Voltage regulating equipment, including capacitor banks and regulators, are also modeled within the network.

Having designed and coded this circuit, the next step was to analyze the voltage and current dynamics of the distribution network, and to assess whether thermal runaway on the transformers could be avoided. Using a series of Monte-Carlo simulations, the worst case scenarios were assessed as occurring when a large number of PEVs was attached to a transformer with significant background load. Even in these instances, however, transformer temperature was successfully constrained below the threshold value by the distributed charging algorithm. Furthermore, the variability in the voltage profile due to this control strategy was minor when compared to other switching phenomena endemic to the network. Thus, control was maintained with minimal system interference.

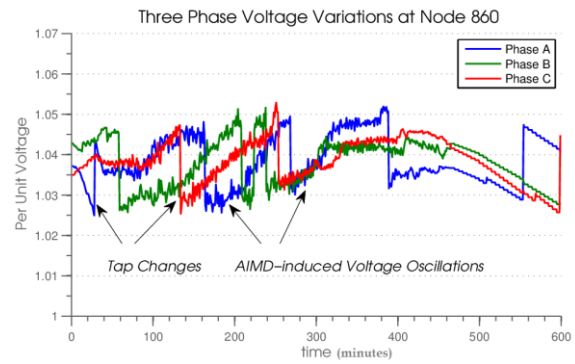


Figure 3. Voltage dynamics at a sample network node. The oscillatory behavior related to AIMD is significantly reduced by the geographic disparity of PEVs within the power system.

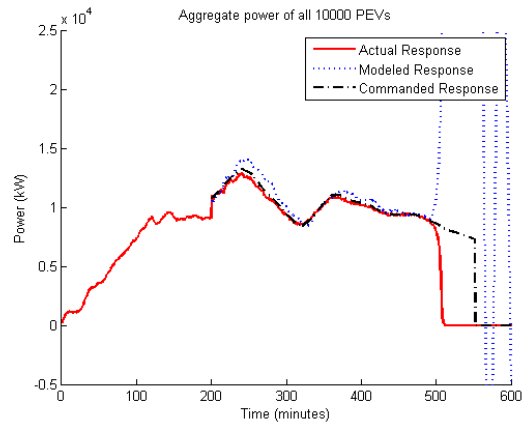


Figure 4. A simulation of a large population of PEVs attempting to track a wind signal while maintaining the lower-level system constraints identified in earlier studies.

These ideas have recently been extended to larger vehicle populations—which are capable of providing transmission-level services, such as frequency regulation, to the grid—but must still adhere to the lower-level distribution dynamics identified previously. Ongoing efforts have focused on ways to ensure transformer health at the local level while introducing a minimum of disturbances to fleet-level power tracking.

## Future Plans

The plan is to extend our ongoing work on PEV populations tracking a wind signal, and possibly a full grid-level frequency regulation signal, to achieve better performance and reduced error between the broadcast signal and the fleet's aggregate power response. To achieve this, the optimal fleet behavior will be defined in terms of distributed control actions. Furthermore, the penalty of ensuring distribution-level protections while providing transmission-level tracking will be quantified in terms of lost capacity and delayed response. Poincare maps will also be used to assess fundamental limits on the type of service that can be provided.

## Expected Outcomes

- Distribution-level control of PEV charging
- Control strategies for grid operational services
- Coordination of PEV charging with renewable generation
- Decentralized control strategies for PEV charging
- An understanding of the impact of non-ideal communications networks and computational limitations on the coordination of PEV charging loads

# A Wireless Magnetic-Resonance Power Transmission System for EV Charging

***Cooperative Project (U.S.)***


## U.S. Research Team Lead

- Chris Mi, San Diego State University

## U.S. Partners

- DENSO International

## China Research Team Lead

- Xinmin Lai, Shanghai Jiao Tong University

## China Partners

- Mia Motors, LLC


## Research Objectives

The overarching objective of the project is to develop theoretical framework and technologies enabling efficient and low cost wireless battery charging of EV and PHEV using wireless magnetic-resonance power transfer theory. Specific objectives include.

- Analyze the resonant condition or near-resonant condition (frequency bandwidth). Perform theoretical analysis of maximum power transfer and maximum efficiency between the transmitter and the receiver, detailing the requirements and constraints of distance, power, geometry, and lateral and angular misalignments.
- Develop analytical methods based on S parameters (including the Smith-chart) for the two-port network to calculate the key parameters, such as the maximum efficiency, the coupling coefficient, the power quality factor Q, the coil's self-inductance and mutual-inductance, the radiation resistance and the Ohmic resistance.
- Develop an analytical model based on C++ or Matlab and numerical models based on finite-element method (FEM) to verify the correctness of the proposed methods.
- Perform analytical analysis on the effects of a finite, conducting body on the charger. Perform FEM simulations in the presence of finite conducting bodies to verify the analysis and explore more complex geometries found in an automotive environment.
- Construct the coils based on the analytical analysis and simulation results, and design the control and energy conversion systems. Develop a hardware prototype with corresponding co-FEM simulation model to verify the key aspects of the analysis.
- Build a hardware prototype for placement in an automotive environment to test the performance.
- Develop an algorithm for object detection between the source and the receiver coils for practical study.
- Evaluate the magnetic field levels using published IEEE/SAE standards as a function of frequency and its impact on human body

## Technical Approach

The Wireless Power Transmission (WPT) technology has solid theoretical support in physics and the basic concepts have been successfully proven by both the literature and the PI's preliminary experiments. But the inductive WPT charger has several disadvantages. Due to the large air-gap between the primary and secondary windings, WPT transformers have large leakage inductances and small mutual inductance, which leads to the weak coupling between transmitting and receiving coils. Weak coupling can result in poor transmission performance, low efficiency and high resistive heating. Some researchers have proposed the method of combining the physical resonance and the inductive WPT, which owns the merits of the inductive method but without the disadvantages. The PI believes that turning the significant resonant discovery in physics into a working WPT charger, called magnetic-resonance WPT, will have strong impact not only on the Electrical Vehicle (EV) battery charging, but also on a variety of other electronic devices. The goals of this project include:

- Literature review, initial design and construction
- Numerical program development and verification

- Proposed FEM-BEM simulation program for system performance study
- System co-simulation study, refined design and construction
- EMI evaluation based on FEM simulation and the measurements
- System evaluation using EV battery model and publications
- Objective detection

## Significant Results

A double sided LCC resonance topology was developed. Two patents were filed. With the proposed topology and its tuning method, the resonant frequency is irrelevant with the coupling coefficient between the two coils, and is also independent of the load condition. It means that the system can work at a constant switching frequency. Analysis in frequency domain is given to show the characteristics of the proposed method. We also propose a method to tune the network to realize zero voltage switching (ZVS) for the primary side switches. Simulation and experimental results verified analysis and validity of the proposed compensation network and the tuning method. A wireless charging system with up to 7.7kW output power for electric vehicles was built, and 96% efficiency from DC power source to battery load is achieved; and system efficiency above 93% efficiency from AC plug to battery.

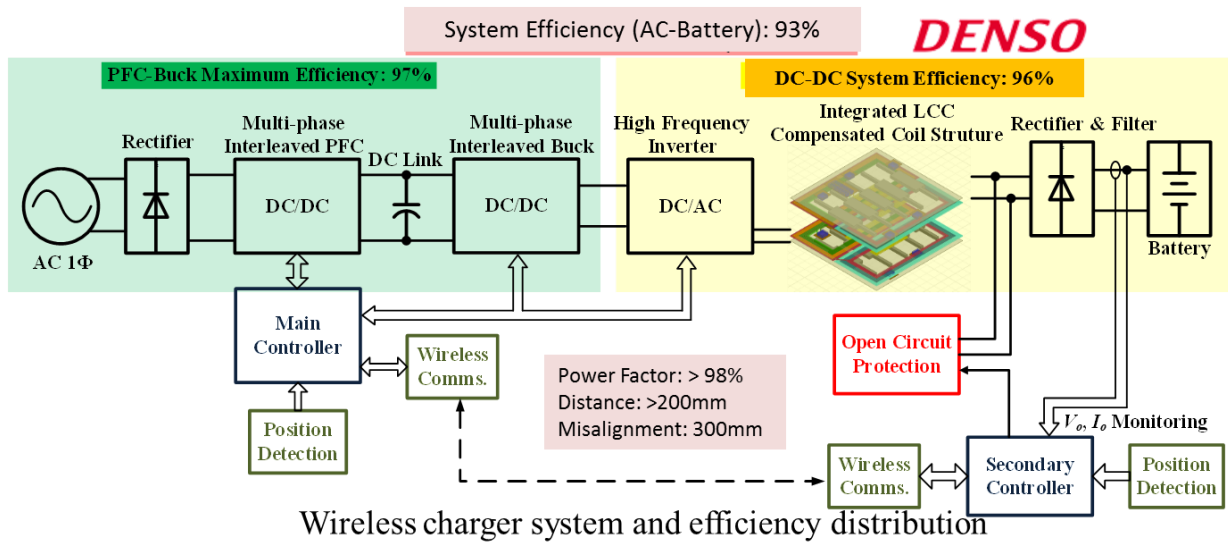


Figure 1: Complete wireless EV Charger with the double-sided LCC topology, segmented coils, and multiphase interleaved power factor correction.

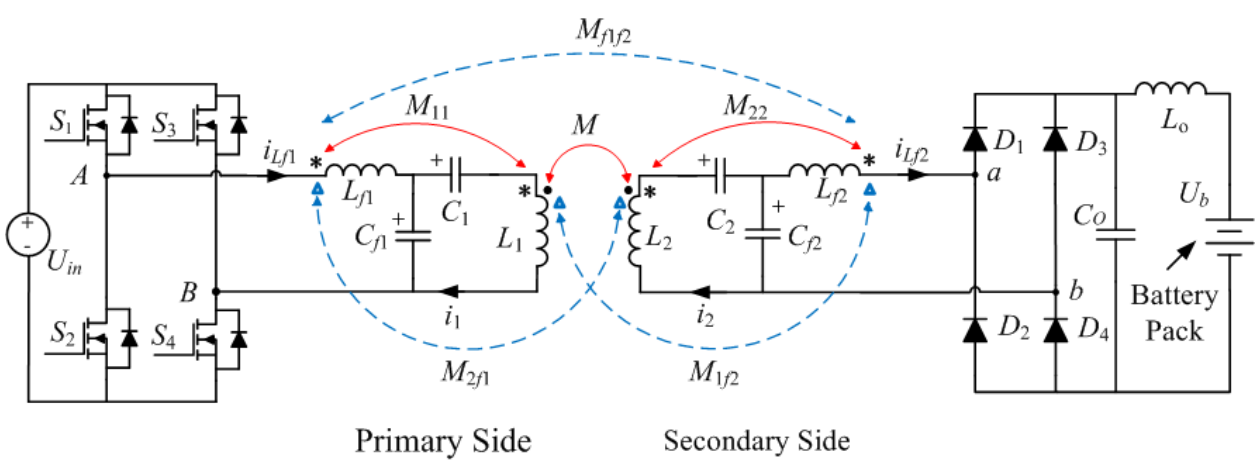


Figure 2: Double sided LCC Topology for the wireless charger.

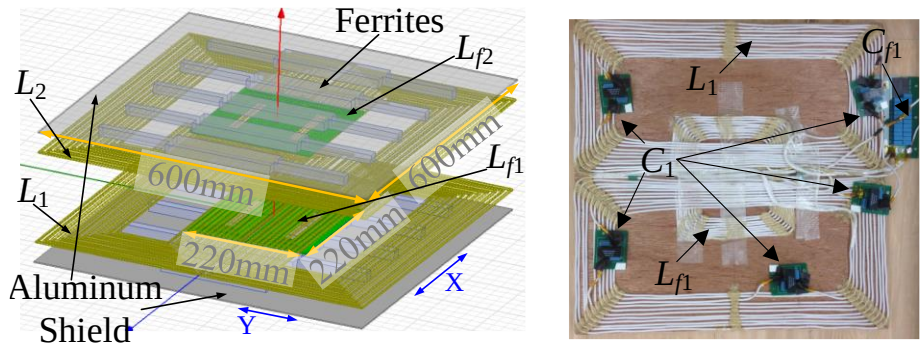


Figure 3: Segmented transmitting and receiving coil with bipolar structure.

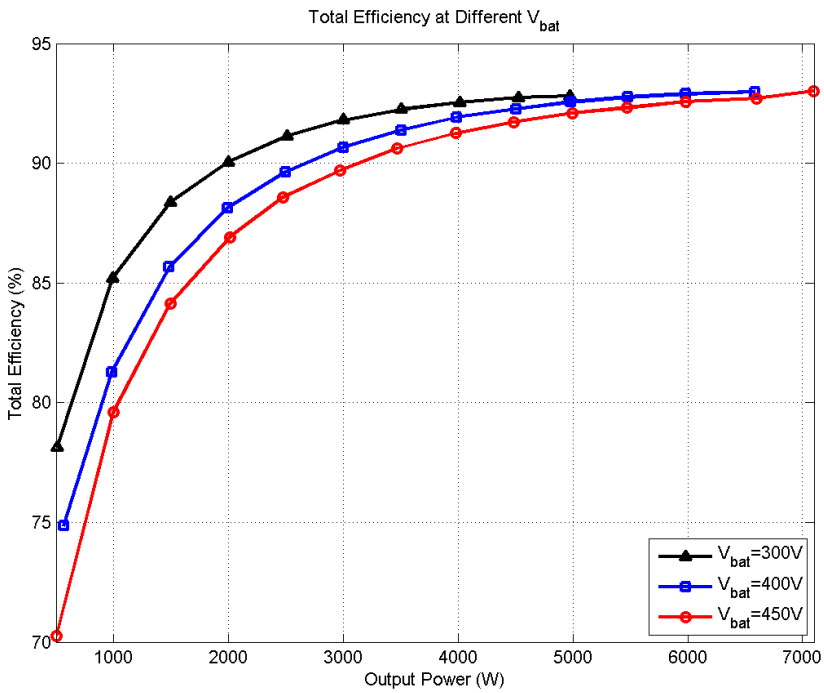


Figure 4: Measured system efficiency (from AC plug to battery).

The parameters of the wireless power transfer system are optimized to reduce the total size and increase the efficiency. The magnetic ferrite is eliminated to reduce the weight of the system, which can help reduce the installation requirement on the vehicle side. When the coupling coefficient of the primary and secondary coils is as low as 10%, the dc-dc efficiency can be maintained higher than 95%. The system sensitivity of parameter variations is analyzed using exhaustive and Monte-Carlo method. It indicates that when the parameter values have $\pm$10% variations, the output power can decease to zero or increase to two times larger than the nominal power.

A 3.3 kW WPT system is installed underneath the vehicle chassis and the system performance is tested. The electromagnetic interference (EMI) issue is also analyzed using finite element analysis (FEA) and practical measurement. Aluminum plates are adopted at both the primary and secondary side to reduce the magnetic fields emission. It shows that the safety range of the WPT system is about 150 mm away from the coils.

A dynamic WPT system is designed to realize vehicle charging in mobile status. Multiple segmented transmitter coils are used at the primary side to reduce the power losses. A receiver coil is moving at the secondary side. The compensation inductors are integrated inside of the main coil to reduce the system size and increase its power density. The transmitters are placed adjacent to each other to reduce the power pulsation during the moving process. The power variation is limited as low as $\pm$2.9% of the nominal power, which means the vehicle can be continuous powered when it is moving on the road.

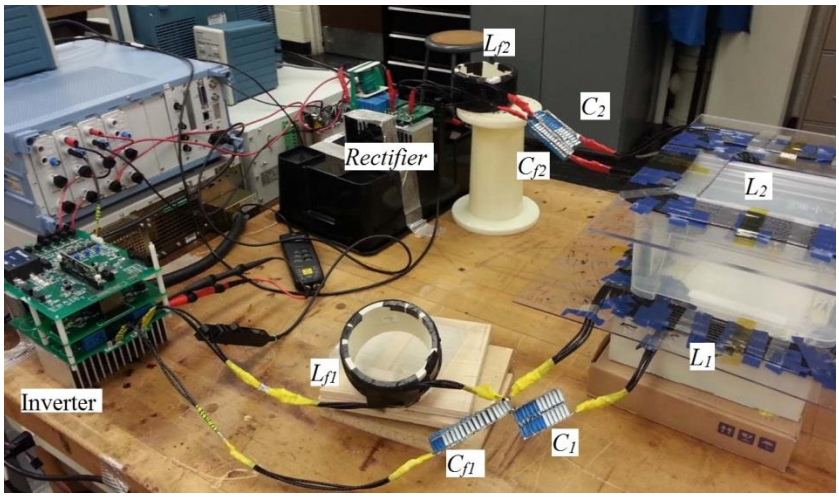


Figure 5: Prototype of a 3.3kW low-weight WPT system without magnetic ferrite.

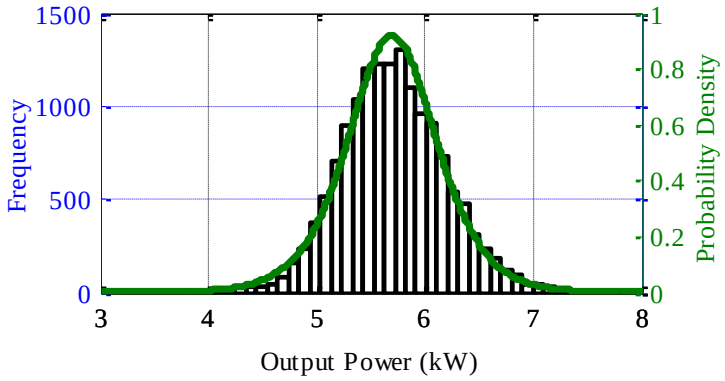


Figure 6: Probability distribution of WPT system output power.

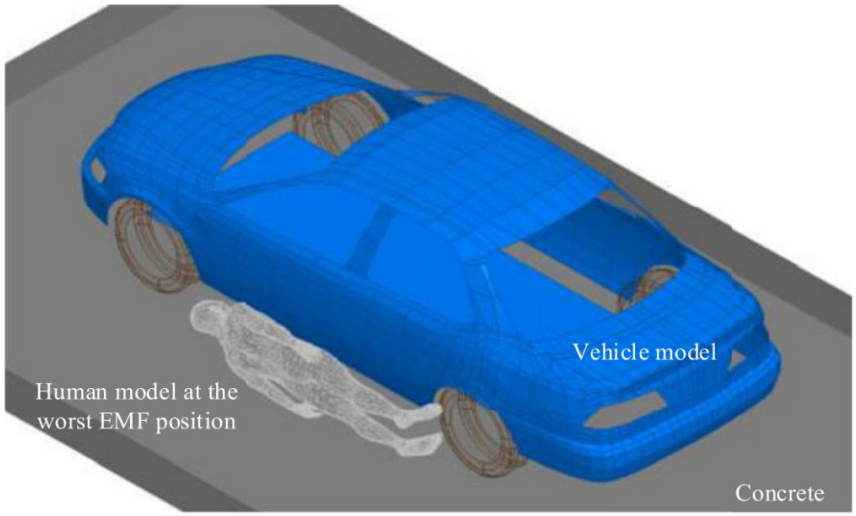


Figure 7: Electromagnetic interference (EMI) analysis of human body at worst radiation scenario.

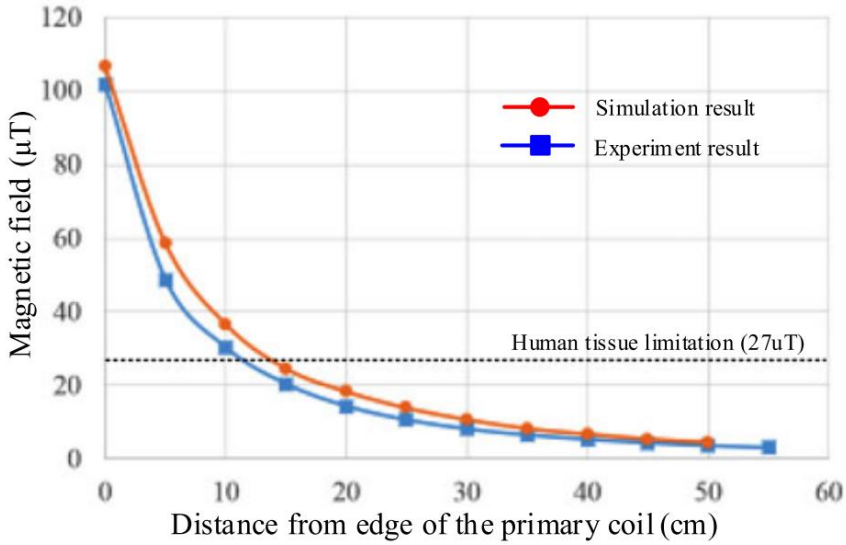


Figure 8: Simulated and measured results of magnetic fields strength.

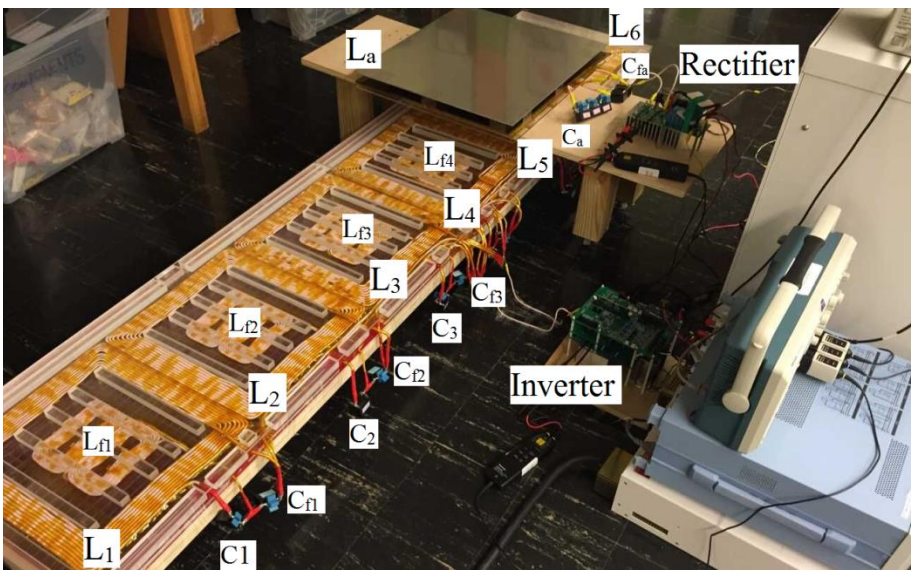


Figure 9: Experimental prototype of a dynamic charging system.

## Future Plans

Future work will focus on

- Commercialization of proposed wireless charging technology
- Work with DENSO and Ford to develop a vehicle level demo of 3.3kW or 6.6 kW wireless charger
- Develop foreign object detection method based on multiple approaches, such as temperature detection, infrared camera, phase detection and others
- Study the safety and electromagnetic emissions of the proposed system
- Develop communication methods for the information exchange between the primary and secondary coils
- Optimize the coil design and efficiency to satisfy the SAE new standard
- To develop workshops, seminars, short courses, tutorials, e-learning modules, and publications to publicize the technology

## Expected Outcomes

The output of the project will include the detailed theory, analytical models, and simulation models, design validation tools, control algorithms, laboratory experiment, measurement prototypes and vehicle testing platform. The PI will work closely with the industry partner to make sure the models and tools developed are compatible with the tools used within

the industry. The models will be delivered to the industry partner and to be incorporated into the current HEV and PHEV charging design and modeling platforms.

# Life Cycle Assessment of Wireless Charging of Electric Vehicles

***Joint Project***


## U.S. Research Team Lead

- Gregory Keoleian, University of Michigan
- Geoffrey M. Lewis, University of Michigan
- Zicheng (Kevin) Bi, University of Michigan

## U.S. Partners

- UM Dearborn (Chris Mi)
- Ford Motor Company
- Delphi Automotive

## China Research Team Lead

- None

## China Partners

- Visiting scholar: Lingjun Song (Beihang University)
- Tsinghua University (Zhengming Zhao)


## Research Objectives

The project seeks to compare the energy, environmental and economic performance of wireless charging to plug-in charging for electric vehicles using life cycle assessment methods. We assess the tradeoffs of wireless charging, including potential lightweighting benefits from battery size reduction for electric vehicles, such as transit buses and passenger cars, and potential increased burdens from infrastructure.

## Technical Approach

- Conduct life cycle inventory analysis of both wired and wireless charging hardware
- Create life cycle models to assess the environmental, energy and economic trade-offs of infrastructure installation vs. subsequent use-phase savings
- Use the Ann Arbor Transit Authority (AATA) and UM blue bus systems as case studies to evaluate the lightweighting benefits of wireless charging, including the fuel economy improvement induced by battery size reduction
- Develop a method to quantify the battery size reduction due to the fact that wireless charged buses can be charged frequently during daily operation and quantify the resulting fuel economy improvement
- Conduct a life cycle cost analysis to evaluate economic performance of wireless charging technology.
- Establish a life cycle optimization model framework to strategically enhance the environmental, energy and economic performance of wireless charging electric vehicles, including transit buses and passenger cars, with a consideration of battery degradation.

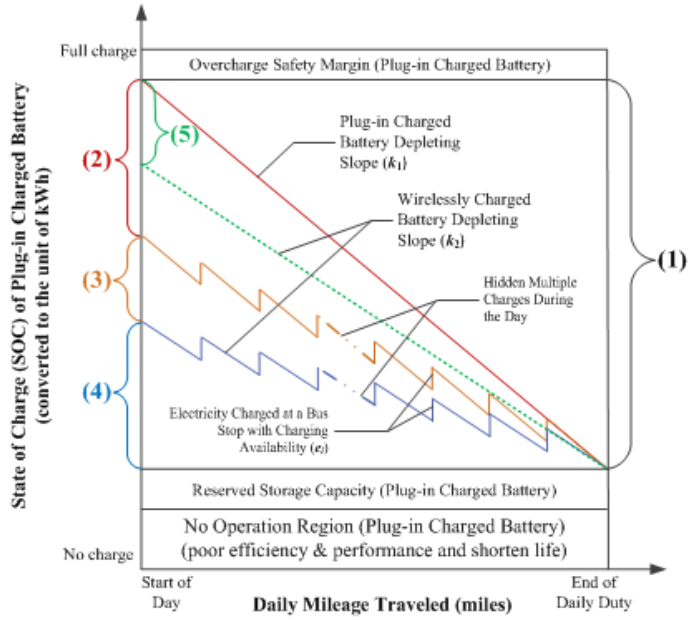


Figure 1: Battery downsizing calculation. Start from a plug-in charged battery to quantify the minimum electricity needed at start of day for a wirelessly charged battery. (1) Operating Region (kWh) of plug-in charged battery; (2) Primary capacity reduction (kWh) due to wireless charging availability; (3) Secondary capacity reduction (kWh) due to fuel economy improvement; (4) Minimum electricity needed (kWh) at start of day for a wirelessly charged battery (not yet including its own Overcharge Safety Margin, Reserved Storage Capacity and No Operation Region); (5) Daily energy saving (battery-to-wheel) due to wireless charging (kWh).

## Significant Results

**An integrated life cycle assessment and life cycle cost model for comparing wireless vs. plug-in charging electric buses**

Figure 2 shows that the wirelessly charged battery can be downsized to 27-44% of a plug-in charged battery. The associated reduction of 12-16% in bus weight for the wireless buses can induce a reduction of 5.4-7.0% in battery-to-wheel energy consumption.

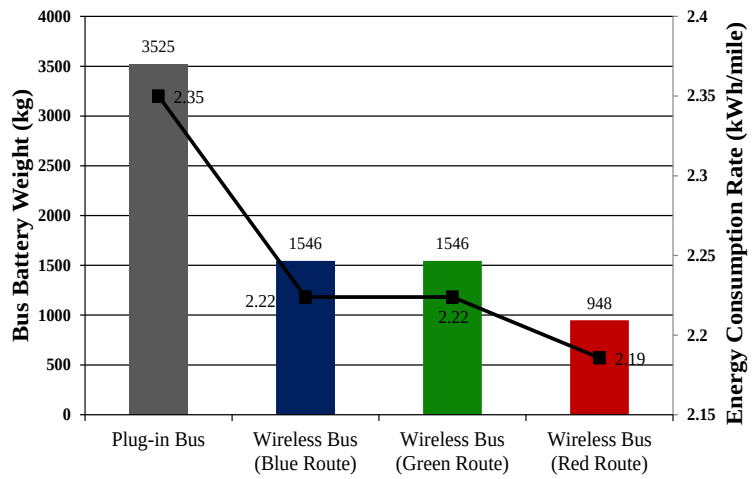


Figure 2: Battery weights and energy consumption rates for plug-in and wirelessly charged buses. Blue routes = Ann Arbor city routes; red routes = Ann Arbor-Ypsilanti intercity routes; green routes = Ypsilanti city routes.

As shown in Figure 3, a wireless charging electric bus system has comparable life cycle energy and greenhouse gas emissions with a plug-in charging electric bus system. To further improve the energy and environmental performance of a wireless charging electric bus system, it is important to focus on key parameters including carbon intensity of the electric grid and wireless charging efficiency. If the wireless charging efficiency is improved to the same level as the assumed plug-in charging efficiency (90%), the difference of life cycle greenhouse gas emissions between the two systems can increase to 6.3%, which means the wireless charging system will have larger advantage.

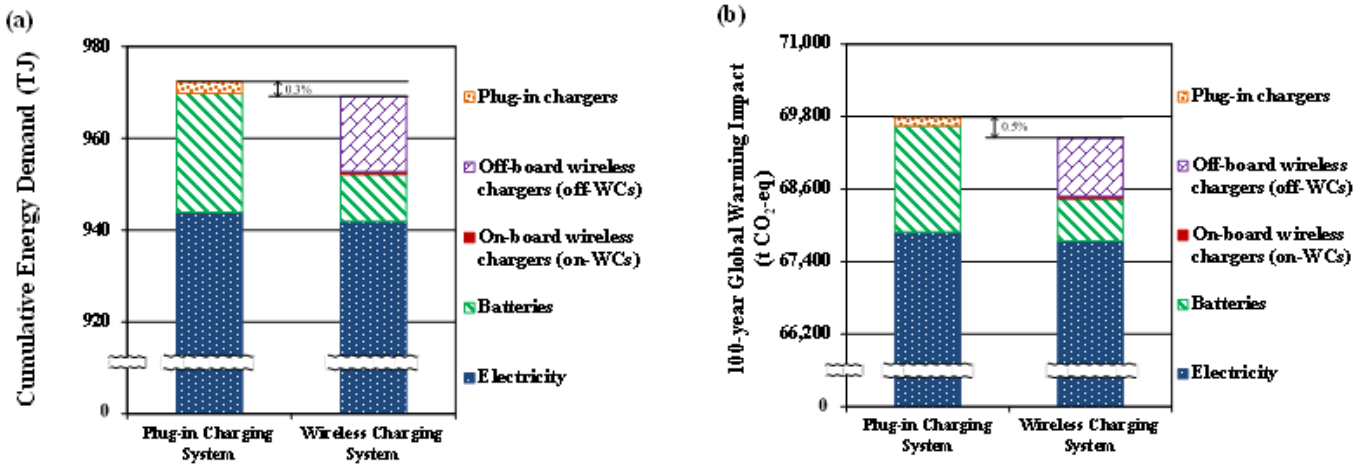


Figure 3: Cumulative Energy Demand (a) and 100-year Global Warming Impact (b) of plug-in and wireless charging electric bus systems.

An integrated life cycle assessment and life cycle cost model was developed to evaluate the life cycle costs for an all-electric bus system utilizing either plug-in or wireless charging and also compare these costs to both conventional pure diesel and hybrid bus systems, as shown in Figure 4. Despite a higher initial infrastructure investment for off-board wireless chargers deployed across the service region, the wireless charging bus system has the least life cycle cost of $0.99 per bus-km among the four systems and has the potential to reduce use-phase carbon emissions due to the lightweighting benefits of onboard battery downsizing compared to plug-in charging. Further uncertainty analysis and sensitivity analysis indicate

that the unit price of battery pack and day or night electricity price are key parameters in differentiating the life cycle costs between plug-in and wireless charging.

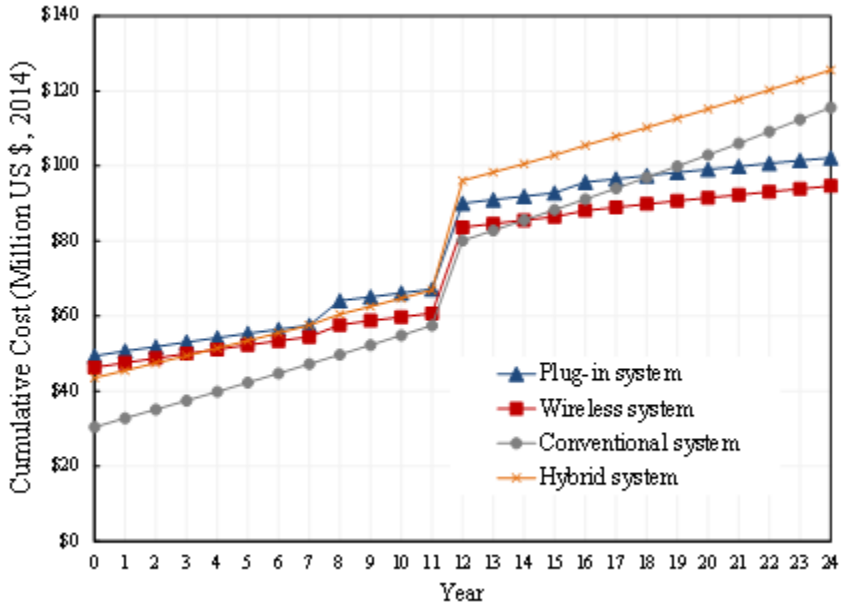


Figure 4: Comparison of cumulative costs of plug-in charging all-electric, wireless charging all-electric, conventional pure diesel and hybrid bus systems

**A life cycle optimization model framework to enhance the environmental, energy and economic performance of wireless charging electric vehicles**

As shown in Figure 5, a life cycle optimization framework has been established for enhancing the economic performance of a wireless charging electric bus fleet, by selecting which bus stops to deploy wireless chargers and determining the battery capacity with a consideration of battery degradation.

The optimization highlighted the trade-off of battery capacity vs. number of selected charging stations, and demonstrated the significance of the optimal charger deployment strategy in real-world applications of wireless charging technology.

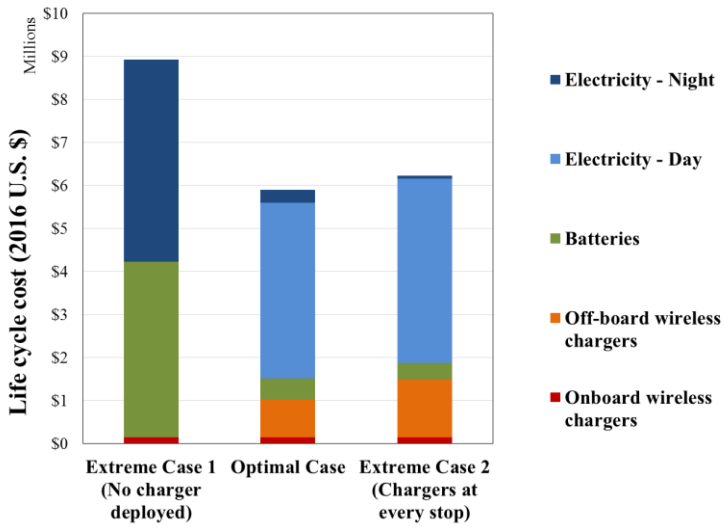


Figure 5: Life cycle costs of three different charger deployment strategies

## Future Plans

- Task 1. Extend the current life cycle cost optimization model to a multi-objective life cycle optimization (LCO) model that achieves optimal environmental, energy and economic performance of a network of wireless charging electric bus routes. Both charger location accounting for charging stops being shared by multiple routes and battery capacity with a consideration of battery degradation will be optimized.
- Task 2. Develop an integrated life cycle assessment and life cycle cost (LCA-LCC) model for evaluating the environmental, energy and economic impacts of a dynamic wireless charging passenger car system on interstate and urban roadways;
- Task 3. Develop a multi-objective LCO model for implementing dynamic wireless charging for passenger cars. The optimization will include both spatial (charger location) and temporal (infrastructure deployment as a function of EV market share) components.

## Expected Outcomes

The following expected optimization model framework and life cycle assessment results will be used to guide real-world deployment of wireless charging technology to enhance sustainable mobility:

- A multi-objective life cycle optimization model framework to evaluate and enhance the environmental, energy and economic performance of wireless charging electric vehicles, including transit buses and passenger cars.
- Life cycle assessment and life cycle cost results of a dynamic wireless charging passenger car system on interstate and urban roadways. Challenges and opportunities for dynamic wireless charging to enhance future sustainable mobility will be highlighted.
- Collaboration with Chinese partners to evaluate and enhance the sustainable performance of wireless charging demonstrations in China

## References/Publications


1. Bi Z, Song L, De Kleine R, Mi C, Keoleian GA. Plug-in vs. wireless charging: Life cycle energy and greenhouse gas emissions for an electric bus system. Applied Energy 2015;146:11–19.
2. Bi Z, De Kleine R, Keoleian GA. Integrated life cycle assessment and life cycle cost model for comparing plug-in versus wireless charging for an electric bus system. Journal of Industrial Ecology 2016;In Press.
3. Bi Z†, Kan T†, Mi C, Zhang Y, Zhao Z, Keoleian GA. A Review of Wireless Power Transfer for Electric Vehicles: Prospects to Enhance Sustainable Mobility. Applied Energy 2016 († Equal contribution from these authors) (Under Review)

# Fuel Mix Strategies and Constraints

***Cooperative Project (U.S.)***

## U.S. Research Team Lead

- **Ming Xu, University of Michigan**

## U.S. Partners

- **Sandia National Laboratories**
- **University of Michigan**

## Research Objective

The objective of this project is to assess the feasibility of alternative vehicle fueling, including biofuels and electricity, for meeting significant penetration of clean vehicles (CVs). This project will highlight critical resource availability and infrastructure constraints for both biofuels and electricity generation. This project will be complemented by activities that will address grid control and resilience in Thrust 6.

## Technical Approach

- Conduct a national assessment to understand resource constraints and competition with demands from other sectors (agriculture, urban, industrial activities, etc.)
- Complete a regional analysis to develop optimized strategies to maximize the reduction of greenhouse gas (GHG) emissions and fossil fuel use, given the resource constraints
- Conduct an assessment of the feasibility and opportunities for large-scale penetration of CV and fuel technologies
- Understand the impact of real-world driving patterns on CV penetration, and that of electric vehicles in particular, based on different consumer responses to cost and range limitations
- Apply the modeling framework to China

## Recent Progress

- Presented results of the ride sharing project at the 2015 Conference of the International Society for Industrial Ecology in Guilford, UK.
- Conducted literature review on using float car data to estimate real-time traffic flows (volume and speed) in August 2015
- Developed an optimization model to evaluate the environmental benefits of ride sharing in cities. Evaluated charging behaviors of electric taxis in Shenzhen, China.
- Developed formulation of an optimization model to site charging stations according to vehicle travel patterns to maximize vehicle-mile-traveled electrification. Tested the sensitivity of the model to travel pattern changes using weekly data.

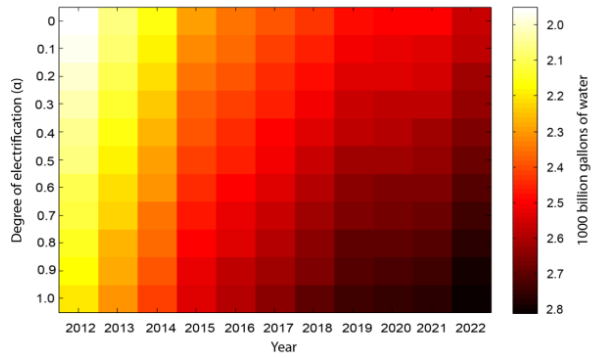


**Figure 1. Projected additional water consumption due to CV deployment. Degree of electrification refers to the percentage of remaining travel demand (after applying biofuels mandated by RFS2) that is fulfilled by electric vehicles (the rest by gasoline).**

- Examined trajectory data collected by Prof. Hewu Wang's group (Tsinghua) for travel pattern analysis and drive cycle emission modeling.

## Significant Results

At the national level, based on existing policies, transitioning the current gasoline-based transportation into one with CVs will increase national annual water consumption by 1,950–2,810 billion gallons of water, or 1.5%–2.2%, depending on the market penetration of electric vehicles (Figure 1).

At the regional level, variances of water efficiency in producing different fuels are significant. Using an optimization approach to further evaluate impacts on regional water stress from a fully implemented CV system, we were able to identify potential roles (fuel producer or consumer) states may play in a real-world CV development scenario (Figure 2).

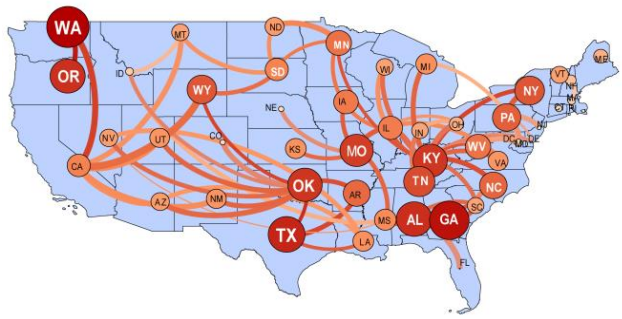


Figure 2. Optimized state-level water consumption and water flows embodied in interstate trade of alternative fuels. Size and color of circles indicate the amount of water consumption related to producing designated fuels, including fuels consumed within the states and those transported to other states. Lines go clockwise from states producing to states consuming designated fuels. Line color indicates the amount of water embodied in interstate trade of fuels.

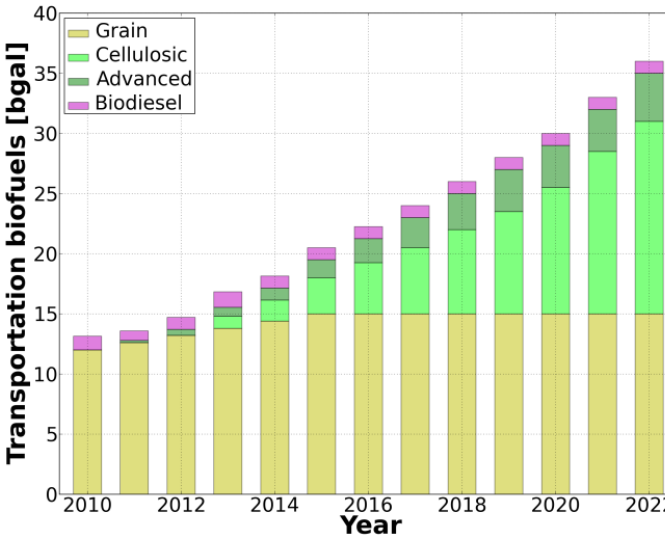


Figure 3. The Renewable Fuel Standard biofuels mandate by year. Figure from Schnepf and Yacobucci, Renewable Fuel Standard (RFS): Overview and Issues. Congressional Research Service (2012).

This analysis has been submitted to *Applied Energy*.

To complement the assessment of water utilization, researchers assessed the feasibility of the U.S. light-duty vehicle (LDV) park to consume biofuels prescribed by the modified Renewable Fuel Standard (RFS2). RFS2 prescribes the annual volume of biofuels to be used in the transportation sector through 2022 (Figure 3).

Sensitivity analyses indicate that the fuel price differential between gasoline and ethanol blendstocks, such as E85, is the principal factor in LDV biofuel consumption. The number of flex fuel vehicles and biofuel refueling stations will grow given a favorable price differential relative to petroleum. However, when considering the longer-term implications beyond 2022 shown in Figure 4, the extreme oil prices that make biofuels favorable in the near term also encourage use of other

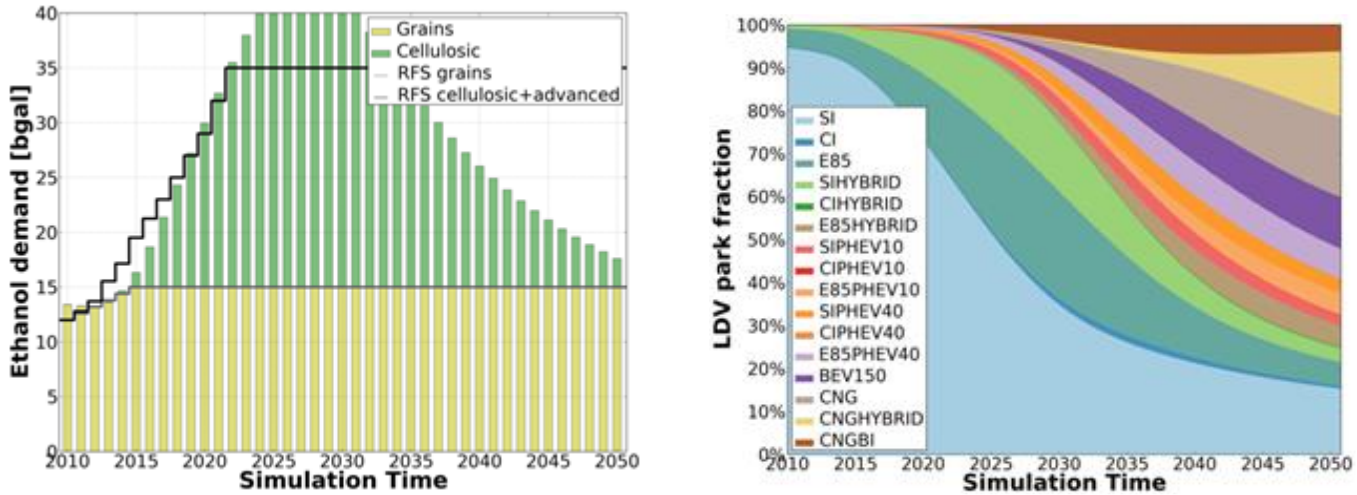


Figure 4. RFS2 can be satisfied at extreme values for oil and biomass, which make gasoline very expensive and biofuels very inexpensive. Longer term, the conditions that encourage biofuel demand also encourage other alternative vehicles and fuels, and thus biofuel demand decreases.

alternative powertrains, such as NGVs and EVs, and thus do not sustain high quantities of biofuel consumption. This analysis has been published in *Energy Policy* (Westbrook et al., 2014).

In addition to examining biofuels in competition with other alternatives, researchers considered the potential impact of

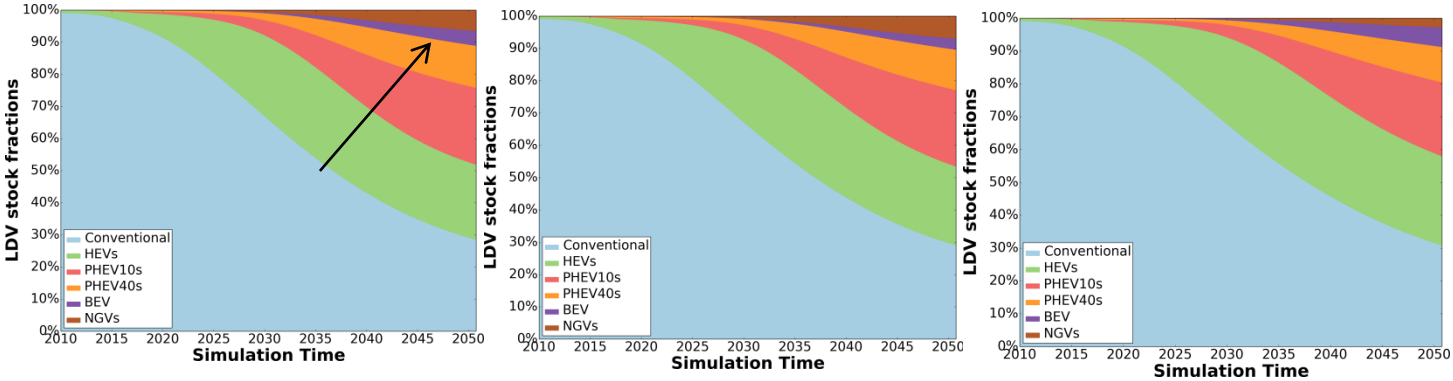


**Figure 5. Light-duty vehicle stock fraction of various powertrains if range limitations were based purely on modeling cost penalties, a threshold of inconvenienced days that requiring renting another vehicle, and a threshold of inconvenience with the availability of another household vehicle.**

range penalties, infrastructure availability, and recharge time on battery electric vehicle (BEV) adoption using driving distributions that represent real-world data. The assessment considered the difference in adoption based on representing penalties as cost versus thresholds for frequency of inconvenience for insufficient range. As shown in Figure 5, the relative impact of a cost penalty, requiring rental of an alternative, and availability of another household vehicle on days of inconvenience had an impact on the magnitude of BEV adoption. This work has been submitted to the *Journal of the Transportation Research Board* (Barter et al., 2014).

## Future Plans

- Investigate impacts to land use intensity due to CV development
- Apply the framework on water implication to CVs in China
- Consider additional consumer choice and behavior factors that have an impact on clean vehicle and fuel adoption patterns and resulting impact on petroleum consumption and greenhouse gas emissions

## Expected Outcomes

- Feasibility assessments of large-scale clean fuel and vehicle technology penetration in the context of national policy goals and consumer behaviors
- Evaluation of constraints posed by critical infrastructure systems and natural resources to meet CV targets in both the United States and China

## Publications and Presentations

- Manuscript titled "Siting Public Electric Vehicle Charging Stations Using Real World Vehicle Travel Patterns" has been submitted to journal Transportation Research Part D: Transportation and Environment
- J. Westbrook, G.E. Barter, D.K. Manley, T.H. West, "A parametric analysis of future ethanol use in the light-duty transportation sector: Can the US meet its Renewable Fuel Standard goals without an enforcement mechanism?" *Energy Policy*, 65, 419-431 (2014)
- G.E. Barter, M.A. Tamor, D.K. Manley, T.H. West, "The implications of modeling range and infrastructure barriers to battery electric vehicle adoption," submitted to *Journal of the Transportation Research Board* (2014)
- Summer Zhao's MIT SM Thesis completed, June 2015: The projected Pathways and Environmental Impacts of China's Electrified Passenger Vehicles
- Presented "Environmental Benefits of Ride Sharing in Urban Cities" in the 2015 International Symposium on Sustainable Systems and Technology (ISSST) conference.

# Fleet Modeling on China's Electric Vehicle Development

***Cooperative Project (U.S.)***


## U.S. Research Team Lead

- John Heywood, Massachusetts Institute of Technology

## U.S. Partners

- Massachusetts Institute of Technology
- University of Michigan
- Argonne National Laboratory
- Oak Ridge National Laboratory

## China Research Team Lead

- Hong Huo, Tsinghua University
- Hewu Wang, Tsinghua University
- Jiuyu Du, Tsinghua University
- Xunming Ou, Tsinghua University

## China Partners

- Tsinghua University
- China Automotive Technology Research Center


## Research Objective

This project will use a Fleet model to forecast and analyze the different scenarios of electric vehicle (EV) penetration in China's in-use vehicle fleet, measuring their impacts on reducing energy consumption and $CO_2$ emissions. The $CO_2$ emission impact is measured by forecasting the electric utilities' expansion and assessing how much greener the electric grid would become in China. This project also conducts a comparison of different forecasting models. Researchers will be able to use the model and results from this project to determine under what scenarios EV development would a make a substantial environmental impact.

## Technical Approach

- Modify the existing Chinese Fleet model to include various detailed assumptions of EV growth in China; collect data on historical sales and mileage traveled (compared to conventional vehicles) for electric vehicles, including battery electric vehicles (BEVs), plug-in hybrid electric vehicles (PHEVs), and hybrid electric vehicles (HEVs)
- Build a utility capacity expansion model to forecast the energy mix in China; if enough information can be extracted from literature reviews, then literature data will be used

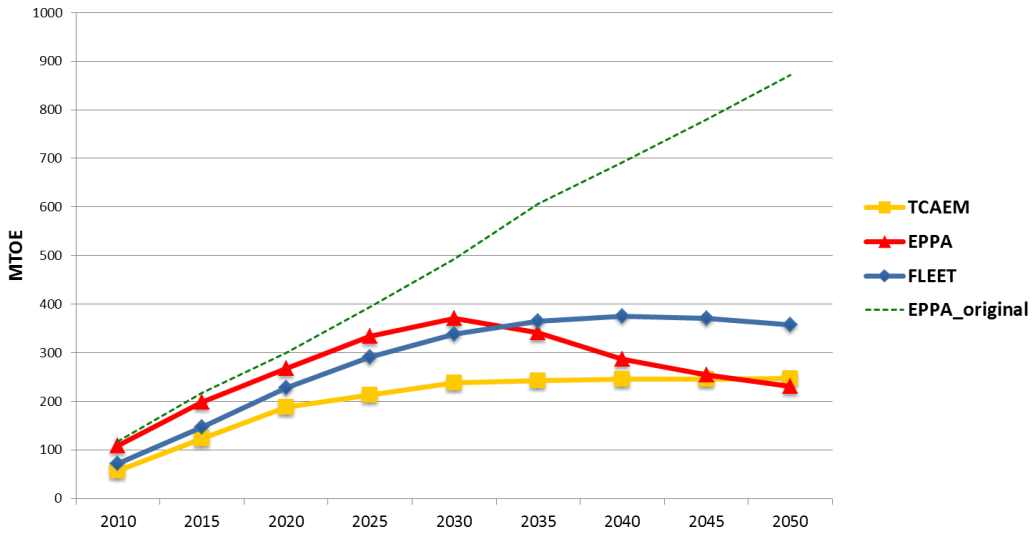


Figure 1. Comparison of energy usage among three models with similar FC assumptions.

- Compare three types of forecasting models by breaking down the underlying logic and assumptions and comparing whether the model results are robust to their input assumptions

## Recent Progress

- Built model to forecast electric power system; researched the market information of the clean energy vehicle industry to better learn about the market dynamics and leading companies; and collected data on the historical sales of HEV, PHEV, and BEV; and on the historical power generation, capacity, and power mix of China, including coal, natural gas, oil, hydro, nuclear, wind, and solar
- Conducted in-depth research to find out the generation, capacity and power mix of six power regions in China, including the north, northeast, east, central, northwest, and south power grids
- Conducted literature review on other people's projections on the power generation mix of China
- Researched the current well-to-meter emission intensity factors (g CO2-equivalent/MJ) of the different power generation technologies
- Built the Electricity Supply and Emissions Model (ESEM) on Excel that forecasts the power capacity, generation, and emissions intensity factors of the grid until 2050. Designed three scenarios for ESEM, including a "planned" that reflects the government's intention; a "more-RE" that reflects a high adoption of renewables in the grid; and a "less-RE" that reflects a low adoption of renewables
- Modified the FLEET model, by dividing the powertrain "BEV" into "regular-BEV" and "micro-BEV", adjusting micro-BEV's electricity efficiency, and changing micro-BEV's mileage driven assumptions (micro-BEV growth is a strong trend in China because it is more energy efficient and convenient than regular vehicles)
- Implemented EV scenarios into the FLEET model, including a "sensible" that is meant to depict the aggressive reality of what would happen in China; an "aggressive" that reflects a high EV penetration in the fleet; and a "passive" that reflects a low EV penetration. Added another scenario in FLEET to represent the case where the total mileage stays the same because other vehicles drive more to compensate the reduction in mileage driven by micro-BEVs
- Ran models with a total of 12 combined scenarios and generated analysis and results; compared the results from all 12 scenarios and derived findings and conclusions
- Conducted further analysis of the derived results from running the different scenarios in the FLEET model and the Electricity Supply and Emissions Model (ESEM)

## Collaboration

Visited Tsinghua University and conducted meetings with Prof. Xunming Ou, Prof. Hewu Wang, and Prof. Guiping Zhu.

## Significant Results

From the comparison analysis, it has been found that the fuel consumption (FC) factor is one of the most important assumptions that drive models' energy usage results. Figure 1 shows that after the fuel consumption input factor for the EPPA model is adjusted to assemble the factor for the other two models, its outcome (the energy usage curve) collides with the other models' outcome curves.

Literature reviews highlight this forecast of electric vehicle development scenarios in China (Figure 2, Wu et al.). The assumption of continued governmental support of BEVs and PHEVs plays a big role in the projection of the shape of the curves. But the inconvenience of charging and lack of infrastructure are critical barriers to the adoption of electric vehicles.

## Future Plans

In the upcoming year, the following activities will be conducted:

- Generate more detailed and realistic EV penetration scenarios by rigorously collecting data on EV technology characteristics, EV sales and mileage, MPG, and government policies for EV support
- Conduct interviews and collect data on historical energy generation/usage from hydro power plants, PVs, wind power plants, and thermal power plants; forecast energy demand for the grid, and use the cost-optimization capacity expansion model to forecast the energy mix in China
- Apply the capacity expansion model for six separate power grids in China to generate the total forecasts
- Explore the interactions between EVs and the electric power systems; if time permits, assume a big EV penetration will change the curves of the hourly load profiles of the grid through both charging and providing storage for the grid; then analyze the impact on energy usage and $CO_2$ emissions

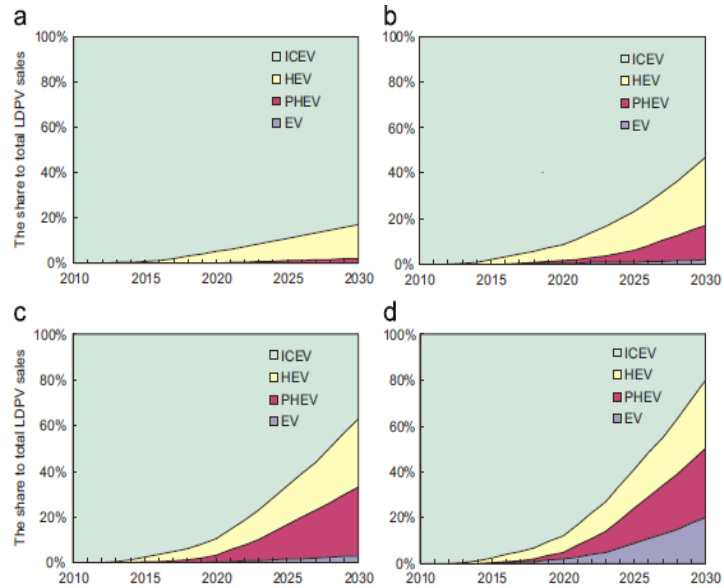


**Figure 2. The share of different powertrain technologies to total LDPV sales market under four difference scenario designs, 2010–2030.**

## Expected Outcomes

- Comparison study of the three different forecasting models (complete)
- Data analysis and a Fleet model that is able to generate different scenarios for EV penetration for light-duty transportation in China (in progress)
- Scenario analysis on different levels of EV penetrations in the fleet, and how they affect energy usage and $CO_2$ emissions (in progress)
- Data analysis and a cost-optimization electric capacity expansion model that forecasts the energy mix of power grids in China (in progress)
- Policy implications on how government support for EV should be conducted to bring the best impact/outcome on reducing energy usage and $CO_2$ emissions (in progress)

# Evaluating the Significance of Allocation Methods on Interpretation of Lightweighting Results

***Cooperative Project (U.S.)***


## U.S. Research Team Lead

- Gregory Keoleian (UM)
- Robert De. Kleine (UM)
- Nolan Orfield (UM)
- Arman (Mohammad) Golrokhian (UM)


## Research Objectives

The objective of this project is to evaluate the significance of resource depletion characterization methods and recycling allocation methods on interpretation of vehicle lightweighting practices. This research uses Life Cycle Assessment (LCA) to model energy consumption, global warming potential, and resource depletion (RD).

The specific goals are as follows:

- To create a LCA model of vehicle lightweighting through Recycled Content (RC) and End-of-Life Recycling (EOLR) allocation methods to account for the environmental benefits of lightweighting.
- To conduct a literature review of the existing resource depletion characterization methods, compile these methods, and summarize strength and shortcomings of each method.
- To explore new approaches for better capturing material scarcity in the context of manufacturing lightweight automobiles.

## Technical Approach

- Life Cycle Assessment is used to evaluate the environmental impacts of recycling allocation methods on vehicle lightweighting taking into account existing recycling infrastructure limitations and to evaluate strategies to improve it.
- Several scenarios have been developed based on the most significant decision factors and the results are compared in a fleet-based model.
- A sensitivity analysis has been conducted to assess the robustness of results in different scenarios.
- Vehicle Lightweighting (LW) with aluminum is evaluated through the eight most well-known existing resource depletion characterization methods: CML, EDIP, ILCD, CExD, EPS, Eco-Indicator, IMPACT 2002+ and ReCiPe.

## Significant Results

The project has developed a comprehensive life cycle model that compares greenhouse gas emissions for various lightweighted vehicle components based on different recycling allocation methods. The fleet based case study of the aluminum hood demonstrates that the results for *recycled content (RC)* and E*nd-of-Life Recycling (EOLR)* allocation methods are significantly different.

Consequently, the selection of allocation methods has a significant impact on accounting for benefits of vehicle lightweighting; both in terms of magnitude of benefits and when they appear.

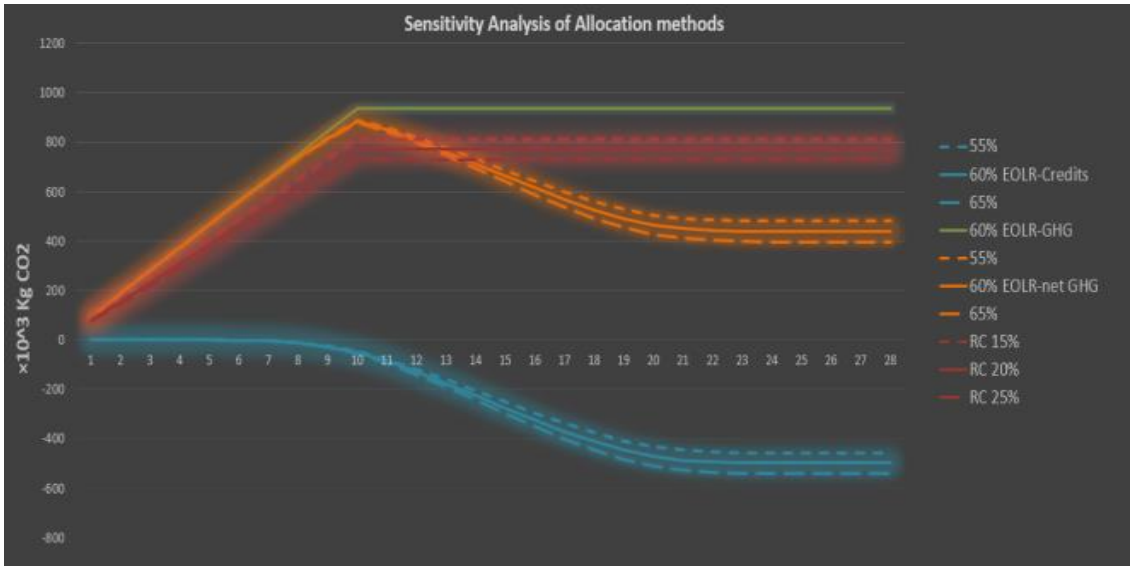


**Figure 1: GHG emissions modeled for the case study of lightweight aluminum hood in a fleet-based model. The results are compared for Recycled Content (RC) and End-of-Life Recycling (EOLR) method.**

We found that selection of recycling allocation method (which is currently not standardized) has a major impact on the aggregate life cycle results compared to any other modeling assumptions. Consequently, standardization of allocation methods is necessary to harmonize modeling and interpretation of lightweighting results across the board for life cycle practitioners in academia and industry.

In the next phase, we extended this model to resource depletion characterization methods. More than 7 distinct recycling allocation methods are in use in the literature. We cataloged these methods as well as any critiques of these methods. The PHEV aluminum hood case study that was used in previous Project 6.5 research is being used to compare the results of each RD method and each impact category.

The results demonstrate how assessment of the same system with different methods leads to significantly varied interpretations and consequently vehicle design solutions in the controversial context of vehicle lightweighting.

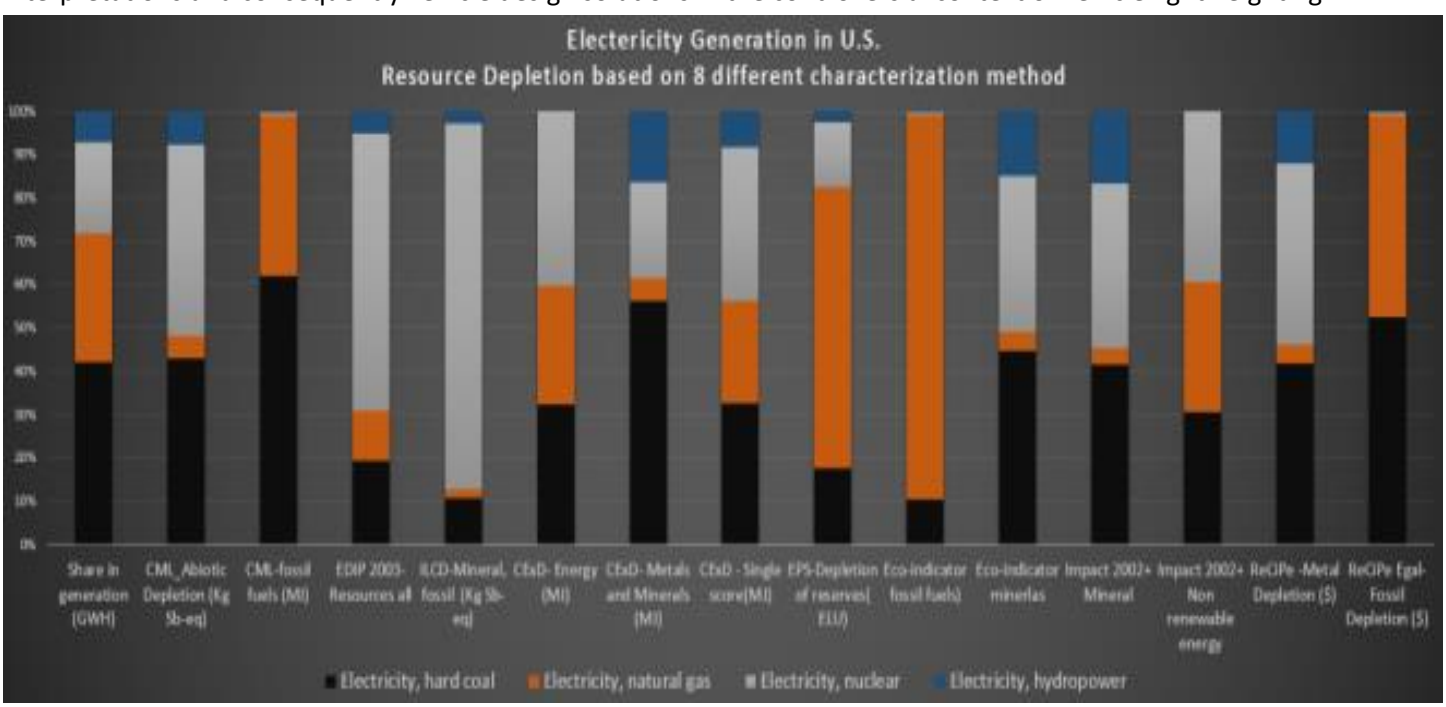


**Figure 2: Comparison of resource depletion results associated with charging a vehicle with 1kWh electricity in the U.S.**

## Future Plans

- Provide recommendations for standardization of recycling allocation methods and resource depletion characterization methods.
- Identify and recommend deficits and strengths of recycling allocation methods and resource depletion characterization methods in the case of vehicle lightweighting with aluminum.
- Explore improvements to current methods (or develop new methods) that take into account the benefits of using recycled materials from a resource depletion avoidance point of view.
- Inform policies to enhance benefits of lightweighting beyond the vehicle's use phase such as material production and improving recycling infrastructure.

## Expected Outcomes

- Recommendations on benefits of vehicle lightweighting's under different recycling allocation methods and resource depletion characterization methods.
- Recommendations on improving the existing recycling allocation methods and resource depletion characterization methods.
- Recommendations for developing strategic standardization in selection of allocation methods and resource depletion characterization methods.

# Improving Precision of Electricity Grid Modeling for Electrified Vehicle Sustainability Assessments

*Collaborative Project (U.S.)*


## U.S. Research Team Lead

- Gregory Keoleian (UM)
- Jeremiah Johnson (UM), Robb De Kleine (UM), Geo
  Lewis (UM)
- Nicole Ryan (UM)


## Research Objectives

The project is developing a comparative assessment of protocols and tools used to estimate emissions from electricity consumption. The analysis will provide the project team with a better understanding of the appropriate applications for existing emissions estimation tools and how their use will effect the life cycle emissions of a product or process. This is very relevant to electrified and lightweight vehicles which are dependent on electricity for charging and material production (e.g. aluminum smelting) respectively. Both private and public electricity allocation protocols are available and each uses a different set of variables in their fuel mix calculations: time, aggregation level, transmission constraints, fuel costs, marginal changes in consumption, etc. The research will focus on how the consideration or omission of these variables effects estimates of emissions, initially, in relation to electric vehicle charging stations. These results will provide the team with the information necessary to develop guidelines for how types of electricity loads should be modeled to more appropriately estimate emissions. Finally, the analysis will show where these tools are lacking and how they could be improved.

## Technical Approach

- Complete a literature review of all public and private electricity allocation protocols to better understand their appropriate applications
- Categorize the protocols into unique categories outlined in Table 1 to aid in providing clear recommendations on protocol selection

Table 1: Emissions model categories

| Category | Characteristics |
|---|---|
| **Empirical Data & Relationship Models** | Emissions Factors (Marginal & Average)<br>Emissions Factor Models with Trading/Imports<br>Statistical Relationship Models |
| **Power System Optimization Models** | Economic Dispatch<br>Unit Commitment<br>Capacity Planning |

- Analyze the variations in emissions estimates from different electricity allocation protocols (e.g. AVERT, PLEXOS, eGRID sub regions, balancing authorities, etc.) when applied to the electricity use at nine plug in vehicle charging stations across the U.S.
- Create emissions estimation heat maps of hourly emission factors, using PLEXOS & AVERT, for representational days in each month in select U.S. regions
- Develop a tool to guild users in selecting the appropriate model for their application

## Significant Results

The team compiled information on 35 plus electricity allocation protocols that can be used to estimate emissions from electricity consumption. The protocols were reviewed in a comparative assessment. Multiple protocol deficits and strengths have been identified. Some deficits found in the many public models include a lack of consideration for time of generation/consumption, electricity trading and for effects of marginal power production changes, along with an inability to account for changes in fuel prices or available generation assets. Many of the average estimations also use data several years old. Ten of the protocols were compared in the electric vehicle charging station case study.

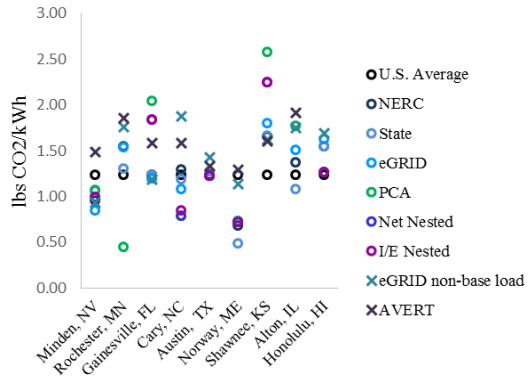


**Figure 1: CO2 emissions, averaged across the year, per kWh based on charging station location [North American Electric Reliability Corporation (NERC), Power Control Area (PCA)]**

Figure 1, shows a comparison of the yearly average emissions factor results from nine of the methods compared in nine electric vehicle charging station locations across the U.S. This demonstrates that the selection of the method will greatly impact the overall estimates of electric vehicle emissions. The instance with the largest variation from the average was the PCA value for Rochester, MN, at 69% lower than the average of all the methods in that location. The largest spread was also in Rochester, MN, at 1.4 lb. $CO_2$/kWh, representing 102% of the average value at that location. Austin, TX had the smallest spread at 0.21 lbs. $CO_2$/kWh. These differences were shown to have varying location specific causes, ranging from the location of interchanges to large regional differences in generation mix.

Even larger differences could be seen when comparing the same location's hourly emissions factors using PLEXOS and AVERT. Not only were the hourly averages for each month different but the overall seasonal and diurnal trends calculated were also different when calculated for the same charging station location, Rochester, MN.

Another important note is the consistent difference between marginal and average emissions factors. The marginal emissions factors averaged 21% higher than the average emissions factors. However, this is not the trend in each location, for Shawnee, KS and Gainesville, FL the average of the average emissions factors was larger than the average of the marginal factors.

The case study results showcase the importance of method selection, and the need for greater consistency in emissions modeling. These results along with the literature review of existing protocols led to the creation of 13 recommendations to aid researchers, analysts and others in selecting the appropriate method to model the emissions from their electricity load. These recommendations can be found in table 2.

**Table 2: Recommendations on model characteristics required based on load features**

| Recommendations |
|---|
| ***Marginal or Average Emissions Factors*** |
| 1) If the load being studied is part of the existing demand or used in an attributional LCA where it does not represent a change, then an AEF is appropriate. |
| 2) If the load being studied causes an incremental change in demand or generation or is part of a consequential LCA, then a MEF is appropriate. |
| ***Regional Boundaries*** |
| 1) Political regions should not be used as boundaries unless electricity flows in and out are minimal or electricity trading is taken into consideration. |
| 2) An average country level emissions factor should only be used for loads distributed evenly throughout the country. |
| 3) If specific plant locations are known, smaller regions like PCAs/BAs can be employed with caution, see recommendation 6. |
| 4) If the load is caused by an industry unevenly distributed across a country and specific production facilities information is unknown regional differences should still be considered. |
| 5) For regional loads, regional EFs using a region of the same size or larger are appropriate. Trading may need to be taken into consideration unless using a NERC region or interconnection. |
| 6) If there is non-trivial trade between surrounding regions and the difference in EFs are large and or the percent imports are large, the user should incorporate the emissions from the imported electricity. |
| ***Historical or Future Perspective*** |
| 1) Recent historical data are appropriate when estimating a product's emissions from electricity consumption at present of in the near future. |
| 2) A prospective model should be used when studying a system that examines fuel prices, grid infrastructure, or policy change. |
| ***Temporal Granularity*** |
| 1) Yearly averages should only be used for loads that are consistent throughout the year. |
| 2) For loads with strong diurnal shapes models that can account for diurnal emissions variation should be used in regions where generation mix varies with time of day. |
| 3) For loads with strong seasonal variation models that can account for seasonal emissions variation should be used in regions where generation mix varies with season. |

## Future Plans

Future work includes creating a decision support tool using the recommendations developed with this work to aid researchers, analysts, policy makers and others interested in modeling electricity emissions from a particular load on the appropriate method to use. This tool is currently being developed and tested.

## Expected Outcomes

- Recommendations for which electricity allocation protocol to apply based on the application
- Analysis of emissions produced from electric vehicle charging station use in a variety of geographic locations
- A publically available tool for selecting the appropriate emissions estimation method for modeling loads

## References/Publications


1. Colett, J.S., J.C. Kelly, and G.A. Keoleian, "Using Nested Average Electricity Allocation Protocols to Characterize Electrical Grids in Life Cycle Assessment: A Case Study of U.S. Primary Aluminum Production" Journal of Industrial Ecology (2016) 20(1): 29–41.
2. Ryan, Nicole A., Jeremiah X. Johnson, and Gregory A. Keoleian. 2016. "Comparative Assessment of Models and Methods to Calculate Grid Electricity Emissions." Environmental Science & Technology. In Review.
3. Ryan, Nicole A., Jeremiah X. Johnson, and Gregory A. Keoleian. 2016. "Selecting the appropriate Electricity Model (SEEM): Technical Support Document, 2016"